Acta Pharmaceutica Sinica B 2025;15(4):2170−2196

Chinese Pharmaceutical Association
Institute of Materia Medica, Chinese Academy of Medical Sciences

Acta Pharmaceutica Sinica B

www.elsevier.com/locate/apsb
www.sciencedirect.com

ORIGINAL ARTICLE

Discovery and mechanism verification of first-in-class hydrophobic tagging-based degraders of HBV core protein

Shujing Xu[a,†], Ya Wang[b,†], Dazhou Shi[a], Shuo Wang[a], Lijun Qiao[b], Ge Yang[b], Yang Zhou[a], Xinyong Liu[a], Shuo Wu[c,*], Yuhuan Li[c,*], Peng Zhan[a,*]

[a]*Department of Medicinal Chemistry, Key Laboratory of Chemical Biology, Ministry of Education, School of Pharmaceutical Sciences, Shandong University, Jinan 250012, China*
[b]*Institute of Medicinal Biotechnology, Chinese Academy of Medical Sciences & Peking Union Medical College, Beijing 100050, China*
[c]*State Key Laboratory of Bioactive Substances and Functions of Natural Medicines, Beijing Key Laboratory of Antimicrobial Agents, NHC Key Laboratory of Biotechnology for Microbial Drugs, CAMS Key Laboratory of Antiviral Drug Research, Institute of Medicinal Biotechnology, Chinese Academy of Medical Sciences & Peking Union Medical College, Beijing 100050, China*

Received 3 June 2024; received in revised form 12 September 2024; accepted 27 February 2025

KEY WORDS

Hepatitis B virus;
Core protein;
Hydrophobic tagging;
Degrader;
Mechanism verification;
Drug resistance;
Autophagy−lysosome pathway;
Drug design

Abstract Interfering hepatitis B virus (HBV) capsid assembly holds promise as a therapeutic approach for chronic hepatitis B (CHB). Novel anti-HBV agents are urgently needed to overcome drug resistance challenges, with targeted protein degradation (TPD) emerging as a hopeful strategy. Herein, we report the first degradation of HBV core protein (HBC), a multifunctional structural protein, using small-molecule degraders developed by hydrophobic tagging (HyT) technology. Structure−activity relationship (SAR) analysis identified compound **HyT-S7**, featuring an adamantyl group, exhibiting potent inhibitory activity (EC_{50} = 0.46 μmol/L, HepAD38 cells) and degradation ability (DC_{50} = 3.02 ± 0.54 μmol/L) in a dose- and time-dependent manner. Mechanistic studies demonstrated that the autophagy−lysosome pathway was a potential driver of **HyT-S7-**induced HBC degradation. Remarkably, **HyT-S7** effectively degraded 11 drug-resistant mutants, including highly resistant strains P25G and T33N, to Phase III drug GLS4. Furthermore, cellular thermal shift assay, surface plasmon resonance assay, and molecular dynamics simulations revealed the precise mode of **HyT-S7** binding to HBC with the adamantyl group potentially

*Corresponding authors.
E-mail addresses: zhanpeng1982@sdu.edu.cn (Peng Zhan), yuhuanlibj@126.com (Yuhuan Li), wushuoimb@126.com (Shuo Wu).
†These authors made equal contributions to this work.

Peer review under the responsibility of Chinese Pharmaceutical Association and Institute of Materia Medica, Chinese Academy of Medical Sciences.

https://doi.org/10.1016/j.apsb.2025.02.033

mimicking protein misfolding to facilitate HBC degradation. This first proof-of-concept study highlights the potential of HyT-mediated TPD in HBC as a promising avenue for discovering novel HBV and other antiviral agents with favorable drug resistance profiles.

1. Introduction

The Hepatitis B virus (HBV) is a hepatotropic pathogen that invades the human body, resulting in hepatitis B infection. Chronic hepatitis B (CHB) may further progress to cirrhosis or liver cancer, ultimately leading to mortality. It is estimated by the World Health Organization (WHO) that approximately 296 million individuals were afflicted with CHB, and 820,000 people died from hepatitis B in 2019. Consequently, Hepatitis B has emerged as a grave global public health concern[1]. Currently, there are two categories of drugs employed in the clinical treatment of CHB: nucleoside analogs (NAs) and interferon (IFN)[2]. Up to now, NAs approved by the US Food and Drug Administration (FDA) for HBV treatment include lamivudine (3TC), telbivudine (LdT), entecavir (ETV), adefovir dipivoxil (ADV) and tenofovir (TAF) prodrugs (tenofovir disololol and tenofovir arafenamide) (Fig. 1A). NAs have demonstrated remarkable efficacy as anti-HBV medications. However, the prolonged use necessary for treating chronic infection may eventually result in the development of drug resistance. For instance, mutations such as M204V/I/S are associated with resistance to lamivudine, while A181T/V mutations confer resistance to adefovir[3]. IFN therapy frequently results in numerous adverse reactions, encompassing flu-like symptoms, gastrointestinal disturbance, thrombocytopenia, neutropenia, and depression[4]. Moreover, the stability of covalently closed circular DNA (cccDNA) in the host nucleus serves as a resilient transcription template and remains a primary factor contributing to persistent HBV infection. Neither of these drugs can eliminate cccDNA and achieve a cure for CHB[5]. Consequently, there is a pressing demand for research and development focused on novel targets and mechanisms for anti-HBV drugs.

HBV capsid protein plays crucial roles in the viral life cycle, such as facilitating nucleocapsid assembly, encapsulating viral pregenomic RNA (pgRNA), and interacting with cccDNA, making it garner considerable interest as a promising target[6–10]. HBV capsid is formed by assembling 90 or 120 dimers of the core protein (HBC)[11]. These dimers are connected through hydrophobic forces, forming hexamers, and then assembled into an icosahedral capsid. Core protein allosteric modulators (CpAMs) bind to the core protein dimer interface, thereby disrupting or interfering with the HBV capsid assembly processes[12]. The chemical structures of representative CpAMs are illustrated in Fig. 1B[6-8]. CpAMs operate through two distinct mechanisms. Type I CpAMs, exemplified by heteroaryldihydropyrimidine derivatives (HAPs) like Bay41-4109 and GLS4, impede virus proliferation by inducing the aggregation of core proteins. This results in the formation of non-capsid structures with compromised functionality and abnormal configuration[13–15]. On the other hand, type II CpAMs, including phenylpropenamides (PPAs) such as AT-130 and sulfamoylbenzamides (SBAs) like NVR 3-778 and JNJ-6379, disrupt the encapsidization of pgRNA. This interference leads to the creation of empty capsids devoid of the viral genome, rendering the virus incapable of infection[16,17].

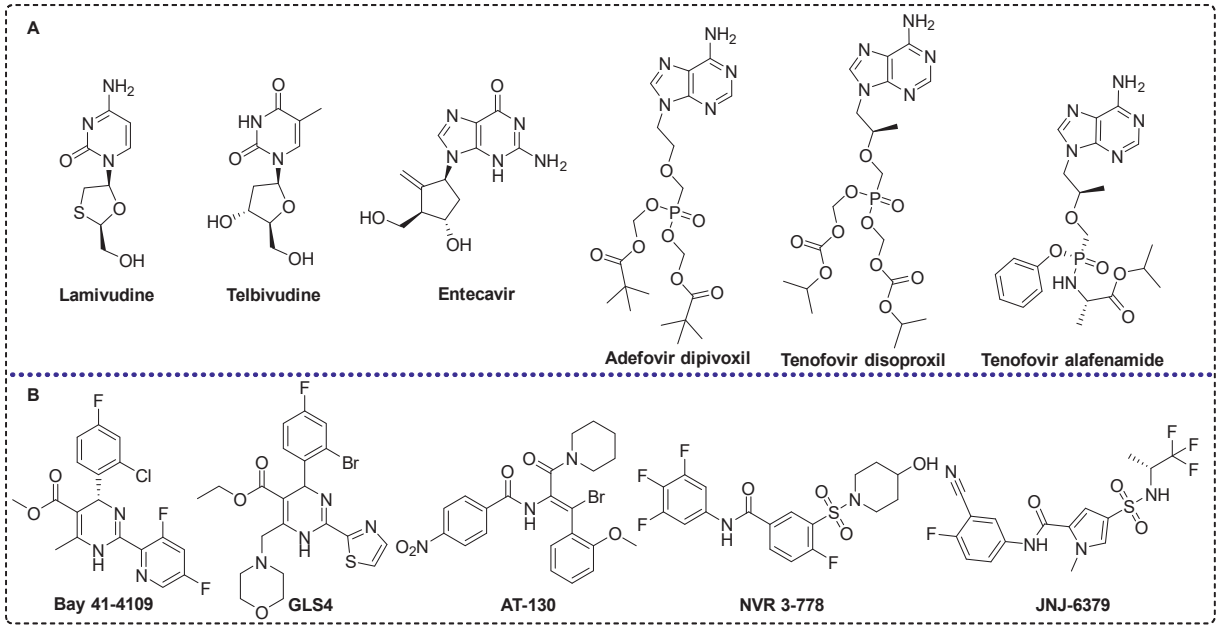

Figure 1 (A) Chemical structures of NAs approved by FDA; (B) Chemical structures of representative CpAMs.

Presently, the effective concentration at which CpAMs inhibit HBV replication *in vitro*, known as EC_{50}, has reached nanomolar levels, with about 20 CpAMs undergoing clinical studies. However, the emergence of accumulated mutations in the binding pocket of CpAMs poses a risk of drug resistance. Up to now, a total of 19 resistant mutations have been identified at 13 different residues (Phe23, Phe24, Pro25, Asp29, Leu30, Thr33, Leu37, Ile105, Thr109, Phe110, Tyr118, Val124 and Arg127)[18]. Notably, the T33N and P25G mutants exhibited a reduction in sensitivity to HBV CpAMs by more than 66 times. Additionally, various mutations can lead to cross-resistance, resulting in decreased sensitivity to different structural types of CpAMs[16]. Therefore, it is imperative to discover novel HBV CpAMs with improved drug resistance profiles urgently.

Employing an event-driven mode, targeted protein degradation (TPD) presents an effective strategy to overcome drug resistance stemming from mutations in the targeted viral protein by facilitating their degradation[19]. Hydrophobic tagging technology (HyT) stands out as a particularly promising TPD method. Serving as a heterobifunctional molecule, HyT comprises three components: a ligand for the protein of interest (POI), a hydrophobic moiety, and a linker connecting these two parts[20]. Recently, SBA-derived structures have undergone rapid development, gaining considerable attention in the field of medicinal chemistry[21,22]. NVR 3-778, representing the extensively studied SBA chemotype, was the first CpAM demonstrating antiviral efficacy in patients with HBV infection[23,24]. Given this significance, we opted to utilize NVR 3-778 as the tool compound for designing HyT degraders. Through analysis of the co-crystal structure between NVR 3-778 and HBC, it was observed that the 3,4,5-trifluorophenyl group penetrates deeply into the hydrophobic pocket of HBC, while the 4-hydroxypiperidine occupies the solvent-exposed region (Fig. 2). Based on the binding pattern of NVR 3-778 in complex with HBC, there were several polar amino acid residues proximate to the hydroxypiperidine moiety of NVR 3-778. Given that introducing more hydrogen bond acceptors or donors might enhance the binding affinity of NVR 3-778-based degraders to HBC, an amino group replaced the hydroxyl group before introducing hydrophobic groups and obtained the POI ligand **SP-5**, which demonstrated anti-HBV activity comparable to that of NVR 3-778. Firstly, target compounds of series I were designed by connecting **SP-5** with an adamantyl group, a commonly used hydrophobic tag, through a linear linker. Following an antiviral activity screening, it was determined that a linker length of seven carbon atoms displayed optimal antiviral efficacy. Subsequently, this advantageous linker was employed to connect various hydrophobic groups in order to generate more potent degraders, and target compounds of series II were designed accordingly. It has been reported that linkers possessing greater rigidity exhibit improved degradation activity and druggability[25]; hence, different ring structures were chosen for designing target compounds of series III (Fig. 2).

All target compounds underwent assessment for their anti-HBV activity, cytotoxicity, and degradation activity toward HBC in HepAD38 cells. These results allowed us to establish a structure−activity relationship (SAR). Furthermore, we conducted a series of Western blot assays to investigate the mechanisms of action of the representative compound and sequentially performed cellular thermal shift assay (CETSA) and surface plasmon resonance (SPR) assay to validate its target. Finally, molecular docking and molecular dynamics simulation were conducted to obtain a comprehensive understanding of the binding mode of representative compound in the binding pocket.

2. Results and discussion

2.1. *Chemistry*

The target compounds in series I were synthesized following the outlined procedures in Scheme 1. Commercially available 3-(chlorosulfonyl)-4-fluorobenzoic acid (**1**) was converted into intermediate **2** by reacting with thionyl chloride. Refluxing intermediate **2** and 3,4,5-trifluoroaniline in toluene yielded the key intermediate **3**. The key intermediate **3** underwent an acylation reaction with 4-Boc-aminopiperidine to give intermediate **4**. Removal of the Boc protecting group using trifluoroacetic acid

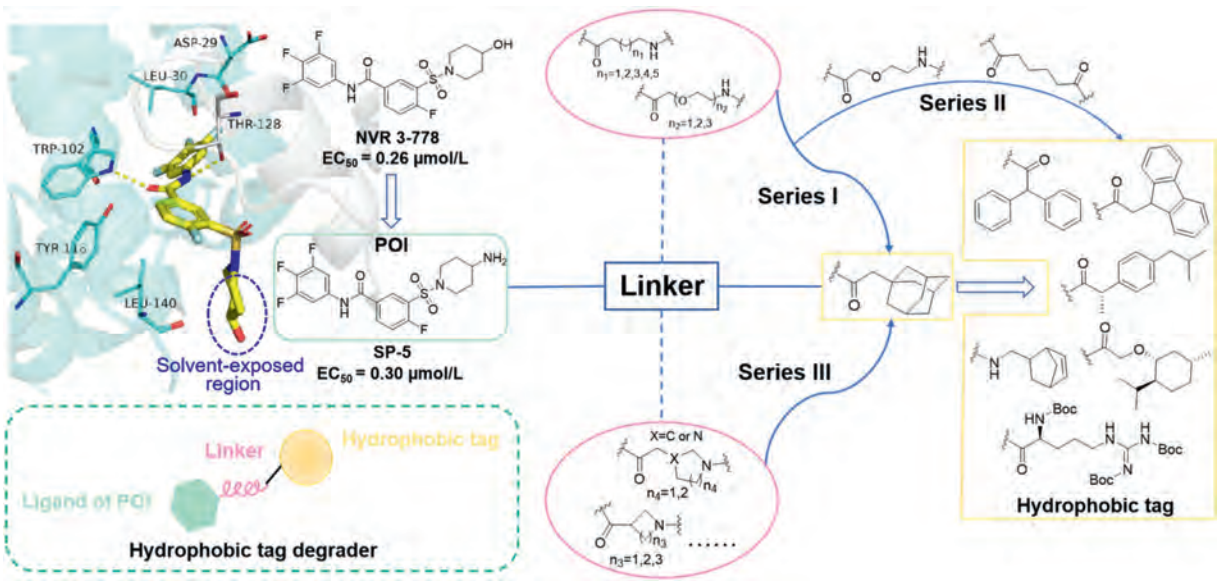

Figure 2 Design idea of HBC degraders based on HyT technology (PDB code: 5T2P). The figure of NVR 3-778 binding with HBC was generated in PyMOL (www.pymol.org).

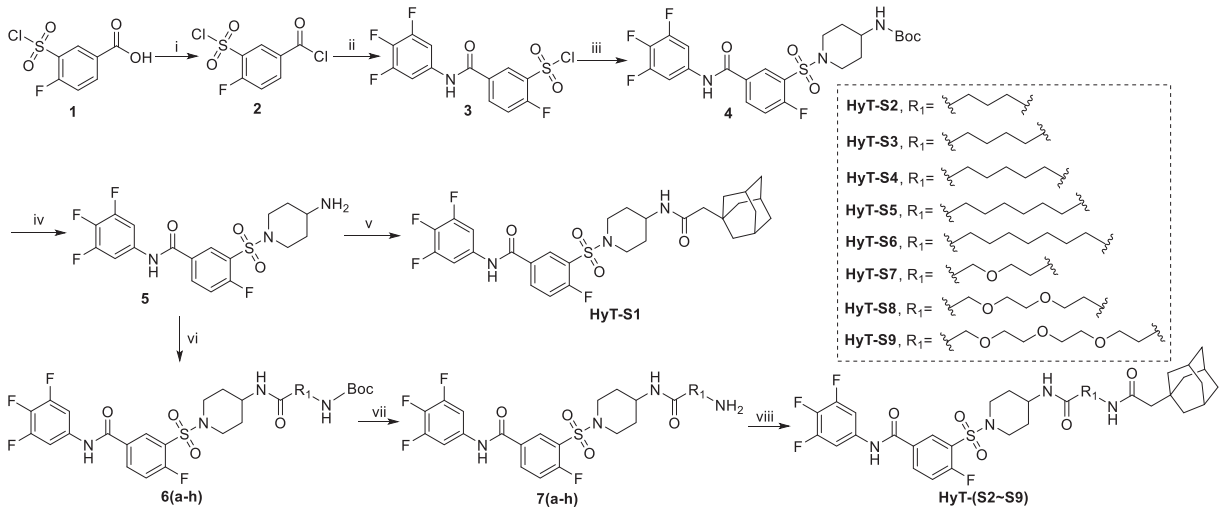

Scheme 1 The synthetic route of series I. Reagents and conditions: (i) $SOCl_2$, toluene, DMF, 120 °C; (ii) 3,4,5-trifluoroaniline, toluene, 120 °C; (iii) 4-Boc-aminopiperidine, DCM, TEA, 0 °C to r.t. Yield: 80%; (iv) TFA, DCM, 0 °C to r.t. Yield: 83%; (v) 1-adamantaneacetic acid, HATU, DIEA, DCM, 0 °C to r.t. Yield: 73%; (vi) different substituted *N*-Boc alkylamino acids, HATU, DIEA, DCM, 0 °C to r.t. Yield: 69%−80%; (vii) TFA, DCM, 0 °C to r.t. Yield: 61%−76%; (viii) 1-adamantaneacetic acid, HATU, DIEA, DCM, 0 °C to r.t. Yield: 67%−77%.

(TFA) generated intermediate **5,** which was subsequently utilized for amide coupling with 1-adamantaneacetic acid to produce target compound **HyT-S1**. In addition, coupling of different substituted *N*-Boc alkylamino acids with intermediate **5** in DCM afforded intermediates **6(a−h)**. The Boc protecting group was then removed using TFA to yield intermediates **7(a−h)**, which were further employed for amide coupling with 1-adamantaneacetic acid to afford target compounds **HyT-(S2−S9)**.

The synthesis of target compounds **HyT-(S10−S11**, **S13−S15)** was achieved using the pathway described in Scheme 2. Coupling of different hydrophobic groups with intermediate **7f** in DCM afforded target compounds **HyT-(S10−S11**, **S13−S14)**. Additionally, coupling of (*tert*-butoxy) carbonyl Arg $(Boc)_2$-OH (symmetrical) with **7f** in acetonitrile yielded the target compound **HyT-S15**.

The synthesis of the target compound **HyT-S12** was accomplished through a pathway outlined in Scheme 3. Intermediate **8** was obtained through an amide condensation reaction with intermediate **5**. Then, intermediate **8** underwent LiOH-mediated hydrolysis to yield intermediate **9**, which was used for the subsequent amide coupling with 1-bicyclo[2.2.1]hept-5-en-2-ylmethanamine to produce the target compound **HyT-S12**.

The synthetic pathway for the preparation of target compounds in series III was illustrated in Scheme 4. Coupling of different substituted *N*-Boc acids with intermediate **5** in DCM afforded intermediates **10(a−n)**; Subsequently, removal of the Boc protecting group using TFA yielded intermediates **11(a−n)**, which were employed for the subsequent amide coupling with 1-adamantaneacetic acid to afford target compounds **HyT-(S16−S29)**.

2.2. *Biological evaluation of **SP-5**-based HBC HyT degraders*

The HepAD38 cell line, derived from HepG2 cells and characterized by tetracycline-inducible HBV expression, exhibited an approximately 11-fold increase in viral DNA production compared to HepG2.2.15 cells[26]. This cell line proved valuable for scrutinizing the viral replication cycle and screening potential anti-HBV drugs. A total of 29 synthesized compounds were assessed for their activity against HBV DNA replication and cytotoxicity in HepAD38 cells using standard quantitative polymerase chain reaction (qPCR) and cytopathic effect (CPE) methods, respectively. The lead compound NVR 3-778 served as a positive control. The EC_{50}, CC_{50}, and selectivity index (SI, CC_{50}/EC_{50}) values of the

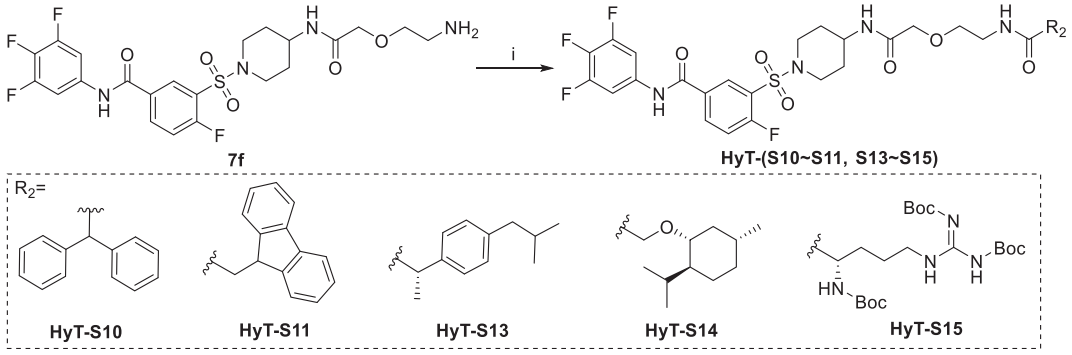

Scheme 2 The synthetic route of target compounds **HyT-(S10−S11**, **S13−S15)**. Reagents and conditions: (i) different acid, HATU, DIEA, DCM, 0 °C to r.t. Yield: 67%−71%; or (*tert*-Butoxy) carbonyl Arg $(Boc)_2$-OH (symmetrical), NMI, TCFH, CH_3CN, r.t. Yield: 65%.

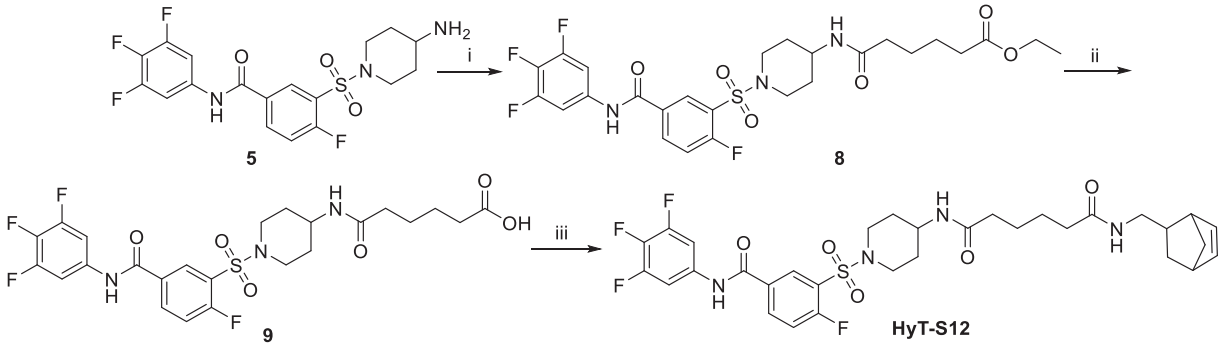

Scheme 3 The synthetic route of target compound **HyT-S12.** Reagents and conditions: (i) monoethyl adipate, HATU, DIEA, DCM, 0 °C to r.t. Yield: 78%; (ii) LiOH, THF: H_2O = 1:1, r.t. Yield: 70%; (iii) 1-bicyclo[2.2.1]hept-5-en-2-ylmethanamine, HATU, DIEA, DCM, 0 °C to r.t. Yield: 65%.

target compounds are presented in Tables 1−3. In consideration of the anti-HBV activities, all target compounds underwent further evaluation for their effects on HBC degradation in the HepAD38 cells by the Western blot analysis (Figs. 3 and 4).

*2.2.1. In vitro anti-HBV assays and degradation activity evaluation of target compounds **HyT-(S1−S15)***

Based on the strategy mentioned above, since there was no report on HyT-based degraders targeting HBC, we first designed and synthesized **HyT-(S1−S6)** connected by six carbon chains (0−10-atom lengths) and **HyT-(S7−S9)** connected by three polyethylene glycol (PEG) chains (7−13-atom lengths) to explore the suitable length range of linker. As detailed in Table 1, most of the target compounds in series I exhibited moderate to excellent anti-HBV activity. Interestingly, the anti-HBV activity first decreased (from **HyT-S1** to **HyT-S5** and from **HyT-S7** to **HyT-S8**) and then increased (from **HyT-S5** to **HyT-S6** and from **HyT-S8** to **HyT-S9**) with the increase of chain length, and **HyT-S1** displayed the most potent anti-HBV activity with an EC_{50} value of 0.40 μmol/L. Compound **HyT-S5**, characterized by an 8-carbon atom linker, displayed approximately 10 times less potent than **HyT-S1**, which indicated that compounds with a shorter linker of fewer than eight atoms exhibit a favorable influence on cellular potency. Despite **HyT-S1** showcasing the most potent antiviral activity in series I, comparable to the positive control NVR 3-778 (EC_{50} = 0.26 μmol/L, CC_{50} = 11.11 μmol/L), it displayed higher cytotoxicity (CC_{50} = 7.70 μmol/L) with a SI value of only 19.25. However, when PEG was employed as a linker with a carbon atom number of seven, **HyT-S7** not only demonstrated good antiviral activity (EC_{50} = 0.46 μmol/L) but also significantly reduced cytotoxicity (CC_{50} = 28.84 μmol/L), making it a promising candidate for further modification as an advantageous linker.

According to the favorable linker identified in series I, different hydrophobic tags with diphenyl (**HyT-S10**), fluorene (**HyT-S11**), norbornene (**HyT-S12**), alkyl-substituted phenyl (**HyT-S13**), (−)-menthoxyacetyl (**HyT-S14**) or Boc protected arginine (**HyT-S15**) were introduced to obtain target compounds in series II. All these compounds exhibited excellent anti-HBV activity (Table 2). Substituting fluorene (**HyT-S11**), norbornene (**HyT-S12**), and Boc-protected arginine (**HyT-S15**) as hydrophobic tags led to a

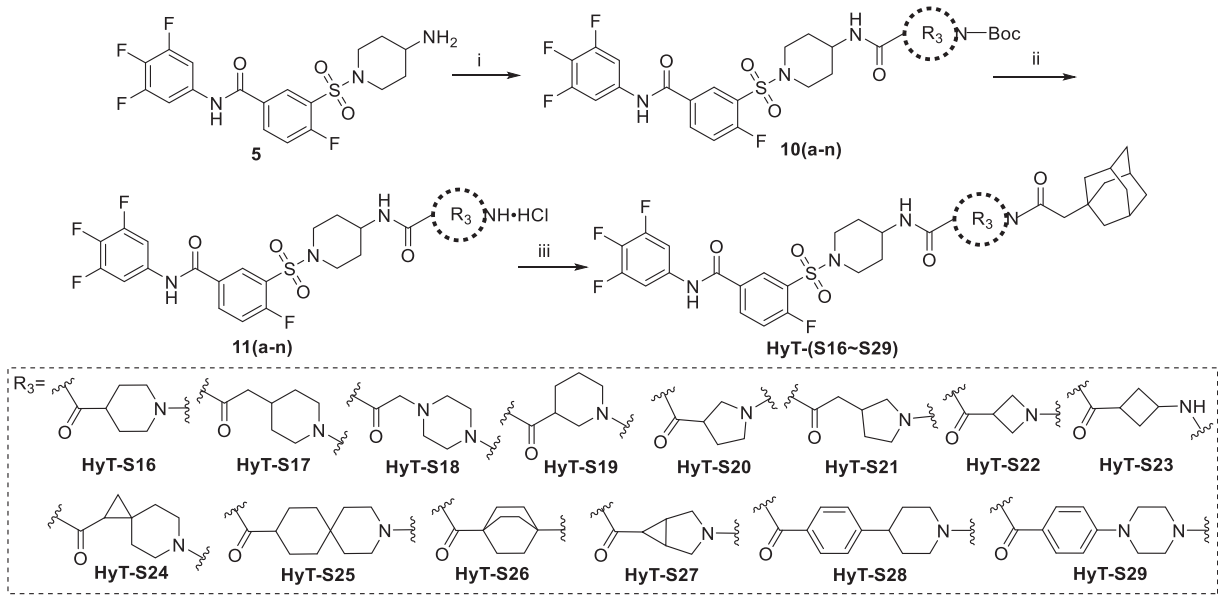

Scheme 4 The synthetic route of series III. Reagents and conditions: (i) differently substituted *N*-Boc acids, HATU, DIEA, DCM, 0 °C to r.t. Yield: 60%−74%; (ii) 4 mol/L HCl in dioxane, DCM, r.t.; (iii) 1-adamantaneacetic acid, HATU, DIEA, DCM, 0 °C to r.t. Yield: 36%−71%.

Table 1 Anti-HBV activity and cytotoxicity of compounds **HyT-(S1−S9).**

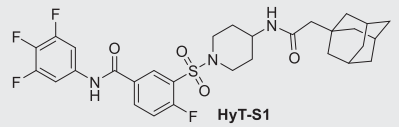

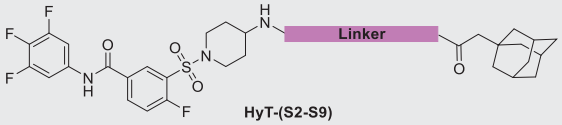

Compd.	Linker	EC_{50}[a] (μmol/L)	CC_{50}[b] (μmol/L)	SI[c]
HyT-S1	–	0.40	7.70	19.25
HyT-S2	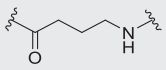	0.47	33.33	70.91
HyT-S3	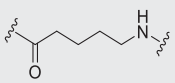	0.89	33.33	37.45
HyT-S4	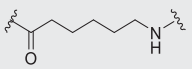	1.80	77.61	43.12
HyT-S5	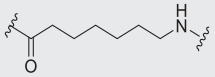	4.46	100.00	22.42
HyT-S6	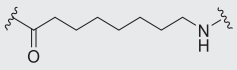	1.29	33.33	25.84
HyT-S7	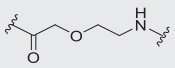	0.46	28.84	62.70
HyT-S8	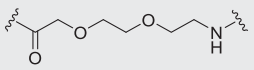	1.42	ND[d]	NA[e]
HyT-S9	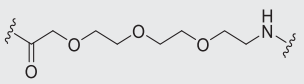	1.19	16.65	13.99
NVR 3-778	–	0.26	11.11	42.73

[a]EC_{50} is the concentration of the test compounds for reduction of HBV DNA by 50% in HepAD38 cells. EC_{50} values were evaluated from HBV DNA by the qPCR assay after 6 days of incubating the cells with the compounds.

[b]CC_{50} is the concentration of the test compounds for reduction of the viability of HepAD38 cells by 50%. CC_{50} values were measured by the CPE method.

[c]Selective index (SI) is the ratio of CC_{50}/EC_{50}.

[d]Not determined.

[e]Not applicable.

significant reduction in cytotoxicity and an increase in the selectivity index. Particularly for **HyT-S11** with an EC_{50} of 0.21 μmol/L, slightly superior to the lead compound NVR 3-778, whose SI value was approximately four times that of NVR 3-778.

To explore whether the synthesized new compounds could degrade HBC, we assessed the degradability of all target compounds in series I and series II, with GAPDH or *β*-Actin as a loading control, and the results were presented in Fig. 3. In series I with adamantyl as the hydrophobic ligand (Fig. 3A), compounds **HyT-S1** and **HyT-S2** effectively induced HBC degradation, while **HyT-(S3−S6)** did not exhibit any degradation activity. This may be attributed to the increased flexibility of the compounds with extended linker length, hindering the stable binding of the hydrophobic groups to the surface of HBC. Compounds **HyT-(S7−S9)** containing PEG linker all demonstrated degradation activity, consistent with their anti-HBV activity order (**HyT-S7** > **HyT-S9** >**HyT-S8**). In series II (Fig. 3B), replacing adamantyl with diphenyl (**HyT-S10**), fluorene (**HyT-S11**), alkyl-substituted phenyl (**HyT-S13**), (−)-menthoxyacetyl (**HyT-S14**), and Boc-protected arginine (**HyT-S15**) still retains some degradation activity. Among them, **HyT-S11** exhibited the highest degradation activity in series II, slightly weaker than **HyT-S7** in series I (Fig. 3C). However, when adamantyl was replaced with norbornene (**HyT-S12**), the degradation activity against HBC was lost. Analysis of SAR for these compounds demonstrates that degradation is dependent on the hydrophobic tag type and length of the linker, and the adamantyl group remains the most effective hydrophobic moiety for inducing HBC degradation.

2.2.2. In vitro anti-HBV assays and degradation activity evaluation of target compounds HyT-(S16−S29)

Building upon the appropriate linker length, we proceeded to examine the impact of a rigid linker on both anti-HBV activity and HBC degradation activity, aiming to identify a potent HBC degrader possessing favorable drug-like properties. Herein, we designed and synthesized 14 HyTs **HyT-(S16−S29)** with different ring linkers and using adamantyl as a hydrophobic group. As presented in Table 3, the different ring linkers in series III can be

Table 2 Anti-HBV activity and cytotoxicity of compounds **HyT-(S10−S15)**.

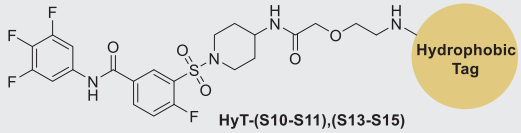

HyT-(S10-S11),(S13-S15)

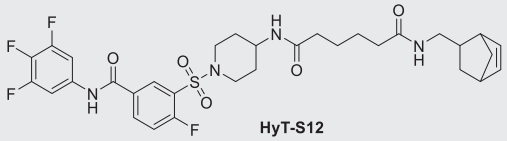

HyT-S12

Compd.	Hydrophobic Tag	EC_{50}[a] (μmol/L)	CC_{50}[b] (μmol/L)	SI[c]
HyT-S10	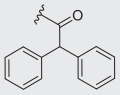	0.26	20.00	76.92
HyT-S11	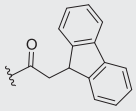	0.21	34.64	164.95
HyT-S12	—	0.22	28.84	131.09
HyT-S13	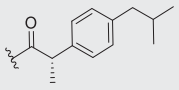	0.59	11.55	19.58
HyT-S14	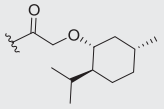	0.29	11.55	39.83
HyT-S15	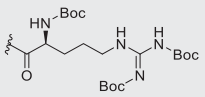	0.45	60.00	133.33
NVR 3-778	—	0.24	ND[d]	NA[e]

[a]EC_{50} is the concentration of the test compounds for reduction of HBV DNA by 50% in HepAD38 cells. EC_{50} values were evaluated from HBV DNA by the qPCR assay after 4 days of incubating the cells with the compounds.

[b]CC_{50} is the concentration of the test compounds for reduction of the viability of HepAD38 cells by 50%. CC_{50} values were measured by the CPE method.

[c]Selective index (SI) is the ratio of CC_{50}/EC_{50}.

[d]Not determined.

[e]Not applicable.

divided into six types: ① six-membered ring (**HyT-S16**−**S19**), ② five-membered ring (**HyT-S20**−**S21**), ③ four-membered ring (**HyT-S22**−**S23**), ④ spiral ring (**HyT-S24**−**S25**), ⑤ bridge ring (**HyT-S26**−**S27**) and ⑥ phenyl connected six-membered ring (**HyT-S28**−**S29**). The SAR of series III can be summarized as follows: (i) Overall, the average anti-HBV activity is ranked in the following order: ③>⑤>①>②>④>⑥; **HyT-S23** with cyclobutylamine as a linker (EC_{50} = 0.20 μmol/L, CC_{50} = 60.00 μmol/L) is the most potent compound in this series, surpassing NVR 3-778 (EC_{50} = 0.31 μmol/L, CC_{50} = 10.00 μmol/L), and exhibiting significantly reduced cytotoxicity compared to NVR 3-778. (ii) In instances where the linker adopts a six-membered ring structure: a) For the piperidine ring, the different positions of the nitrogen atom lead to significant differences in activity (**HyT-S19** > **HyT-S16**); b) Compound **HyT-S17** with one additional methylene improved the anti-HBV activity relative to **HyT-S16**; c) The efficacy of a six-membered ring with two nitrogen atoms surpasses that of a counterpart with only one nitrogen atom (**HyT-S18** > **HyT-S17**); (iii) In cases where the linker takes the form of a five-membered ring, compound **HyT-S21**, featuring a one-carbon atom extension in the linker, demonstrated heightened anti-HBV activity compared to **HyT-S20**. This trend aligns with observations seen with a six-membered ring linker, implying that the incorporation of a methylene group enhances flexibility and facilitates the binding of the small molecule to the target; (iv) The replacement of azazocyclobutane (**HyT-S22**) with cyclobutylamine (**HyT-S23**) resulted in an improvement in activity, potentially attributed to the increased interactions between NH and the binding site; (v) The effectiveness of 6-azaspiro[2.5]octane (**HyT-S24**) markedly outperformed that of 3-azaspiro[5.5]undecane (**HyT-S25**); (vi) The efficacy of 3-azabicyclo[3.1.0]hexane (**HyT-S27**) exceeded that of bicyclo[2.2.2]octane (**HyT-S26**); (vii) When the linker adopts a phenyl connected six-membered ring: a) The presence of two nitrogen atoms in the six-membered ring enhanced its effectiveness compared to a counterpart with one nitrogen atom (**HyT-S29** > **HyT-S28**), aligning with the rule for a six-membered ring linker and indicating that the nitrogen atom of piperazine is more favorable for activity than the CH group of piperidine. This phenomenon may be explained by the typical "necessary nitrogen atom" concept[27]; Thus, according to the bioisosteric replacement criteria (positional analog scanning)[28], the application of the

Table 3 Anti-HBV activity and cytotoxicity of compounds **HyT-(S16−S29)**.

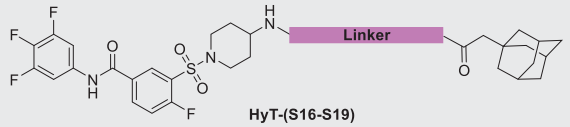

HyT-(S16-S19)

Compd.	Linker	EC_{50}[a] (μmol/L)	CC_{50}[b] (μmol/L)	SI[c]
HyT-S16	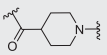	1.10	>60	>54.55
HyT-S17	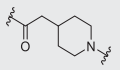	0.65	28.84	44.37
HyT-S18	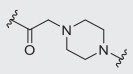	0.57	60.00	105.26
HyT-S19	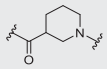	0.27	60.00	222.22
HyT-S20	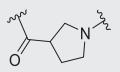	1.38	>60	>43.48
HyT-S21	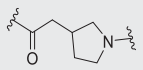	0.56	>60	>107.14
HyT-S22	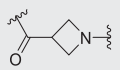	0.44	60.00	136.36
HyT-S23	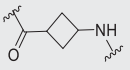	0.20	60.00	300.00
HyT-S24	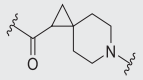	0.48	>60	>125.00
HyT-S25		2.71	>60	>22.14
HyT-S26	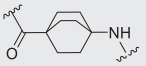	0.56	60.00	107.14
HyT-S27	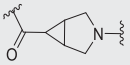	0.45	>60	>133.33
HyT-S28	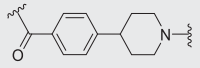	5.34	>60	>11.24
HyT-S29	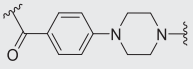	0.93	>60	>64.52
NVR 3-778	—	0.31	10.00	32.26

[a]EC_{50} is the concentration of the test compounds for reduction of HBV DNA by 50% in HepAD38 cells. EC_{50} values were evaluated from HBV DNA by the qPCR assay after 4 days of incubating the cells with the compounds.

[b]CC_{50} is the concentration of the test compounds for reduction of the viability of HepAD38 cells by 50%. CC_{50} values were measured by the CPE method.

[c]Selective index (SI) is the ratio of CC_{50}/EC_{50}.

nitrogen-walk or nitrogen-scan (N-scan) approach will be more beneficial to systematically investigate the influence of the linker on the activity[29−31] and drug-like profiles; b) The introduction of an additional phenyl group led to a significant decrease in activity compared to a six-membered ring linker (**HyT-S28** < **HyT-S16**); c) Substituting methylene with phenyl resulted in reduced activity (**HyT-S28** < **HyT-S17**, **HyT-S29** < **HyT-S18**). Despite the initial design intention of introducing the phenyl group to enhance linker rigidity in compounds **HyT-S28** and **HyT-S29**, their anti-HBV efficacy was notably reduced. It is essential to highlight the substantial decrease in cytotoxicity observed for this series of compounds.

In addition to an assessment of the cellular inhibitory activity, the potency of these compounds for their HBC degradative activity was evaluated in HepAD38 cells. As depicted in Fig. 4, this series comprises eight compounds capable of inducing HBC degradation. Among them, **HyT-S18** and **HyT-S19** exhibit excellent degradation activity at 10 μmol/L (Fig. 4A), with **HyT-S19** demonstrating superior degradation activity compared to **HyT-S18**, consistent with their antiviral activities (**HyT-S19**: EC_{50} = 0.27 μmol/L; **HyT-S18**: EC_{50} = 0.57 μmol/L). Although significantly inhibiting the growth of HepAD38 cells, **HyT-S23** still failed to decrease the level of HBC (Fig. 4B). Thus, increasing the rigidity of the linker does not seem to favor the enhancement of compound degradation activity (Fig. 4C).

The gross SAR indicated that compounds with adamantyl as the hydrophobic ligand and containing a PEG linker may facilitate these HyTs in achieving the potency for HBC degradation. Among them, **HyT-S7** showed the best degradation activity. Subsequently, we further determined its efficacy in another cell line,

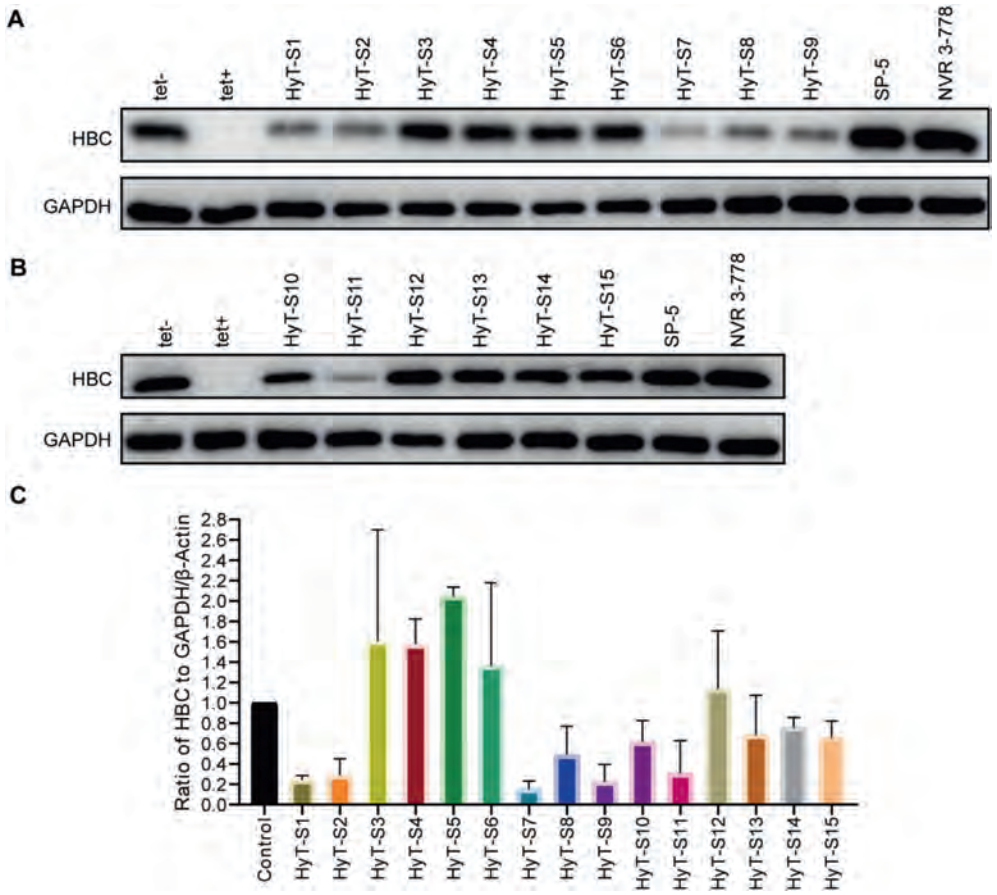

Figure 3 Degradation test for HBC with target compounds **HyT-(S1−S15)**. HepAD38 cells were cultured in the presence of tetracycline (tet+) or in the absence of tetracycline and mock treated (tet−) or treated with **HyT-(S1−S15)** (maximum non-toxic concentration by CPE method, **HyT-S1**: 4 μmol/L; **HyT-(S2−S6)**: 5 μmol/L; **HyT-(S7−S12)**: 6 μmol/L; **HyT-(S13−S14)**: 2 μmol/L; **HyT-S15**: 20 μmol/L; **SP-5** (20 μmol/L) or NVR 3-778 (6 μmol/L) for 72 h. (A, B) HBV core protein (HBC) expression was detected by Western blot assay with a rabbit polyclonal antibody. GAPDH served as the loading control. (C) The quantification results of HBC/GAPDH (or β-actin) ratio from two independent immunoblots are shown.

Hep2.2.15 cells (Supporting Information Table S1, Supporting Information Fig. S1), and tested its effect on other HBV replication intermediates, including intracellular HBV DNA intermediates (Supporting Information Fig. S2A), extracellular HBsAg (Fig. S2B), and HBeAg (Fig. S2C) of HepAD38 cells. The results showed that **HyT-S7** also had a good inhibitory effect on these related indicators. Therefore, compound **HyT-S7** was selected as a representative HBC degrader for further characterization.

*2.3. **HyT-S7** degraded HBC in concentration- and time-dependent manner*

To further evaluate the degradation efficiency of **HyT-S7**, HepAD38 cells were treated with gradient-diluted **HyT-S7**, followed by cell lysis 24 h later and Western blot assay. The results of three independent replicate experiments were selected for quantitative analysis. As depicted in Fig. 5A and B, **HyT-S7** could degrade HBC in a concentration-dependent manner. Based on the quantified results, the half-maximal degradation concentration (DC_{50}) of **HyT-S7** for HBC was calculated to be 3.02 ± 0.54 μmol/L.

Meanwhile, to confirm whether the compound **HyT-S7** induces the degradation of HBC by introducing a hydrophobic group to mimic the misfolded protein state, we designed and synthesized a compound called **SP-O-7 (7f)** lacking hydrophobic groups as a negative control. We evaluated its cellular activity in inhibiting HBV DNA replication (EC_{50} = 4.89 μmol/L) as well as its ability to induce degradation of HBC. Despite exhibiting certain cellular activity, **SP-O-7** (20 μmol/L) was unable to induce degradation of HBC (Fig. 5A and B), thus demonstrating that the degradation activity of **HyT-S7** depends on the introduction of the hydrophobic group. Since **SP-O-7** lacks degradation activity and only exerts an inhibitory effect, its activity in inhibiting HBV DNA replication is more than ten times weaker than that of **HyT-S7**, thereby substantiating that the excellent anti-HBV activity of compound **HyT-S7** originates from its degradation activity.

Furthermore, to evaluate the degradation kinetics of compound **HyT-S7**, we selected different time points to examine the expression levels of HBC in HepAD38 cells after incubation. As shown in Fig. 5C, after 4 h of administration, there was a slight decrease in the expression level of HBC in HepAD38 cells. With prolonged incubation time, the degradation effect became more pronounced, indicating that **HyT-S7** can degrade HBC in HepAD38 cells in a time-dependent manner.

*2.4. **HyT-S7** degraded HBC through the autophagy pathway*

It has been reported that the processing of misfolded proteins may involve the ubiquitin-proteasome pathway, chaperone-mediated

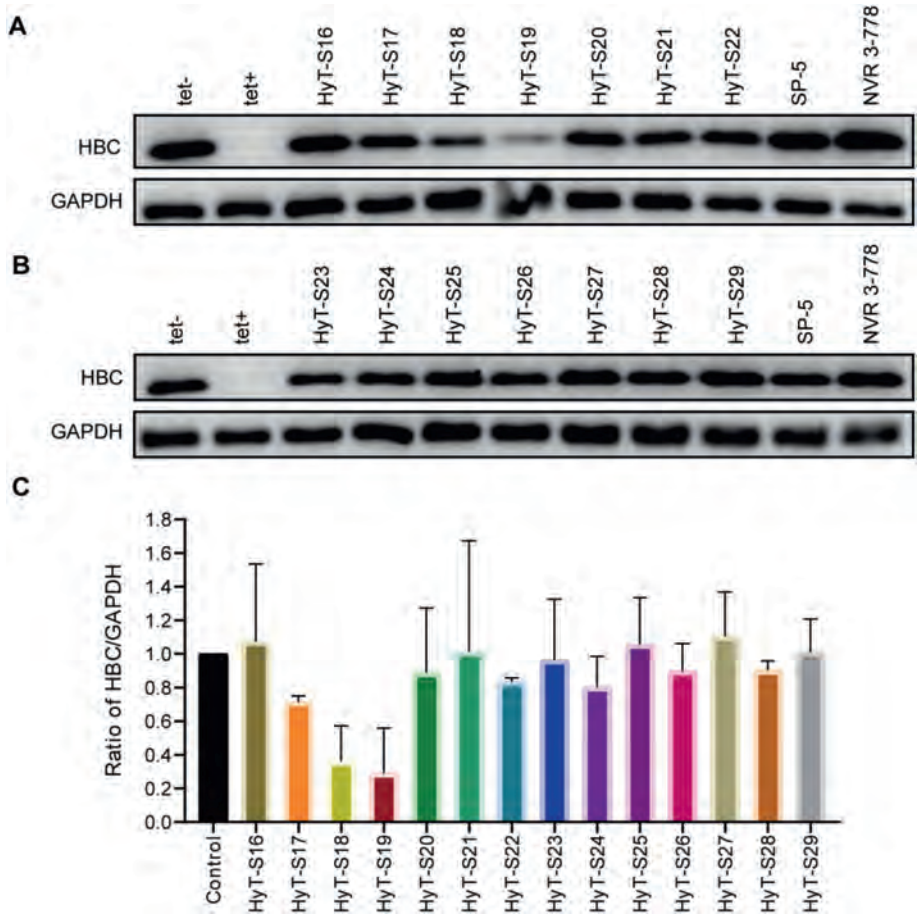

Figure 4 Degradation test for HBC with target compounds **HyT-(S16−S29)**. HepAD38 cells were cultured in the presence of tetracycline (tet+) or in the absence of tetracycline and mock treated (tet−) or treated with **HyT-(S16−S29)** (maximum non-toxic concentration by CPE method, **HyT-S16**: 60 μmol/L; **HyT-S17**: 2 μmol/L; **HyT-S18**: 10 μmol/L; **HyT-S19**: 10 μmol/L; **HyT-S20**: 30 μmol/L; **HyT-S21**: 30 μmol/L; **HyT-S22**: 15 μmol/L; **HyT-S23**: 30 μmol/L; **HyT-S24**: 60 μmol/L; **HyT-S25**: 15 μmol/L; **HyT-S26**: 30 μmol/L; **HyT-S27**: 60 μmol/L; **HyT-S28**: 30 μmol/L; **HyT-S29**: 30 μmol/L; **SP-5** (20 μmol/L) or NVR 3-778 (6 μmol/L) for 72 h. (A, B) HBC expression was detected by Western blot assay. GAPDH served as the loading control. (C) The quantification results of HBC/GAPDH ratio from two independent immunoblots are shown.

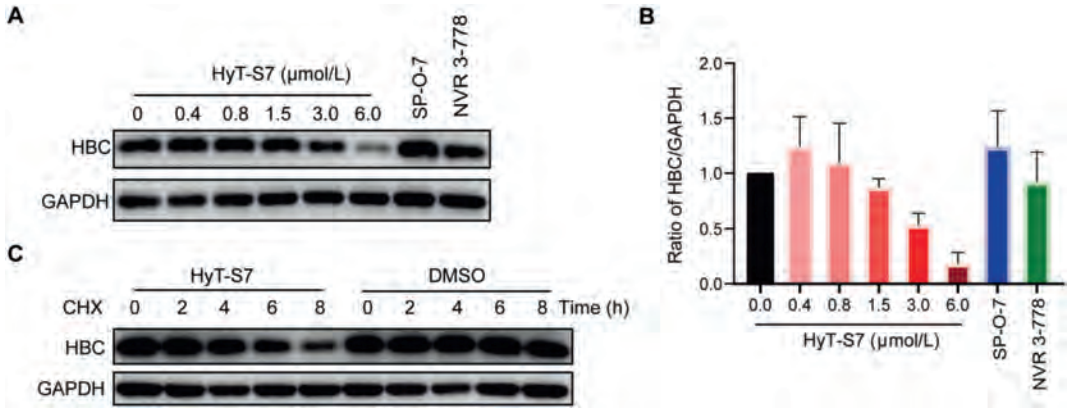

Figure 5 **HyT-S7** degraded HBC in concentration-and time-dependent manner. (A, B) HepAD38 cells cultured in the absence of tetracycline were treated with the indicated concentrations of the compound **HyT-S7**, SP-O-7 (20 μmol/L) or NVR 3-778 (6 μmol/L) for 24 h. HBC expression was detected by Western blot assay. GAPDH served as the loading control. The quantification results of HBC/GAPDH ratio from three independent immunoblots are shown. (C) HepAD38 cells were cultured in tetracycline-free complete medium for 24 h and then incubated with treated with 6 μmol/L **HyT-S7** or DMSO in the presence of 50 μg/mL cycloheximide (CHX) for the indicated time. After washing with pre-chilled PBS, the cells were lysed and HBV core protein levels were determined by Western blot assay.

pathway, and autophagy−lysosome pathway[32]. MG132 and bortezomib can effectively inhibit the activity of the 20S proteasome by targeting threonine residues and effectively block the protein hydrolysis activity of the 26S proteasome complex[33,34], making them widely used proteasome inhibitors for mechanistic studies. The chaperone protein Hsp70 can recognize unfolded or misfolded proteins exposed in hydrophobic regions and mediate polyubiquitination and proteasomal degradation[35]. Compound 17-AAG can induce upregulation of Hsp70 expression[36]and is commonly used to investigate whether the degradation of target compounds is related to Hsp70. 3-Methyladenine (3-MA) inhibits the early stages of autophagosome formation[37], while chloroquine (CQ) prevents the late-stage degradation of autolysosomes by lysosomes[38], thus serving as autophagy inhibitors to explore the influence of the autophagy−lysosome system on target compound degradation. In this study, we systematically investigated whether the degradation of HBC by compound **HyT-S7** is related to the above three pathways.

Firstly, to confirm whether the ubiquitin-proteasome system is involved in the degradation of HBC induced by **HyT-S7**, we investigated the effect of proteasome inhibitors on the degradation efficacy of **HyT-S7**. As shown in Fig. 6A, MG132, and bortezomib failed to reverse the degradation effect of **HyT-S7** on HBC. Subsequently, as illustrated in Fig. 6B, the addition of 17-AAG did not affect the degradation of HBC by **HyT-S7**. These experimental findings suggest that **HyT-S7** does not induce the degradation of HBC through the ubiquitin-proteasome system mediated by Hsp70. Next, we co-treated HepAD38 cells with autophagy inhibitors and **HyT-S7**, and the results were illustrated in Fig. 6C. Both 3-MA and HCQ could reverse the degradation effect of **HyT-S7** on HBC. Additionally, it has been reported that MG132 could act as an autophagy activator[39−41], which can be observed from Fig. 6A that the addition of MG132 promotes the degradation of HBC induced by **HyT-S7**. Furthermore, a data-independent acquisition (DIA)-based proteomic analysis was performed to evaluate differentially expressed proteins on HepAD38 cells

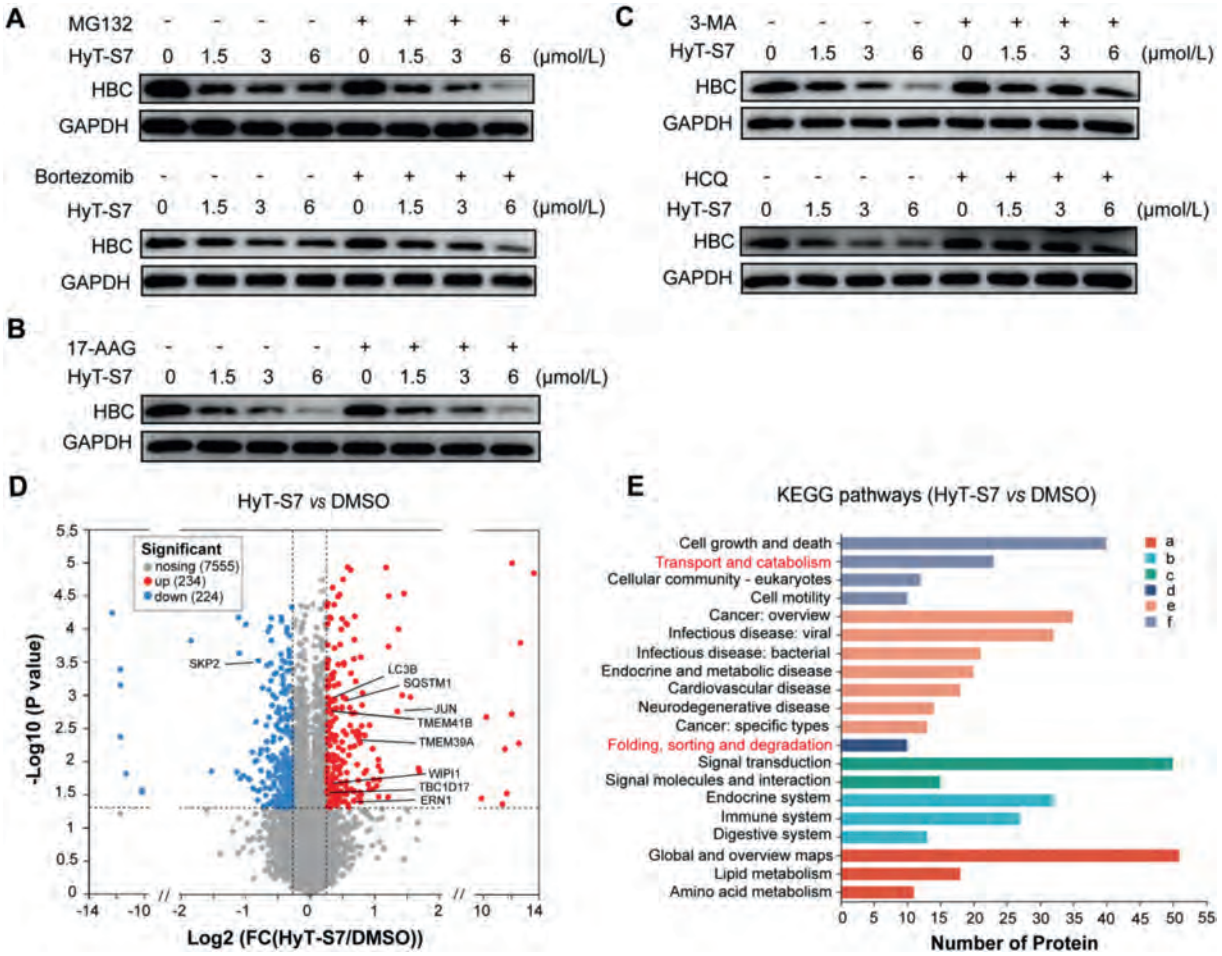

Figure 6 Degradation mechanism analysis of **HyT-S7**. (A) HepAD38 cells cultured in the absence of tetracycline were treated with the indicated concentrations of **HyT-S7** with or without proteasome inhibitor MG132 (5 μmol/L) or bortezomib (0.5 μmol/L); (B) Hsp70 inducer 17-AAG (2 μmol/L); (C) autophagy inhibitor 3-MA (5 mmol/L) or hydroxychloroquine (HCQ) sulfate (50 μmol/L) for 8 h. HBC and GAPDH proteins were detected by Western blot assay. (D, E) The data-independent acquisition (DIA)-based proteomic analysis of HepAD38 cells treated with DMSO or 6 μmol/L **HyT-S7** for 24 h. (D) Volcano plots demonstrating global changes in protein abundance. The x axis displays the relative abundance of all identified proteins (8013) in compound **HyT-S7**-treated cells (log2 FC) *vs*. DMSO-treated cells. The y axis displays *P* values (−log10) from triplicate experiments. (E) Kyoto Encyclopedia of Genes and Genomes (KEGG) pathways analysis of differentially expressed proteins. a: Metabolism; b: Organismal systems; c: Environmental information processing; d: Genetic information processing; e: Human diseases; f: Cellular processes.

treated with **HyT-S7**. In total, 8013 proteins were identified and quantified from our proteomic data. Based on fold-change screening and comparison with the DMSO group, we identified 234 upregulated proteins and 224 downregulated proteins (fold change >1.2 or <0.83, $P < 0.05$) after **HyT-S7** treatment. We did observe a significant increase or decrease in proteins involved in the autophagy pathway, such as JUN, SQSTM1 (p62), LC3B, WIPI1, TBC1D17, ERN1, TMEM39A, TMEM41B and SKP2 (Fig. 6D). Moreover, the KEGG pathways analysis showed that there are 33 proteins related to transport, catabolism, fording, sorting and degradation underwent significant systemic changes in the presence of **HyT-S7** (Fig. 6E). Collectively, these results indicate that **HyT-S7** can induce the degradation of HBC through the autophagy pathway.

2.5. *HyT-S7 exhibited remarkable degradation activity against 11 CpAMs-resistant mutant HBC*

As mentioned earlier, mutations accumulated within the binding pocket of CpAMs can easily lead to resistance, and many mutations can result in cross-resistance, whereby sensitivity to CpAMs of different structural types decreases[16]. Protein degraders, due to their "event-driven" mechanism of action, do not rely on potent interactions with the target protein, providing an effective solution to overcome resistance caused by amino acid residue mutations in the binding site. Therefore, we utilized Western blot assays to test the degradation activity of compound **HyT-S7** and its controls (with non-toxic concentration, Supporting Information Fig. S3) in HepG2 cells against 11 common CpAMs-resistant mutant proteins (P25A, P25G, D29L, D29W, T33N, I105F, I105W, I105Y, T109A, V124W, and V124F).

In this experiment, in addition to the lead compound NVR 3-778, we also included the clinically used nucleoside analog anti-HBV drug 3TC and the class I CpAM Bay 41-4109 as control drugs. It is noteworthy that Bay 41-4109 can induce the misassembly of core proteins into non-capsid structures followed by cellular degradation[18]. This property can be utilized to assess better whether **HyT-S7** possesses an advantage in degrading mutant HBC. As depicted in Fig. 7, neither NVR 3-778 nor 3TC showed any degradation effect on either wild-type or 11 mutant types of HBC. In the wild-type, Bay 41-4109 could completely degrade HBC in HepG2 cells, and **HyT-S7** also demonstrated excellent degradation capability. However, the degradation activity of Bay 41-4109 against mutant strains was significantly reduced (P25G, D29L, T33N, T109A, V124W, V124F) or even lost (P25A, D29W, I105F, I105Y, I105W) (Supporting Information Fig. S4). In contrast, **HyT-S7** maintained good degradation efficiency against all 11 mutant HBC in a dose-dependent manner (Fig. S4, Supporting Information Fig. S5), particularly for the highly resistant strains P25G and T33N to a Phase III CpAM GLS4. These results indicate that **HyT-S7** can effectively induce the degradation of both HBC and its drug-resistant mutants. Therefore, the application of HyT technology to HBV CpAMs holds promise for addressing potential drug resistance issues.

2.6. *Compound **HyT-S7** binds to HBC*

To confirm that the target of compound **HyT-S7** is HBC, we sequentially conducted cellular thermal shift assay (CETSA) and surface plasmon resonance (SPR) assay, with NVR 3-778, SP-5, and SP-O-7 as controls.

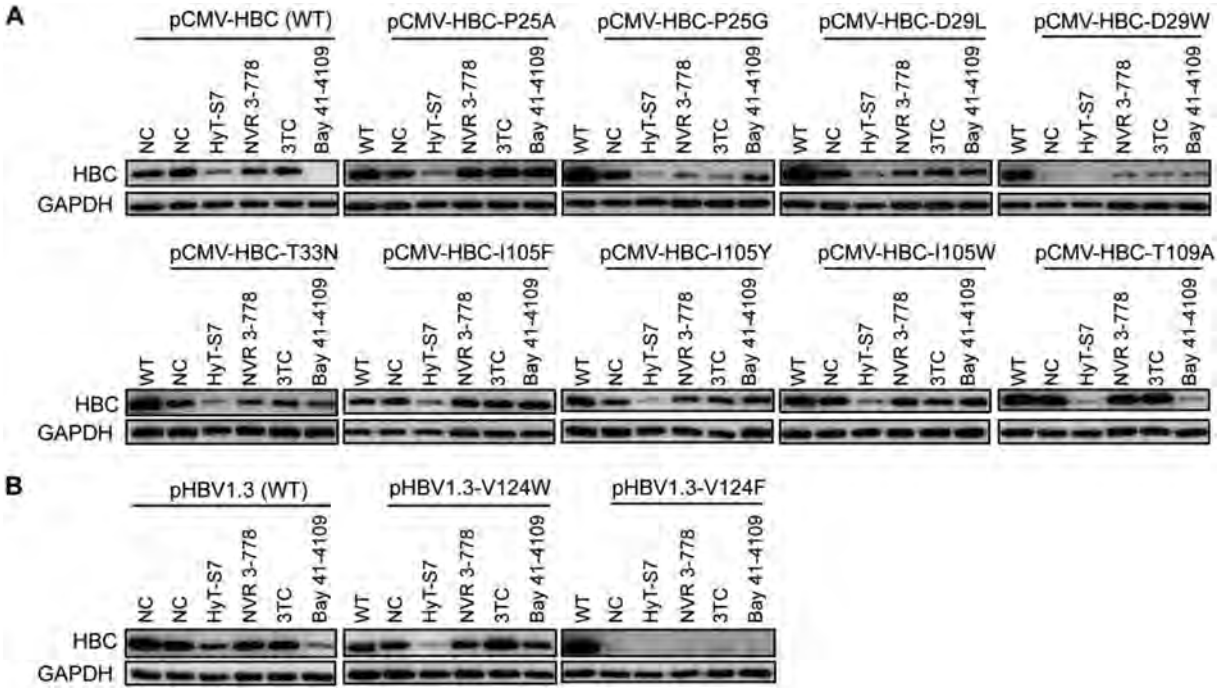

Figure 7 Degradation test for HBC with amino acid mutations reported in CpAMs resistance. HepG2 cells transfected with pCMV-HBC or pCMV-HBC-derived plasmids expressing core protein with indicated charged amino acid mutation (A), or transfected with pHBV1.3, pHBV1.3-V124F, or pHBV1.3-V124W (B). 6 h post transfection, the culture media were replaced with fresh media (NC) or media containing **HyT-S7** (6 μmol/L), NVR 3-778 (3 μmol/L), 3 TC (1 μmol/L) or Bay 41-4109 (1 μmol/L) and cultured for additional 18 h. Intracellular HBV core protein were examined with the Western blot assay. GAPDH served as the loading control.

Firstly, CETSA was conducted in HepAD38 cells to validate whether compound **HyT-S7** can bind to HBC in cells. As shown in Fig. 8A and B, upon elevating HBC the temperature beyond 57 °C, a significant increase in HBC expression level was observed in the **HyT-S7**-treated group compared to the control group (DMSO), accompanied by a remarkable rightward shift of the CETSA melting curve with ΔTm value of 5.4 °C. Since the thermodynamic stability of the protein is enhanced after binding with the compound, it can be demonstrated that compound **HyT-S7** can bind to HBC in the cells.

Next, an SPR assay was performed to test the interaction between compound **HyT-S7** and HBC at different concentrations, along with control compounds NVR 3-778, SP-5, and SP-O-7. As shown in Fig. 8C—F, the K_D value of **HyT-S7** was determined to be 0.78 μmol/L, indicating a potent binding affinity with HBC, far superior to the control compounds. Notably, compared with NVR 3-778, **HyT-S7** exhibited a similar K_{on} value but a much lower K_{off} value (Supporting Information Table S2), indicating that the presence of the hydrophobic tag of adamantyl induced a robust interaction between the HBC and **HyT-S7** and enhanced the stability of the complex. Conversely, the binding kinetics of NVR 3-778 and SP-5 with HBC reveal both fast association and dissociation rates, suggesting a weaker interaction between HBC and these two compounds. In general, these results demonstrate that the introduction of adamantyl (hydrophobic moiety) not only enables **HyT-S7** to induce the degradation of HBC but also

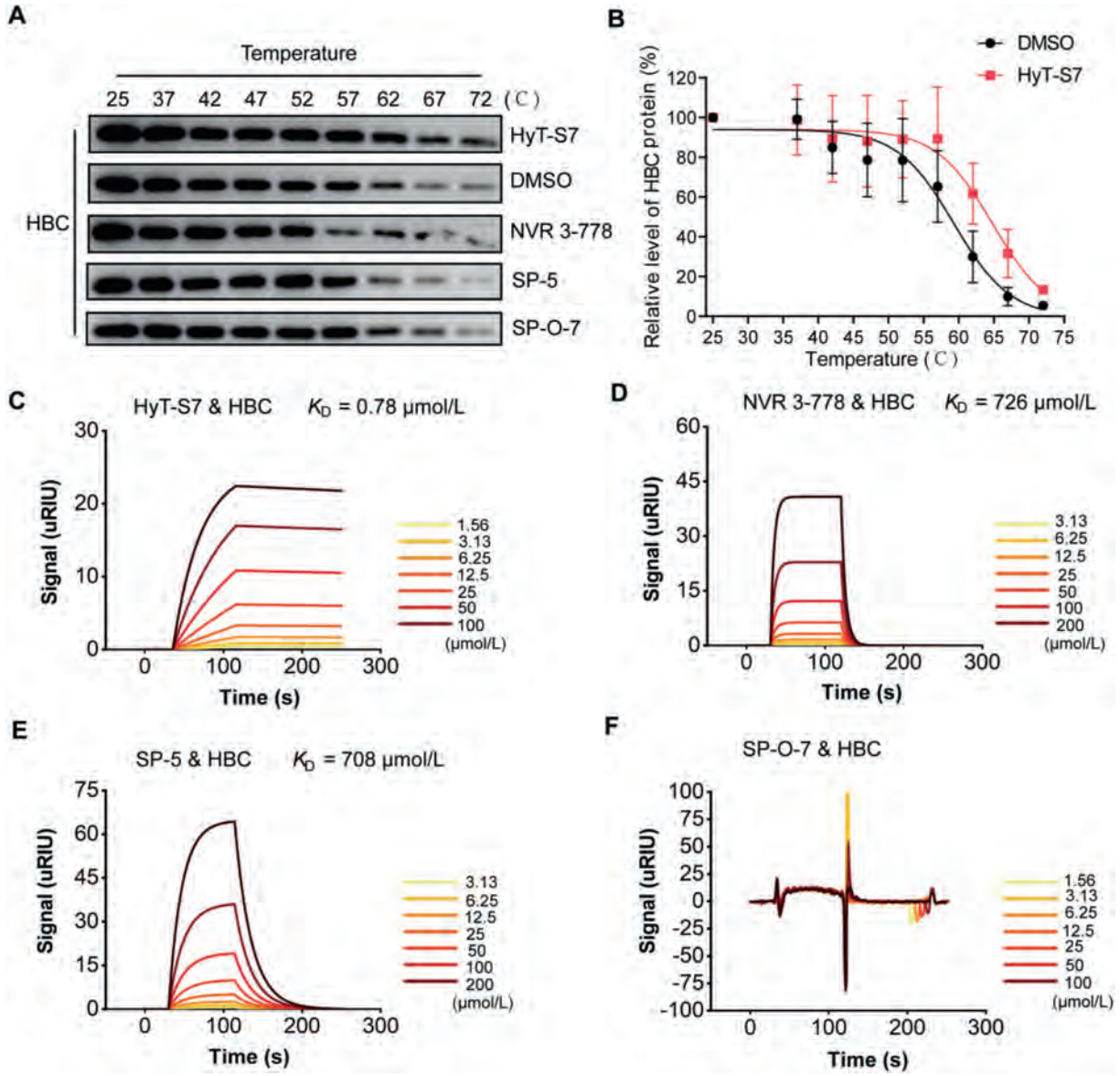

Figure 8 Compound **HyT-S7** binds to HBC. (A, B) Cellular thermal shift assay (CETSA). Incubate the cell lysate from HepAD38 cells cultured in complete culture medium without tetracycline for 96 h with DMSO, **HyT-S7** (6 μmol/L), NVR 3-778 (6 μmol/L), SP-5 (20 μmol/L), or SP-O-7 (20 μmol/L) for 30 min at room temperature. Then the mixtures were heated on a gradient from 37 to 72 °C for 3 min. The supernatant was collected and loaded onto a 10% SDS-PAGE gel. The levels of HBC were detected by Western blot assay. The quantitative results of HBC of group DMSO and **HyT-S7** are shown. Data are shown as mean ± SD from three independent experiments. (C—F) The interactions between HBC protein, and the compound **HyT-S7**, NVR 3-778, SP-5, or SP-O-7 were analyzed by a SPR assay performed on a CM5 chip integrated in the Reichert4 SPR system.

enhances the affinity of the SBA scaffold for HBC. Therefore, CETSA, SPR, and previous degradation studies collectively demonstrate that compound **HyT-S7** can target and degrade HBC.

2.7. Molecular docking and molecular dynamics simulation of HyT-S7

In order to comprehend the interaction between the target compounds and HBC, we conducted molecular docking simulations for the optimal compound, **HyT-S7**, using Schrödinger software, and the resulting binding mode was visualized by PyMOL. Our docking analysis relied on the co-crystal structure of NVR 3-778 and HBC (PDB: 5T2P). The results revealed a good overlap between **HyT-S7** and NVR 3-778 within the identical pocket of HBC, as illustrated in Fig. 9A. The 3,4,5-trifluorophenyl group of **HyT-S7** and NVR 3-778 was situated within the large hydrophobic pocket defined by residues Pro25, Leu30, Thr33, and Trp102. Hydrogen bonds were observed between the amide oxygen of **HyT-S7** and the side chains of both Trp102 and Ser106. Additionally, the amide nitrogen of **HyT-S7** formed hydrogen bonds with the side chain of Thr128 from the adjacent capsid dimer, which is crucial for its inhibitory activity. Furthermore, the phenyl group of **HyT-S7** engaged in a $\pi-\pi$ stacking interaction with Tyr118, while the oxygen atom and amino hydrogen atom of the linker act as hydrogen bond acceptor and donor, respectively, forming dual hydrogen bonds with Ile139 (Fig. 9B), which may facilitate the attachment of hydrophobic groups onto the surface of the protein.

To obtain a more comprehensive understanding of the favored binding mode of **HyT-S7** in the binding pocket, we conducted molecular dynamics (MD) simulations on the complex of **HyT-S7** with HBC (PDB code: 5T2P) using the Desmond module within the Schrodinger suite, spanning a duration of 250 ns. As depicted in Fig. 9C, the average root-mean-square deviation (RMSD) of the protein-**HyT-S7** complex exhibited oscillations around 4.0 Å throughout the 250 ns simulation period, which suggested that **HyT-S7** was stable in several conformers relative to the initial docked structure. Fig. 9D and E depict the protein-ligand contacts between **HyT-S7** and HBC, highlighting the detailed interactions involving specific residues, including hydrogen bonds, hydrophobic contacts, and water bridges. Of particular note, the interactions fraction plot suggests that certain interactions persist consistently throughout a percentage of the 250 ns simulations, while multiple contacts between individual residues and the ligand may result in an interaction fraction exceeding 1.0 (Fig. 9D). Furthermore, in Fig. 9E visualizes

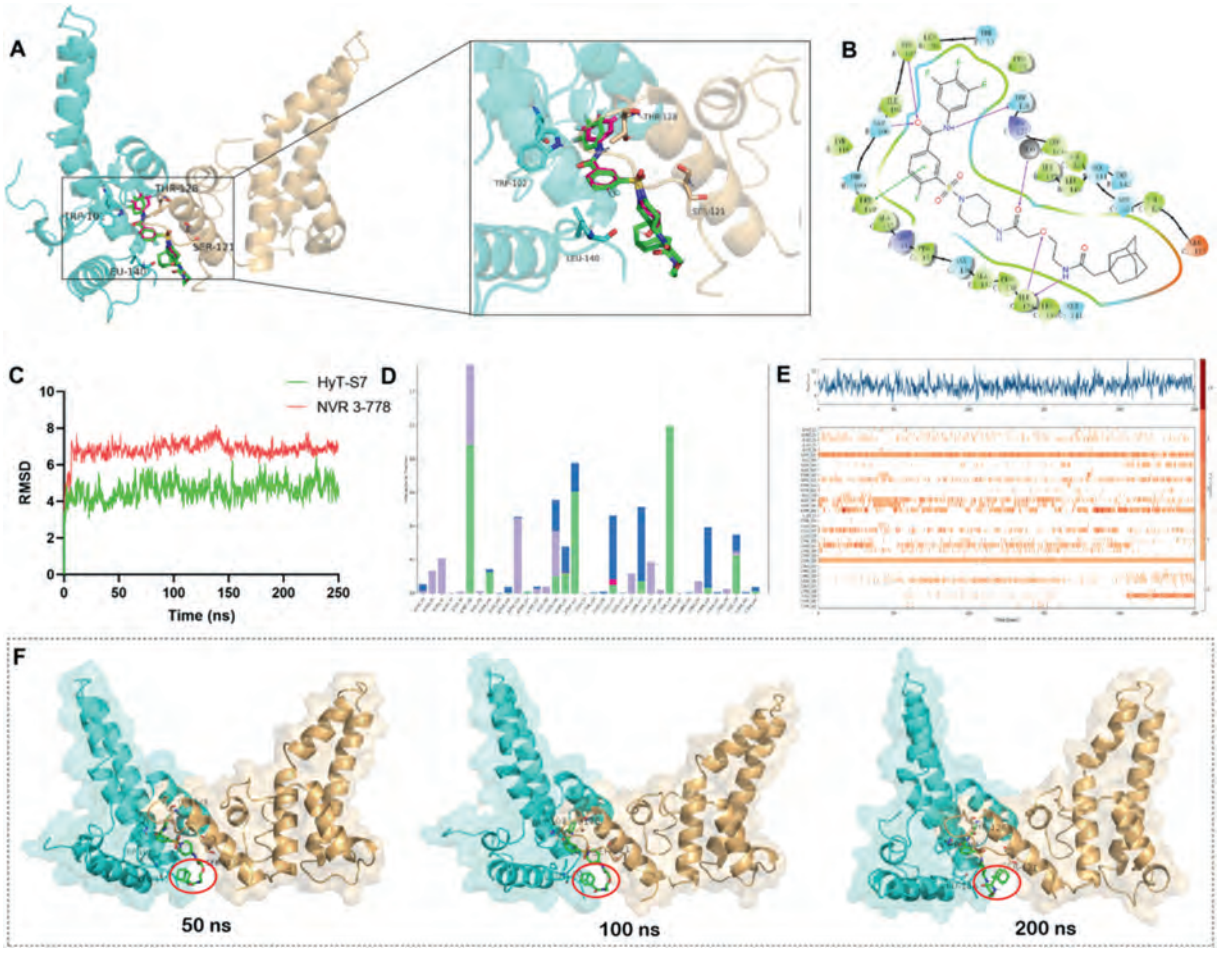

Figure 9 Molecular docking and molecular dynamics simulation of **HyT-S7**. (A) Cartoon mode of interactions between **HyT-S7** and HBC; (B) Two-dimensional diagram of interactions between **HyT-S7** and HBC; (C) Protein RMSD plots of the MD simulations of HBC in complex with **HyT-S7** (green line) and NVR 3-778 (red line); (D) Number of protein-ligand contacts in each trajectory frame for **HyT-S7** with HBC; (E) Interactions fraction plots of **HyT-S7** with specific amino acid residues of HBC, green: H-bonds, purple: Hydrophobic, red: ionic, blue: water bridges; (F) Different frames of docking modes of HBC in complex with **HyT-S7** in 250 ns simulations. The figures were generated by PyMOL (www.pymol.org).

the count of contact forces between **HyT-S7** and HBC in each trajectory frame, alongside the specific residue codes involved in ligand interaction, with darker shades of orange indicating more robust interactions. The enduring presence of characteristic hydrogen bonds with Thr128 and Trp102 remained with **HyT-S7** throughout the simulation, underscoring the significance of these interactions in maintaining complex stability. Examining different frames in Fig. 9F from the MD simulations indicated that the adamantyl group (red line) could always extend on the surface of the protein, which may facilitate **HyT-S7** to mimic the protein misfold state to achieve HBC degradation. These observations elucidate the underlying structural factor to facilitate the HBC degradation induced by **HyT-S7** and provide a theoretical foundation for the subsequent phase of rational structure optimization.

3. Conclusions

Herein, the degradation of HBV core protein with SBA-based small-molecule degraders was revealed as the first example of hydrophobically tagged degraders targeting viral proteins. In this work, compound **HyT-S7** with adamantyl group exhibited potent anti-HBV activity (EC_{50} = 0.46 μmol/L, HepAD38 cells) and degradation activity for HBC, being selected as a representative compound for further mechanistic investigation.

Firstly, **HyT-S7** had been demonstrated to degrade HBC in a dose- and time-dependent manner (DC_{50} = 3.02 ± 0.54 μmol/L), and the degradation activity of **HyT-S7** depends on the introduction of the hydrophobic group. To investigate the mechanisms of action of **HyT-S7**, we systematically conducted a series of Western blot assays related to the ubiquitin-proteasome pathway, chaperone-mediated pathway, and autophagy−lysosome pathway, as well as DIA-based proteomic analysis, and found that autophagy−lysosome pathway was a potential driver of **HyT-S7**-induced HBC degradation. Notably, **HyT-S7** showed excellent degradation efficiency against 11 CpAMs-resistant mutant HBC (P25A, P25G, D29L, D29W, T33N, I105F, I105W, I105Y, T109A, V124W, and V124F) with a concentration-dependent manner, particularly for the highly resistant strains P25G and T33N to Phase III CpAM GLS4, which represents a promising approach to address potential drug resistance issues of HBV CpAMs. Furthermore, CETSA and SPR assay collectively demonstrated that compound **HyT-S7** could directly bind to HBC. Finally, molecular docking and molecular dynamics simulation results elucidated the key interactions between **HyT-S7** and HBC, as well as the underlying structural factor that facilitates HBC degradation.

In conclusion, this work successfully applied HyT to HBV core protein for the first time and elucidated the mechanism of action of the representative compound as well as its advantage in overcoming drug resistance, providing a valuable reference for addressing resistance issues associated with other antiviral medications.

4. Experimental

4.1. Chemistry

All new compound's melting points (mp) were determined using a micro melting point apparatus (RY-1G, Tianjin Skylight). ^{1}H NMR and ^{13}C NMR spectra were obtained in DMSO-d_6 on Bruker AV-400 or Bruker AV-600 MHz spectrometer using tetramethylsilane (TMS) as the internal reference. Chemical shifts were reported in δ values (ppm), and J values were expressed in hertz (Hz). Thin layer chromatography (TLC) was performed to monitor reactions or purify products on Silica Gel GF254 and HUANGHAI_HSGF254, 0.15−0.2 mm (Merck), respectively. Spots were visualized with iodine vapor or by irradiation with UV light (λ = 254 or 365 nm). Mass spectra (MS) were carried out on an LC Autosampler Device: Standard G1313A instrument (TSQ Vantage LC−MS/MS, ThermoFisher). Flash column chromatography was performed on a column packed with Silica Gel60 (200−300 mesh, Shanghai Haohong Scientific Co., Ltd.). Solvents were of reagent grade and, if needed, were purified and dried by standard methods. Rotary evaporators were involved in the concentration of the reaction solutions under reduced pressure. The solvents DCM, acetonitrile, methanol, etc., were obtained from Sinopharm Chemical Reagent Co., Ltd. (SCRC) and were of AR grade. The key reactants, including 3-chlorosulfonyl-4-fluorobenzoic acid (Cat No.1109322, Leyan, Shanghai, China), 3,4,5-trifluoroaniline (Cat No.1023036, Leyan, Shanghai, China), 4-Boc-aminopiperidine (Cat 1041132, Leyan, Shanghai, China), etc. were purchased from Shanghai Haohong Scientific Co., Ltd. The purity of target compounds was evaluated using a Shimadzu HPLC system (Shimadzu SPD-20A/20AV). HPLC conditions were as follows: Agilent ZORBAX, SB-C18 column (250 mm × 4.6 mm × 5 μm); isocratic elution method: mobile phase A: methanol (80%); mobile phase B: water (20%); flow rate: 1.0 mL/min; wavelength: 254.4 or 250.4 nm, temperature: 30 °C, injection volume: 10 μL. All tested target compounds possessed purities of >95%.

*4.1.1. tert-Butyl (1-((2-fluoro-5-((3,4,5-trifluorophenyl) carbamoyl)phenyl)sulfonyl)piperidin-4-yl)carbamate (**4**)*

A solution of 3-(chlorosulfonyl)-4-fluorobenzoic acid (**1**, 1.0 equiv.) in toluene (30 mL) at ambient temperature was successively added to thionyl chloride (6.0 equiv.) and DMF (1 mL), and the resulting yellowish solution was heated to 120 °C for 4 h (monitored by TLC), giving a slurry. The solvent was removed *in vacuo* by coevaporation with toluene, providing 3-(chlorosulfonyl)-4-fluorobenzoyl chloride (**2**) as a brown oil, which was used in the next step without purification. Intermediate **2** (1.0 equiv.) was dissolved in toluene (30 mL), and then a solution of 3,4,5-trifluoroaniline (1.0 equiv.) in toluene (3 mL) was added dropwise over 10 min. The mixture was heated to 120 °C for 2 h (monitored by TLC). The reaction was cooled to room temperature and filtered, and the obtained cake was washed with a small amount of toluene, resulting in 2-fluoro-5-((3,4,5-trifluorophenyl) carbamoyl) benzenesulfonyl chloride (**3**), which was applied to the next step without further purification. Under an ice bath, the 4-Boc-aminopiperidine (1.0 equiv.), TEA (2.0 equiv.), and intermediate **3** (1.2 equiv.) were successively dissolved in DCM (20 mL). The resulting mixture was then stirred at room temperature (monitored by TLC). Then, the reaction mixture was filtered under reduced pressure, and the filter cake was washed with DCM. Finally, intermediate **4** was obtained after drying the filter cake. White solid, yield: 80%. ^{1}H NMR (400 MHz, DMSO-d_6) δ 10.82 (s, 1H), 8.34 (t, J = 6.3 Hz, 2H), 7.72 (dt, J = 14.0, 7.2 Hz, 3H), 6.88 (d, J = 6.6 Hz, 1H), 3.60 (d, J = 12.1 Hz, 2H), 3.42−3.34 (m, 1H), 2.78 (t, J = 11.3 Hz, 2H), 1.79 (d, J = 11.3 Hz, 2H), 1.40 (d, J = 9.4 Hz, 2H), 1.36 (s, 9H). ESI-MS: m/z 530.43 $[M-H]^-$, $C_{23}H_{25}F_4N_3O_5S$ [531.15].

*4.1.2. 3-((4-Aminopiperidin-1-yl)sulfonyl)-4-fluoro-N-(3,4,5-trifluorophenyl)benzamide (**5**)*

Under an ice bath, TFA was added dropwise to intermediate **4** in 30 mL of DCM (monitored by TLC). Then, the resulting mixture

solution was alkalized to pH∼7 with a saturated sodium bicarbonate solution and then extracted with DCM (40 mL). Then, the combined organic layer was washed with saturated sodium bicarbonate (3 × 20 mL), dried over anhydrous Na_2SO_4, filtered, and concentrated under reduced pressure to afford the intermediate **5**. White solid, yield: 83%. ^{1}H NMR (400 MHz, DMSO-d_6) δ 10.84 (s, 1H), 8.34 (dd, J = 9.7, 3.8 Hz, 2H), 7.72 (td, J = 10.5, 9.6, 6.1 Hz, 3H), 3.74 (d, J = 12.6 Hz, 2H), 3.19−3.07 (m, 1H), 2.75 (t, J = 11.8 Hz, 2H), 1.99−1.92 (m, 2H), 1.51 (qd, J = 12.1, 3.5 Hz, 2H). ESI-MS: m/z 432.84 $[M+H]^+$, $C_{18}H_{17}F_4N_3O_3S$ [431.09].

*4.1.3. 3-((4-(2-((1S,3S)-Adamantan-1-yl)acetamido)piperidin-1-yl)sulfonyl)-4-fluoro-N-(3,4,5-trifluorophenyl)benzamide (**HyT-S1**)*

1-Adamantaneacetic acid (1.2 equiv.) and HATU (1.5 equiv.) were mixed in 30 mL of DCM and stirred in an ice bath for 30 min. Subsequently, DIEA (2.0 equiv.) and intermediate **5** (1.0 equiv.) were added to the mixture and then stirred at room temperature (monitored by TLC). The resulting mixture was evaporated under reduced pressure, and the residue was initially washed with 1 mol/L HCl and extracted with ethyl acetate (3 × 20 mL). Then, the combined organic layer was washed with saturated sodium bicarbonate (3 × 20 mL), dried over anhydrous Na_2SO_4, filtered, and concentrated under reduced pressure to afford the corresponding crude product, which was purified by flash column chromatography (ethyl acetate) to afford the target compound **HyT-S1**. White solid, yield: 73%. Mp: >200 °C. ^{1}H NMR (400 MHz, DMSO-d_6) δ 10.77 (s, 1H, NH), 8.38−8.34 (m, 1H, NH), 8.34−8.29 (m, 1H, Ph-H), 7.75−7.67 (m, 3H, Ph-H), 7.64 (d, J = 7.5 Hz, 1H, Ph-H), 3.72−3.62 (m, 1H, Ph-H), 3.59 (d, J = 12.4 Hz, 2H), 2.84 (t, J = 11.0 Hz, 2H), 1.89 (s, 3H), 1.83−1.78 (m, 2H), 1.78 (s, 2H), 1.67−1.50 (m, 12H), 1.45−1.34 (m, 2H). ^{13}C NMR (150 MHz, DMSO-d_6) δ 169.69, 164.00, 160.67 (d, J = 259.7 Hz), 150.48 (d, J = 253.4 Hz), 135.72 (d, J = 9.8 Hz), 131.34 (d, J = 3.2 Hz), 130.85, 126.08 (d, J = 15.2 Hz), 118.55 (d, J = 22.9 Hz), 105.39 (dd, J = 25.5, 5.4 Hz), 105.33, 105.30, 50.37, 44.79, 44.66, 42.59, 36.94, 32.65, 31.41, 28.53. HRMS (ESI): m/z Calcd. for $C_{30}H_{33}F_4N_3O_4NaS$ $[M+Na]^+$ 630.2026; found 630.2024. HPLC purity: 96.3%.

*4.1.4. General procedure for the synthesis of **6(a−h)***

Boc-protected amine-terminated linkers (1.2 equiv.) and HATU (1.5 equiv.) were mixed in 30 mL of DCM and stirred in an ice bath for 30 min. Subsequently, DIEA (2.0 equiv.) and intermediate **5** (1.0 equiv.) were added to the mixture and then stirred at room temperature (monitored by TLC). The resulting mixture was evaporated under reduced pressure, and the residue was initially washed with 1 mol/L HCl and extracted with ethyl acetate (3 × 20 mL). Then, the combined organic layer was washed with saturated sodium bicarbonate (3 × 20 mL), dried over anhydrous Na_2SO_4, filtered, and concentrated under reduced pressure to afford the corresponding crude product, which was purified by flash column chromatography (ethyl acetate) to afford the intermediates **6(a−h)**.

*4.1.4.1. tert-Butyl (4-((1-((2-fluoro-5-((3,4,5-trifluorophenyl) carbamoyl)phenyl)sulfonyl)piperidin-4-yl)amino)-4-oxobutyl) carbamate (**6a**).* White solid, yield: 76%. ^{1}H NMR (400 MHz, DMSO-d_6) δ 10.78 (s, 1H), 8.39−8.28 (m, 2H), 7.73 (dt, J = 17.0, 8.5 Hz, 4H), 6.74 (s, 1H), 3.73−3.54 (m, 3H), 2.94−2.76 (m, 4H), 2.00 (t, J = 7.1 Hz, 2H), 1.80 (d, J = 12.2 Hz, 2H), 1.54 (dd, J = 13.5, 6.6 Hz, 2H), 1.41 (d, J = 14.3 Hz, 2H), 1.36 (s, 9H). ESI-MS: m/z 639.11 $[M+Na]^+$, 615.11 $[M-H]^-$. $C_{27}H_{32}F_4N_4O_6S$ [616.20].

*4.1.4.2. tert-Butyl (5-((1-((2-fluoro-5-((3,4,5-trifluorophenyl) carbamoyl)phenyl)sulfonyl)piperidin-4-yl)amino)-5-oxopentyl) carbamate (**6b**).* White solid, yield: 80%. ^{1}H NMR (400 MHz, DMSO-d_6) δ 10.81 (s, 1H), 8.34 (dd, J = 12.2, 6.8 Hz, 2H), 7.76 (dd, J = 18.3, 7.4 Hz, 4H), 6.79 (s, 1H), 3.73−3.53 (m, 3H), 2.92−2.83 (m, 4H), 2.01 (t, J = 7.2 Hz, 2H), 1.85−1.73 (m, 2H), 1.50−1.41 (m, 4H), 1.36 (s, 9H), 1.32−1.27 (m, 2H). ESI-MS: m/z 652.82 $[M+Na]^+$, 629.02 $[M-H]^-$. $C_{28}H_{34}F_4N_4O_6S$ [630.21].

*4.1.4.3. tert-Butyl (6-((1-((2-fluoro-5-((3,4,5-trifluorophenyl) carbamoyl)phenyl)sulfonyl)piperidin-4-yl)amino)-6-oxohexyl) carbamate (**6c**).* White solid, yield: 77%. ^{1}H NMR (400 MHz, DMSO-d_6) δ 10.78 (s, 1H), 8.40−8.27 (m, 2H), 7.80−7.65 (m, 4H), 6.72 (s, 1H), 3.64 (dd, J = 25.8, 10.9 Hz, 3H), 2.84 (dq, J = 21.0, 11.2, 8.8 Hz, 4H), 2.00 (t, J = 7.2 Hz, 2H), 1.79 (d, J = 10.4 Hz, 2H), 1.44 (dt, J = 19.5, 9.6 Hz, 4H), 1.36 (s, 9H), 1.32 (d, J = 7.3 Hz, 2H), 1.17 (dt, J = 14.3, 7.3 Hz, 2H). ESI-MS: m/z 666.94 $[M+Na]^+$, 643.23 $[M-H]^-$. $C_{29}H_{36}F_4N_4O_6S$ [644.23].

*4.1.4.4. tert-Butyl (7-((1-((2-fluoro-5-((3,4,5-trifluorophenyl) carbamoyl)phenyl)sulfonyl)piperidin-4-yl)amino)-7-oxoheptyl) carbamate (**6d**).* White solid, yield: 75%. ^{1}H NMR (400 MHz, DMSO-d_6) δ 11.23 (s, 1H), 8.41−8.28 (m, 2H), 7.93−7.78 (m, 3H), 7.74−7.64 (m, 1H), 6.78 (s, 1H), 3.69−3.57 (m, 5H), 3.08 (dd, J = 12.1, 5.9 Hz, 2H), 2.76−2.68 (m, 2H), 2.06−1.94 (m, 2H), 1.78 (d, J = 10.4 Hz, 2H), 1.36 (s, 9H), 1.29 (dd, J = 5.8, 3.0 Hz, 6H), 1.21−1.17 (m, 2H). ESI-MS: m/z 680.87 $[M+Na]^+$, 657.06 $[M-H]^-$. $C_{30}H_{38}F_4N_4O_6S$ [658.24].

*4.1.4.5. tert-Butyl (8-((1-((2-fluoro-5-((3,4,5-trifluorophenyl) carbamoyl)phenyl)sulfonyl)piperidin-4-yl)amino)-8-oxooctyl) carbamate (**6e**).* White solid, yield: 69%. ^{1}H NMR (400 MHz, DMSO-d_6) δ 10.79 (s, 1H), 8.40−8.28 (m, 2H), 7.73 (q, J = 9.4, 8.1 Hz, 4H), 6.73 (s, 1H), 3.73−3.54 (m, 3H), 2.94−2.75 (m, 4H), 2.01 (t, J = 7.0 Hz, 2H), 1.80 (d, J = 11.5 Hz, 2H), 1.50−1.39 (m, 4H), 1.37 (s, 9H), 1.35−1.29 (m, 2H), 1.24−1.15 (m, 6H). ESI-MS: m/z 695.07 $[M+H]^+$, 671.61 $[M-H]^-$. $C_{31}H_{40}F_4N_4O_6S$ [672.26].

*4.1.4.6. tert-Butyl (2-(2-((1-((2-fluoro-5-((3,4,5-trifluorophenyl) carbamoyl)phenyl)sulfonyl)piperidin-4-yl)amino)-2-oxoethoxy) ethyl)carbamate (**6f**).* White solid, yield: 78%. ^{1}H NMR (400 MHz, DMSO-d_6) δ 10.80 (s, 1H), 8.38−8.28 (m, 2H), 7.77−7.62 (m, 4H), 6.93 (t, J = 5.4 Hz, 1H), 3.81 (s, 2H), 3.79−3.65 (m, 3H), 3.39 (t, J = 5.4 Hz, 2H), 3.11 (q, J = 5.4 Hz, 2H), 2.75 (t, J = 11.8 Hz, 2H), 1.79 (d, J = 10.4 Hz, 2H), 1.53 (qd, J = 12.5, 3.9 Hz, 2H), 1.38 (s, 9H). ESI-MS: m/z 654.80 $[M+Na]^+$, 631.04 $[M-H]^-$. $C_{27}H_{32}F_4N_4O_7S$ [632.19].

*4.1.4.7. tert-Butyl (2-(2-(2-(((1-((2-fluoro-5-((3,4,5-trifluorophenyl)carbamoyl)phenyl)sulfonyl)piperidin-4-yl)amino)-2-oxoethoxy)ethoxy)ethyl)carbamate (**6g**).* White solid, yield: 71%. ^{1}H NMR (400 MHz, DMSO-d_6) δ 10.80 (s, 1H), 8.39−8.28 (m, 2H), 7.76−7.67 (m, 3H), 7.64 (d, J = 7.9 Hz, 1H), 6.79 (t,

J = 5.5 Hz, 1H), 3.84 (s, 2H), 3.77−3.62 (m, 3H), 3.58−3.49 (m, 4H), 3.37 (t, J = 6.1 Hz, 2H), 3.06 (q, J = 5.9 Hz, 2H), 2.76 (t, J = 11.6 Hz, 2H), 1.79 (d, J = 10.6 Hz, 2H), 1.52 (td, J = 13.1, 11.2, 6.4 Hz, 2H), 1.37 (s, 9H). ESI-MS: *m/z* 698.81 $[M+Na]^+$, 675.06 $[M-H]^-$. $C_{29}H_{36}F_4N_4O_8S$ [676.22].

*4.1.4.8. tert-Butyl (2-(2-(2-(2-(((1-((2-fluoro-5-((3,4,5-trifluorophenyl)carbamoyl)phenyl)sulfonyl)piperidin-4-yl)amino)-2-oxoethoxy)ethoxy)ethoxy)ethyl)carbamate (**6h**).* White solid, yield: 70%. ^{1}H NMR (400 MHz, DMSO-d_6) δ 10.80 (s, 1H), 8.40−8.28 (m, 2H), 7.76−7.67 (m, 3H), 7.63 (d, J = 8.0 Hz, 1H), 6.75 (t, J = 5.4 Hz, 1H), 3.84 (s, 2H), 3.76−3.64 (m, 3H), 3.54 (s, 4H), 3.53−3.47 (m, 4H), 3.37 (t, J = 6.1 Hz, 2H), 3.06 (q, J = 5.9 Hz, 2H), 2.76 (t, J = 11.6 Hz, 2H), 1.83−1.74 (m, 2H), 1.57−1.45 (m, 2H), 1.36 (s, 9H). ESI-MS: *m/z* 742.87 $[M+Na]^+$, 719.06 $[M-H]^-$. $C_{31}H_{40}F_4N_4O_9S$ [720.25].

*4.1.5. General procedure for the synthesis of **7(a−h)***

Under an ice bath, TFA was added dropwise to intermediates **6(a−h)** in 30 mL of DCM (monitored by TLC). Then, the resulting mixture solution was alkalized to pH ~ 7 with a saturated sodium bicarbonate solution and then extracted with DCM (40 mL). Then, the combined organic layer was washed with saturated sodium bicarbonate (3 × 20 mL), dried over anhydrous Na_2SO_4, filtered, and concentrated under reduced pressure to afford the intermediates **7(a−h)**.

*4.1.5.1. 3-((4-(4-Aminobutanamido)piperidin-1-yl)sulfonyl)-4-fluoro-N-(3,4,5-trifluorophenyl)benzamide (**7a**).* White solid, yield: 72%. ^{1}H NMR (400 MHz, DMSO-d_6) δ 8.35 (m, 2H), 7.90 (d, J = 9.9 Hz, 1H), 7.72 (dt, J = 11.9, 6.3 Hz, 4H), 3.63 (d, J = 12.7 Hz, 3H), 2.94−2.75 (m, 4H), 2.01 (s, 2H), 1.82 (d, J = 12.9 Hz, 2H), 1.54 (q, J = 6.8 Hz, 2H), 1.41 (d, J = 11.6 Hz, 2H). ESI-MS: *m/z* 517.23 $[M+H]^+$, 515.13 $[M-H]^-$. $C_{22}H_{24}F_4N_4O_4S$ [516.51].

*4.1.5.2. 3-((4-(5-Aminopentanamido)piperidin-1-yl)sulfonyl)-4-fluoro-N-(3,4,5-trifluoro- phenyl)benzamide (**7b**).* White solid, yield: 68%. ^{1}H NMR (400 MHz, DMSO-d_6) δ 8.36 (m, 2H), 7.82 (t, J = 10.1 Hz, 1H), 7.72 (dt, J = 7.3, 3.7 Hz, 4H), 3.62 (d, J = 13.7 Hz, 3H), 2.78 (dd, J = 26.8, 6.1 Hz, 4H), 2.01 (d, J = 7.9 Hz, 2H), 1.78 (m, 2H), 1.56 (tt, J = 14.8, 7.3 Hz, 4H), 1.39 (m, 2H). ESI-MS: *m/z* 531.18 $[M+H]^+$. $C_{23}H_{26}F_4N_4O_4S$ [530.54].

*4.1.5.3. 3-((4-(6-Aminohexanamido)piperidin-1-yl)sulfonyl)-4-fluoro-N-(3,4,5-trifluorophenyl)benzamide (**7c**).* White solid, yield: 70%. ^{1}H NMR (400 MHz, DMSO-d_6) δ 8.39−8.30 (m, 2H), 7.82 (d, J = 7.4 Hz, 1H), 7.71 (dt, J = 9.7, 5.0 Hz, 4H), 3.64 (t, J = 15.8 Hz, 3H), 2.78 (dt, J = 15.4, 9.5 Hz, 4H), 2.03 (t, J = 7.2 Hz, 2H), 1.78 (t, J = 13.4 Hz, 2H), 1.49 (tt, J = 14.6, 7.4 Hz, 4H), 1.42−1.33 (m, 2H), 1.25 (p, J = 7.6, 7.1 Hz, 2H). ESI-MS: *m/z* 545.10 $[M+H]^+$, 543.21 $[M-H]^-$. $C_{24}H_{28}F_4N_4O_4S$ [544.57].

*4.1.5.4. 3-((4-(7-Aminoheptanamido)piperidin-1-yl)sulfonyl)-4-fluoro-N-(3,4,5-trifluorophenyl)benzamide (**7d**).* White solid, yield: 76%. ^{1}H NMR (400 MHz, DMSO-d_6) δ 8.38−8.30 (m, 2H), 7.81 (d, J = 7.6 Hz, 1H), 7.71 (d, J = 9.4 Hz, 4H), 3.61 (d, J = 11.3 Hz, 3H), 2.84−2.71 (m, 4H), 2.01 (d, J = 7.3 Hz, 2H), 1.79 (d, J = 14.2 Hz, 2H), 1.50−1.44 (m, 4H), 1.38 (d, J = 10.5 Hz, 2H), 1.32 (d, J = 10.4 Hz, 2H), 1.25 (m, 2H). ESI-MS: *m/z* 559.38 $[M+H]^+$, 557.28 $[M-H]^-$. $C_{25}H_{30}F_4N_4O_4S$ [558.59].

*4.1.5.5. 3-((4-(8-Aminooctanamido)piperidin-1-yl)sulfonyl)-4-fluoro-N-(3,4,5-trifluorophenyl)benzamide (**7e**).* White solid, yield: 65%. ^{1}H NMR (400 MHz, DMSO-d_6) δ 8.18 (m, 2H), 7.80 (s, 1H), 7.72 (d, J = 4.1 Hz, 4H), 3.58 (dd, J = 8.1, 4.4 Hz, 3H), 2.78−2.70 (m, 4H), 2.00 (m, 2H), 1.76 (d, J = 2.0 Hz, 2H), 1.57 (dd, J = 4.4, 2.1 Hz, 4H), 1.45−1.42 (m, 4H), 1.36 (d, J = 2.0 Hz, 2H), 1.33 (d, J = 1.2 Hz, 2H). ESI-MS: *m/z* 573.45 $[M+H]^+$. $C_{26}H_{32}F_4N_4O_4S$ [572.62].

*4.1.5.6. 3-((4-(2-(2-Aminoethoxy)acetamido)piperidin-1-yl)sulfonyl)-4-fluoro-N-(3,4,5-trifluorophenyl)benzamide (**7f**).* White solid, yield: 63%. ^{1}H NMR (400 MHz, DMSO-d_6) δ 8.34 (m, 2H), 7.85 (d, J = 8.1 Hz, 1H), 7.72 (dq, J = 10.6, 5.2, 4.3 Hz, 4H), 3.81−3.62 (m, 4H), 3.57 (t, J = 5.1 Hz, 2H), 3.53−3.44 (m, 1H), 2.97 (t, J = 5.2 Hz, 2H), 2.77 (t, J = 12.3 Hz, 2H), 1.88−1.72 (m, 2H), 1.52 (qd, J = 12.1, 3.7 Hz, 2H). ESI-MS: *m/z* 533.09 $[M+H]^+$, 531.18 $[M-H]^-$. $C_{22}H_{24}F_4N_4O_5S$ [532.51].

*4.1.5.7. 3-((4-(2-(2-(2-Aminoethoxy)ethoxy)acetamido)piperidin-1-yl)sulfonyl)-4-fluoro-N-(3,4,5-trifluorophenyl)benzamide (**7g**).* White solid, yield: 66%. ^{1}H NMR (400 MHz, DMSO-d_6) δ 8.20 (m, 2H), 7.84 (d, J = 14.6 Hz, 4H), 7.71−7.64 (m, 1H), 3.87 (d, J = 11.3 Hz, 3H), 3.68 (d, J = 16.7 Hz, 4H), 3.56 (m, 2H), 3.14−2.87 (m, 2H), 2.73 (d, J = 30.9 Hz, 2H), 2.61 (d, J = 11.5 Hz, 2H), 1.76 (d, J = 13.0 Hz, 2H), 1.51 (td, J = 13.1, 4.0 Hz, 2H). ESI-MS: *m/z* 577.19 $[M+H]^+$, $C_{24}H_{28}F_4N_4O_6S$ [576.56].

*4.1.5.8. 3-((4-(2-(2-(2-(2-Aminoethoxy)ethoxy)ethoxy)acetamido)piperidin-1-yl)sulfonyl)-4-fluoro-N-(3,4,5-trifluorophenyl) benzamide (**7h**).* White solid, yield: 61%. ^{1}H NMR (400 MHz, DMSO-d_6) δ 8.23−8.11 (m, 2H), 7.77 (qt, J = 11.3, 5.2 Hz, 4H), 7.70−7.60 (m, 1H), 3.85 (dd, J = 10.7, 5.2 Hz, 3H), 3.72−3.64 (m, 4H), 3.63−3.59 (m, 2H), 3.55 (d, J = 3.0 Hz, 4H), 3.43 (dt, J = 8.0, 4.1 Hz, 2H), 2.96 (q, J = 5.1 Hz, 1H), 2.83−2.71 (m, 1H), 2.61 (t, J = 12.2 Hz, 2H), 1.79 (t, J = 6.8 Hz, 2H), 1.50 (td, J = 12.3, 3.9 Hz, 2H). ESI-MS: *m/z* 620.99 $[M+H]^+$. $C_{26}H_{32}F_4N_4O_7S$ [620.62].

*4.1.6. General procedure for the synthesis of **HyT-(S2−S9)***

1-Adamantaneacetic acid (1.2 equiv.) and HATU (1.5 equiv.) were mixed in 30 mL of DCM and stirred in an ice bath for 30 min. Subsequently, DIEA (2.0 equiv.) and intermediates **7(a−h)** (1.0 equiv.) were added to the mixture and then stirred at room temperature (monitored by TLC). The resulting mixture was evaporated under reduced pressure, and the residue was initially washed with 1 mol/L HCl and extracted with ethyl acetate (3 × 20 mL). Then, the combined organic layer was washed with saturated sodium bicarbonate (3 × 20 mL), dried over anhydrous Na_2SO_4, filtered, and concentrated under reduced pressure to afford the corresponding crude product, which was purified by flash column chromatography (ethyl acetate) to afford the target compounds **HyT-(S2−S9)**.

*4.1.6.1. 3-((4-(4-(2-((1S,3S)-Adamantan-1-yl)acetamido)butanamido)piperidin-1-yl)sulfonyl)-4-fluoro-N-(3,4,5-trifluorophenyl) benzamide (**HyT-S2**).* White solid, yield: 67%. Mp:

211−212 °C. ^{1}H NMR (400 MHz, DMSO-d_6) δ 10.79 (s, 1H, NH), 8.38−8.34 (m, 1H, NH), 8.34−8.28 (m, 1H, NH), 7.80 (d, J = 7.5 Hz, 1H, Ph-H), 7.76−7.68 (m, 3H, Ph-H), 7.65 (t, J = 5.5 Hz, 1H, Ph-H), 3.71−3.63 (m, 1H), 3.60 (d, J = 12.5 Hz, 2H), 2.96 (q, J = 6.6 Hz, 2H), 2.82 (t, J = 11.0 Hz, 2H), 2.01 (q, J = 6.8, 6.1 Hz, 2H), 1.89 (s, 3H), 1.85−1.79 (m, 2H), 1.78 (s, 2H), 1.74−1.48 (m, 14H), 1.46−1.31 (m, 2H). ^{13}C NMR (150 MHz, DMSO-d_6) δ 171.59, 170.27, 164.01, 160.67 (d, J = 260.0 Hz), 150.48 (d, J = 253.9 Hz), 135.73 (d, J = 9.7 Hz), 131.36 (d, J = 3.0 Hz), 130.85, 126.06 (d, J = 15.7 Hz), 118.56 (d, J = 22.4 Hz), 105.38 (dd, J = 25.1, 5.2 Hz), 50.55, 44.93, 44.68, 42.62, 38.51, 36.95, 33.45, 32.60, 31.36, 28.55, 25.98. HRMS (ESI): m/z Calcd. for $C_{34}H_{40}F_4N_4O_5NaS$ $[M+Na]^+$ 715.2553; found 715.2562. HPLC purity: 97.2%.

*4.1.6.2. 3-((4-(5-(2-((3r,5r,7r)-Adamantan-1-yl)acetamido)pentanamido)piperidin-1-yl)sulfonyl)-4-fluoro-N-(3,4,5-trifluorophenyl)benzamide (**HyT-S3**).* White solid, yield: 72%. Mp: 218−219 °C. ^{1}H NMR (600 MHz, DMSO-d_6) δ 10.78 (s, 1H, NH), 8.36 (dd, J = 6.5, 2.1 Hz, 1H, NH), 8.32 (ddd, J = 8.1, 4.2, 2.3 Hz, 1H, NH), 7.75 (d, J = 7.6 Hz, 1H, Ph-H), 7.74−7.69 (m, 3H, Ph-H), 7.61 (t, J = 5.4 Hz, 1H, Ph-H), 3.66 (ddt, J = 14.1, 10.6, 5.8 Hz, 1H), 3.61 (d, J = 12.4 Hz, 2H), 2.98 (q, J = 6.8 Hz, 2H), 2.82 (t, J = 11.0 Hz, 2H), 2.02 (t, J = 7.3 Hz, 2H), 1.89 (s, 3H), 1.80 (d, J = 6.5 Hz, 4H), 1.67−1.50 (m, 12H), 1.46 (dt, J = 15.2, 7.4 Hz, 2H), 1.40 (dd, J = 17.1, 6.1 Hz, 2H), 1.33 (dt, J = 14.4, 7.3 Hz, 2H). ^{13}C NMR (150 MHz, DMSO-d_6) δ 171.80, 170.13, 164.01, 160.67 (d, J = 259.6 Hz), 150.46 (d, J = 249.3 Hz), 135.73 (d, J = 9.5 Hz), 131.36 (d, J = 3.2 Hz), 126.06 (d, J = 15.3 Hz), 118.56 (d, J = 22.8 Hz), 105.46, 105.38 (dd, J = 25.3, 5.2 Hz), 105.29, 50.56, 44.90, 44.70, 42.63, 38.54, 36.96, 35.50, 32.61, 31.39, 29.30, 28.56, 23.28. HRMS (ESI): m/z Calcd. for $C_{35}H_{42}F_4N_4O_5NaS$ $[M+Na]^+$ 729.2710; found 729.2706. HPLC purity: 95.6%.

*4.1.6.3. 3-((4-(6-(2-((1S,3S)-Adamantan-1-yl)acetamido)hexanamido)piperidin-1-yl)sulfonyl)-4-fluoro-N-(3,4,5-trifluorophenyl)benzamide (**HyT-S4**).* White solid, yield: 74%. Mp: 186−187 °C. ^{1}H NMR (600 MHz, DMSO-d_6) δ 10.78 (s, 1H, NH), 8.35 (dd, J = 6.5, 2.2 Hz, 1H, NH), 8.32 (ddd, J = 8.2, 4.3, 2.3 Hz, 1H, NH), 7.75−7.67 (m, 4H, Ph-H), 7.59 (t, J = 5.4 Hz, 1H, Ph-H), 3.65 (dq, J = 10.7, 3.7 Hz, 1H), 3.61 (d, J = 12.5 Hz, 2H), 2.97 (q, J = 6.7 Hz, 2H), 2.81 (t, J = 11.0 Hz, 2H), 2.00 (t, J = 7.4 Hz, 2H), 1.89 (s, 3H), 1.79 (d, J = 9.8 Hz, 4H), 1.67−1.50 (m, 12H), 1.45 (p, J = 7.6 Hz, 2H), 1.42−1.36 (m, 2H), 1.36−1.31 (m, 2H), 1.20 (dq, J = 15.0, 6.9, 6.5 Hz, 2H). ^{13}C NMR (150 MHz, DMSO-d_6) δ 171.85, 170.13, 164.01, 160.67 (d, J = 259.6 Hz), 150.48 (d, J = 254.1 Hz), 135.73 (d, J = 9.9 Hz), 131.36 (d, J = 3.0 Hz), 130.86, 126.03 (d, J = 15.5 Hz), 118.56 (d, J = 22.7 Hz), 105.46, 105.38 (dd, J = 25.5, 5.3 Hz), 105.29, 50.56, 44.93, 44.73, 42.63, 38.68, 36.97, 35.84, 32.60, 31.38, 29.44, 28.55, 26.60, 25.42. HRMS (ESI): m/z Calcd. for $C_{36}H_{44}F_4N_4O_5NaS$ $[M+Na]^+$ 743.2866; found 743.2875. HPLC purity: 97.4%.

*4.1.6.4. 3-((4-(7-(2-((3R,5R,7R)-Adamantan-1-yl)acetamido)heptanamido)piperidin-1-yl)sulfonyl)-4-fluoro-N-(3,4,5-trifluorophenyl)benzamide (**HyT-S5**).* White solid, yield: 68%. Mp: 187−188 °C. ^{1}H NMR (600 MHz, DMSO-d_6) δ 10.78 (s, 1H, NH), 8.36 (dd, J = 6.5, 2.2 Hz, 1H, NH), 8.32 (ddd, J = 8.4, 4.4, 2.3 Hz, 1H, NH), 7.77−7.69 (m, 4H, Ph-H), 7.59 (t, J = 5.4 Hz, 1H, Ph-H), 3.69−3.63 (m, 1H), 3.63−3.58 (m, 2H), 2.98 (q, J = 6.8 Hz, 2H), 2.82 (t, J = 10.9 Hz, 2H), 2.01 (t, J = 7.5 Hz, 2H), 1.90 (s, 3H), 1.80 (d, J = 4.3 Hz, 4H), 1.67−1.51 (m, 12H), 1.48−1.42 (m, 2H), 1.42−1.37 (m, 2H), 1.36−1.31 (m, 2H), 1.22 (tt, J = 10.9, 4.4 Hz, 4H). ^{13}C NMR (150 MHz, DMSO-d_6) δ 171.91, 170.12, 164.02, 160.67 (d, J = 259.9 Hz), 150.46 (d, J = 249.3 Hz), 135.73 (d, J = 9.8 Hz), 131.36 (d, J = 3.0 Hz), 130.86, 126.05 (d, J = 15.7 Hz), 118.56 (d, J = 22.9 Hz), 105.47, 105.38 (dd, J = 25.3, 4.8 Hz), 105.30, 50.57, 44.89, 44.72, 42.64, 38.67, 36.97, 35.85, 32.61, 31.38, 29.53, 28.76, 28.56, 26.64, 25.70. HRMS (ESI): m/z Calcd. for $C_{37}H_{46}F_4N_4O_5NaS$ $[M+Na]^+$ 757.3023; found 757.3029. HPLC purity: 96.2%.

*4.1.6.5. 3-((4-(8-(2-((1S,3S)-Adamantan-1-yl)acetamido)octanamido)piperidin-1-yl)sulfonyl)-4-fluoro-N-(3,4,5-trifluorophenyl)benzamide (**HyT-S6**).* White solid, yield: 77%. Mp: 201−202 °C. ^{1}H NMR (600 MHz, DMSO-d_6) δ 10.79 (s, 1H, NH), 8.36 (dd, J = 6.5, 2.2 Hz, 1H, NH), 8.32 (ddd, J = 8.4, 4.3, 2.3 Hz, 1H, NH), 7.76−7.69 (m, 4H, Ph-H), 7.59 (t, J = 5.4 Hz, 1H, Ph-H), 3.66 (ddt, J = 10.1, 6.5, 3.7 Hz, 1H), 3.61 (d, J = 12.5 Hz, 2H), 2.99 (q, J = 6.7 Hz, 2H), 2.82 (t, J = 11.0 Hz, 2H), 2.01 (t, J = 7.4 Hz, 2H), 1.90 (s, 3H), 1.79 (d, J = 5.9 Hz, 4H), 1.68−1.51 (m, 12H), 1.45 (dt, J = 14.3, 7.4 Hz, 2H), 1.40 (dd, J = 17.3, 6.6 Hz, 2H), 1.37−1.32 (m, 2H), 1.26−1.17 (m, 6H). ^{13}C NMR (150 MHz, DMSO-d_6) δ 171.88, 170.10, 164.00, 160.68 (d, J = 259.6 Hz), 150.43 (d, J = 248.8 Hz), 135.79 (d, J = 9.9 Hz), 131.32 (d, J = 2.9 Hz), 130.88, 125.85 (d, J = 15.6 Hz), 118.61 (d, J = 22.6 Hz), 105.41, 105.33 (dd, J = 25.4, 5.1 Hz), 105.25, 50.56, 44.84, 44.74, 42.61, 38.66, 36.94, 35.83, 32.59, 31.37, 29.62, 29.04, 28.91, 28.52, 26.79, 25.65. HRMS (ESI): m/z Calcd. for $C_{38}H_{48}F_4N_4O_5NaS$ $[M+Na]^+$ 771.3179; found 771.3181. HPLC purity: 97.8%.

*4.1.6.6. 3-((4-(2-(2-(2-((3R,5R,7R)-Adamantan-1-yl)acetamido)ethoxy)acetamido)piperidin-1-yl)sulfonyl)-4-fluoro-N-(3,4,5-trifluorophenyl)benzamide (**HyT-S7**).* White solid, yield: 69%. Mp: 221−222 °C. ^{1}H NMR (600 MHz, DMSO-d_6) δ 10.77 (s, 1H, NH), 8.36 (dd, J = 6.4, 2.0 Hz, 1H, NH), 8.32 (dq, J = 5.8, 2.1 Hz, 1H, NH), 7.76 (t, J = 5.5 Hz, 1H, Ph-H), 7.73−7.68 (m, 3H, Ph-H), 7.65 (d, J = 8.0 Hz, 1H, Ph-H), 3.82 (s, 2H), 3.74 (ddt, J = 10.5, 6.6, 3.4 Hz, 1H), 3.68 (d, J = 12.4 Hz, 2H), 3.41 (t, J = 5.6 Hz, 2H), 3.21 (q, J = 5.6 Hz, 2H), 2.77 (t, J = 11.6 Hz, 2H), 1.89 (s, 3H), 1.82 (s, 2H), 1.78 (d, J = 10.3 Hz, 2H), 1.66−1.53 (m, 12H), 1.53−1.48 (m, 2H). ^{13}C NMR (150 MHz, DMSO-d_6) δ 170.52, 168.88, 164.01, 160.69 (d, J = 259.7 Hz), 150.46 (d, J = 248.2 Hz), 135.73 (d, J = 9.7 Hz), 131.35 (d, J = 3.2 Hz), 130.84, 126.01 (d, J = 16.0 Hz), 118.56 (d, J = 22.6 Hz), 105.46, 105.38 (dd, J = 25.1, 5.0 Hz), 105.29, 70.36, 70.28, 50.54, 45.07, 44.99, 42.59, 38.64, 36.94, 32.63, 31.32, 28.55. HRMS (ESI): m/z Calcd. for $C_{34}H_{40}F_4N_4O_6NaS$ $[M+Na]^+$ 731.2502; found 731.2509. HPLC purity: 97.5%.

*4.1.6.7. 3-((4-(2-(2-(2-(2-((3R,5R,7R)-Adamantan-1-yl)acetamido)ethoxy)ethoxy)acetamido)piperidin-1-yl)sulfonyl)-4-fluoro-N-(3,4,5-trifluorophenyl)benzamide (**HyT-S8**).* White solid, yield: 71%. Mp: 212−213 °C. ^{1}H NMR (600 MHz, DMSO-d_6) δ 10.77 (s, 1H, NH), 8.35 (dd, J = 6.5, 2.1 Hz, 1H, NH), 8.32 (ddd, J = 8.1, 4.2, 2.3 Hz, 1H, NH), 7.71 (dd, J = 10.0, 7.0 Hz, 3H, Ph-H), 7.67 (dd, J = 7.2, 4.4 Hz, 1H, Ph-H), 7.63 (d, J = 7.9 Hz, 1H, Ph-H), 3.84 (s, 2H), 3.72 (ddt, J = 14.3, 6.7, 3.6 Hz, 1H), 3.67 (d, J = 12.4 Hz, 2H), 3.58−3.50 (m, 4H), 3.40

(t, J = 5.9 Hz, 2H), 3.17 (q, J = 5.8 Hz, 2H), 2.76 (t, J = 11.6 Hz, 2H), 1.89 (s, 3H), 1.82 (s, 2H), 1.81−1.76 (m, 2H), 1.66−1.53 (m, 12H), 1.53−1.48 (m, 2H). ^{13}C NMR (150 MHz, DMSO-d_6) δ 170.46, 169.01, 164.00, 160.70 (d, J = 259.7 Hz), 150.43 (d, J = 248.2 Hz), 135.80 (d, J = 9.7 Hz), 131.32 (d, J = 2.9 Hz), 130.90, 125.69 (d, J = 15.5 Hz), 118.62 (d, J = 22.8 Hz), 105.42, 105.34 (dd, J = 25.1, 4.9 Hz), 105.25, 70.60, 70.40, 69.72, 69.63, 50.43, 45.05, 45.02, 42.54, 38.69, 36.93, 32.60, 31.22, 28.51. HRMS (ESI): *m/z* Calcd. for $C_{36}H_{44}F_4N_4O_7NaS$ $[M+Na]^+$ 775.2765; found 775.2757. HPLC purity: 98.0%.

*4.1.6.8. 3-((4-(1-((3R,5R,7R)-Adamantan-1-yl)-2-oxo-6,9,12-trioxa-3-azatetradecan-14-amido)piperidin-1-yl)sulfonyl)-4-fluoro-N-(3,4,5-trifluorophenyl)benzamide (**HyT-S9**).* White solid, yield: 70%. Mp: 120−121 °C. ^{1}H NMR (600 MHz, DMSO-d_6) δ 10.77 (s, 1H, NH), 8.35 (dd, J = 6.5, 2.2 Hz, 1H, NH), 8.32 (ddd, J = 8.2, 4.3, 2.3 Hz, 1H, NH), 7.71 (dd, J = 10.4, 7.5 Hz, 3H, Ph-H), 7.66 (t, J = 5.5 Hz, 1H, Ph-H), 7.61 (d, J = 8.0 Hz, 1H, Ph-H), 3.85 (s, 2H), 3.72 (ddt, J = 15.0, 7.7, 4.1 Hz, 1H), 3.67 (d, J = 12.3 Hz, 2H), 3.54 (s, 4H), 3.51 (qd, J = 7.6, 5.1 Hz, 4H), 3.39 (t, J = 5.9 Hz, 2H), 3.17 (q, J = 5.8 Hz, 2H), 2.77 (t, J = 11.5 Hz, 2H), 1.89 (s, 3H), 1.80 (d, J = 17.1 Hz, 4H), 1.66−1.53 (m, 12H), 1.50 (dd, J = 11.6, 8.7 Hz, 2H). ^{13}C NMR (150 MHz, DMSO-d_6) δ 170.43, 169.01, 164.01, 160.70 (d, J = 259.6 Hz), 150.43 (d, J = 248.4 Hz), 135.80 (d, J = 9.5 Hz), 131.32 (d, J = 3.2 Hz), 130.89, 125.73 (d, J = 15.8 Hz), 118.63 (d, J = 23.1 Hz), 105.43, 105.34 (dd, J = 25.2, 4.9 Hz), 105.26, 70.58, 70.31, 70.22, 70.03, 69.98, 69.68, 50.43, 45.00, 42.54, 38.77, 36.93, 32.60, 31.26, 28.52. HRMS (ESI): *m/z* Calcd. for $C_{38}H_{48}F_4N_4O_8NaS$ $[M+Na]^+$ 819.3027; found 819.3032. HPLC purity: 97.9%.

*4.1.7. General procedure for the synthesis of **HyT-(S10−S11, S13−S14)***

Carboxylic acid with different hydrophobic groups (1.2 equiv.) and HATU (1.5 equiv.) were mixed in 30 mL of DCM and stirred in an ice bath for 30 min. Subsequently, DIEA (2.0 equiv.) and intermediate **7f** (1.0 equiv.) were added to the mixture and then stirred at room temperature (monitored by TLC). The resulting mixture was evaporated under reduced pressure, and the residue was initially washed with 1 mol/L HCl and extracted with ethyl acetate (3 × 20 mL). Then, the combined organic layer was washed with saturated sodium bicarbonate (3 × 20 mL), dried over anhydrous Na_2SO_4, filtered, and concentrated under reduced pressure to afford the corresponding crude product, which was purified by flash column chromatography (ethyl acetate) to afford the target compounds **HyT-(S10∼S11, S13∼S14)**.

*4.1.7.1. 3-((4-(2-(2-(2,2-Diphenylacetamido)ethoxy)acetamido)piperidin-1-yl)sulfonyl)-4-fluoro-N-(3,4,5-trifluorophenyl)benzamide (**HyT-S10**).* White solid, yield: 71%. Mp: 172−173 °C. ^{1}H NMR (600 MHz, DMSO-d_6) δ 10.81 (s, 1H, NH), 8.43 (t, J = 5.5 Hz, 1H, NH), 8.36 (dd, J = 6.5, 2.2 Hz, 1H, NH), 8.32 (ddd, J = 8.1, 4.2, 2.3 Hz, 1H, Ph-H), 7.71 (dd, J = 10.0, 6.8 Hz, 3H, Ph-H), 7.67 (d, J = 8.1 Hz, 1H, Ph-H), 7.30 (d, J = 4.2 Hz, 8H, Ph-H), 7.22 (dq, J = 8.7, 4.2 Hz, 2H, Ph-H), 4.96 (s, 1H), 3.82 (s, 2H), 3.73−3.69 (m, 1H), 3.67 (d, J = 12.4 Hz, 2H), 3.45 (t, J = 5.5 Hz, 2H), 3.29 (q, J = 5.5 Hz, 2H), 2.72 (t, J = 11.7 Hz, 2H), 1.76−1.69 (m, 2H), 1.47 (qd, J = 12.5, 4.0 Hz, 2H). ^{13}C NMR (150 MHz, DMSO-d_6) δ 171.62, 168.81, 164.02, 160.70 (d, J = 259.6 Hz), 150.43 (d, J = 248.9 Hz), 140.86, 135.79 (d, J = 9.6 Hz), 131.32 (d, J = 3.1 Hz), 130.90, 128.94, 128.67, 127.07, 125.76 (d, J = 15.4 Hz), 118.62 (d, J = 23.1 Hz), 105.44, 105.35 (dd, J = 25.0, 5.0 Hz), 105.27, 70.21, 70.13, 56.95, 45.03, 45.02, 39.04, 31.25. HRMS (ESI): *m/z* Calcd. for $C_{36}H_{34}F_4N_4O_6NaS$ $[M+Na]^+$ 749.2033; found 749.2037. HPLC purity: 97.5%.

*4.1.7.2. 3-((4-(2-(2-(2-(9H-Fluoren-9-yl)acetamido)ethoxy)acetamido)piperidin-1-yl)sulfonyl)-4-fluoro-N-(3,4,5-trifluorophenyl)benzamide (**HyT-S11**).* White solid, yield: 67%. Mp: 141−142 °C. ^{1}H NMR (600 MHz, DMSO-d_6) δ 10.80 (s, 1H, NH), 8.35 (dd, J = 6.5, 2.1 Hz, 1H, NH), 8.31 (ddd, J = 8.3, 4.3, 2.3 Hz, 1H, NH), 8.16 (t, J = 5.5 Hz, 1H, Ph-H), 7.87 (d, J = 7.5 Hz, 2H, Ph-H), 7.71 (dd, J = 9.6, 6.2 Hz, 3H, Ph-H), 7.68 (d, J = 9.4 Hz, 1H, Ph-H), 7.53 (d, J = 7.5 Hz, 2H, Ph-H), 7.37 (t, J = 7.4 Hz, 2H, Ph-H), 7.32−7.27 (m, 2H, Ph-H), 4.36 (t, J = 7.7 Hz, 1H), 3.88 (s, 2H), 3.73−3.67 (m, 1H), 3.64 (d, J = 12.4 Hz, 2H), 3.52 (t, J = 5.4 Hz, 2H), 3.41−3.39 (m, 2H), 2.72 (t, J = 11.9 Hz, 2H), 2.53 (d, J = 7.8 Hz, 2H), 1.76−1.68 (m, 2H), 1.47 (qd, J = 12.5, 3.9 Hz, 2H). ^{13}C NMR (100 MHz, DMSO-d_6) δ 171.36, 168.89, 164.02, 160.68 (d, J = 259.3 Hz), 150.23 (d, J = 248.3 Hz), 147.11, 140.55, 135.79 (d, J = 10.1 Hz), 131.30 (d, J = 3.1 Hz), 127.70, 127.55, 125.73 (d, J = 15.8 Hz), 125.02, 120.44, 118.60 (d, J = 22.3 Hz), 105.49, 105.36 (d, J = 25.2, 6.0 Hz), 105.24, 70.37, 70.25, 45.02, 44.01, 38.93, 31.24. HRMS (ESI): *m/z* Calcd. for $C_{37}H_{34}F_4N_4O_6NaS$ $[M+Na]^+$ 761.2033; found 761.2040. HPLC purity: 98.1%.

*4.1.7.3. (S)-4-Fluoro-3-((4-(2-(2-(2-(4-isobutylphenyl)propanamido)ethoxy)acetamido)piperidin-1-yl)sulfonyl)-N-(3,4,5-trifluorophenyl)benzamide (**HyT-S13**).* White solid, yield: 68%. Mp: 182−183 °C. ^{1}H NMR (600 MHz, DMSO-d_6) δ 10.81 (s, 1H, NH), 8.36 (dd, J = 6.5, 2.2 Hz, 1H, NH), 8.32 (ddd, J = 8.3, 4.3, 2.3 Hz, 1H, NH), 8.08 (t, J = 5.6 Hz, 1H, Ph-H), 7.75−7.66 (m, 4H, Ph-H), 7.20 (d, J = 8.0 Hz, 2H, Ph-H), 7.06 (d, J = 8.0 Hz, 2H, Ph-H), 3.80 (s, 2H), 3.76−3.71 (m, 1H), 3.71−3.66 (m, 2H), 3.56 (q, J = 7.0 Hz, 1H), 3.40 (dt, J = 12.1, 5.1 Hz, 2H), 3.28−3.16 (m, 2H), 2.75 (t, J = 11.8 Hz, 2H), 2.38 (d, J = 7.1 Hz, 2H), 1.82−1.78 (m, 1H), 1.76 (dd, J = 8.1, 5.0 Hz, 2H), 1.51 (q, J = 10.1, 9.2 Hz, 2H), 1.30 (d, J = 7.0 Hz, 3H), 0.84 (d, J = 6.6 Hz, 6H). ^{13}C NMR (150 MHz, DMSO-d_6) δ 174.09, 168.88, 164.02, 160.69 (d, J = 259.3 Hz), 150.46 (d, J = 249.3 Hz), 139.98, 139.63, 135.73 (d, J = 9.8 Hz), 131.35 (d, J = 3.1 Hz), 130.86, 129.18, 127.39, 126.00 (d, J = 15.4 Hz), 118.57 (d, J = 23.1 Hz), 105.46, 105.38 (dd, J = 25.2, 4.8 Hz), 105.30, 70.28, 70.21, 45.22, 45.07, 44.99, 44.72, 38.93, 31.30, 30.02, 22.62, 19.11. HRMS (ESI): *m/z* Calcd. for $C_{35}H_{40}F_4N_4O_6NaS$ $[M+Na]^+$ 743.2502; found 743.2511. HPLC purity: 99.2%.

*4.1.7.4. 4-Fluoro-3-((4-(2-(2-(2-(((1R,2S,5R)-2-isopropyl-5-methylcyclohexyl)oxy)acetamido)ethoxy)acetamido)piperidin-1-yl)sulfonyl)-N-(3,4,5-trifluorophenyl)benzamide (**HyT-S14**).* White solid, yield: 69%. Mp: 106−107 °C. ^{1}H NMR (600 MHz, DMSO-d_6) δ 10.81 (s, 1H, NH), 8.36 (dd, J = 6.5, 2.2 Hz, 1H, NH), 8.32 (ddd, J = 8.3, 4.3, 2.3 Hz, 1H, NH), 7.75−7.69 (m, 4H, Ph-H), 7.64 (t, J = 5.8 Hz, 1H, Ph-H), 4.05−3.88 (m, 2H), 3.82 (s, 2H), 3.80 (d, J = 14.9 Hz, 1H), 3.73 (ddt, J = 10.6, 6.7, 3.7 Hz, 1H), 3.68 (d, J = 12.3 Hz, 2H), 3.45 (h, J = 5.4, 5.0 Hz, 2H), 3.33−3.26 (m, 2H), 3.12 (td,

J = 10.5, 4.0 Hz, 2H), 2.76 (t, J = 11.5 Hz, 2H), 2.17 (ddq, J = 9.6, 6.9, 3.4, 2.6 Hz, 1H), 2.05−1.97 (m, 1H), 1.82−1.75 (m, 2H), 1.60 (d, J = 11.8 Hz, 1H), 1.55 (dd, J = 11.3, 4.9 Hz, 2H), 1.27−1.23 (m, 4H), 0.87−0.85 (m, 6H), 0.73 (d, J = 6.9 Hz, 3H). ^{13}C NMR (100 MHz, DMSO-d_6) δ 170.26, 168.83, 164.00, 160.70 (d, J = 259.5 Hz), 150.43 (d, J = 248.5 Hz), 135.81 (d, J = 10.0 Hz), 131.30 (d, J = 3.1 Hz), 130.89, 125.75 (d, J = 15.5 Hz), 118.64 (d, J = 22.5 Hz), 105.33 (dd, J = 24.7, 6.4 Hz), 79.93, 79.11, 70.13, 68.24, 65.62, 48.32, 47.84, 45.00, 44.96, 38.40, 34.50, 34.47, 31.32, 31.30, 25.58, 25.45, 23.36, 23.19, 22.69, 22.63, 21.33, 16.77, 16.50. HRMS (ESI): m/z Calcd. for $C_{34}H_{44}F_4N_4O_7NaS$ $[M+Na]^+$ 751.2765; found 751.2770. HPLC purity: 96.8%.

*4.1.8. 2-Methylpropan-2-yl {[(6E,11S)-18-({1-[(2-fluoro-5-{[(3,4,5-trifluorophenyl)amino]carbonyl}phenyl)dioxo-λ6-sulfanyl]hexahydropyridin-4-yl}amino)-2,2-dimethyl-11-({[(2-methylprop-2-yl)oxy]carbonyl}amino)-4,12,18-trioxo-3,16-dioxa-5,7,13-triazaoctadecan-6-ylidene]amino}methanoate (**HyT-S15**)*

A mixture of intermediate **7f** (1.0 equiv.), (*tert*-butoxy) carbonyl Arg (Boc)$_2$-OH (symmetrical) (1.0 equiv.), and NMI (3.0 equiv.) in MeCN (10 mL) was stirred 10 min before TCFH (1.1 equiv.) was added. The mixture was stirred at room temperature overnight (monitored by TLC). The resulting mixture was evaporated under reduced pressure, and the residue was extracted with ethyl acetate (3 × 20 mL) and water. Then, the combined organic layer was washed with saturated sodium bicarbonate (3 × 20 mL), dried over anhydrous Na_2SO_4, filtered, and concentrated under reduced pressure to afford the corresponding crude product, which was purified by flash column chromatography (ethyl acetate) to afford the target compound **HyT-S15**. White solid, yield: 65%. Mp: 132−133 °C. ^{1}H NMR (600 MHz, DMSO-d_6) δ 11.46 (s, 1H, NH), 10.78 (s, 1H, NH), 8.33 (dd, J = 6.4, 2.0 Hz, 1H, NH), 8.29 (ddd, J = 8.0, 4.2, 2.3 Hz, 1H, NH), 8.24 (t, J = 5.5 Hz, 1H, NH), 7.95 (t, J = 5.3 Hz, 1H, NH), 7.72−7.65 (m, 4H, Ph-H), 6.85 (d, J = 8.0 Hz, 1H, Ph-H), 3.89−3.83 (m, 1H), 3.80 (s, 2H), 3.71 (dd, J = 11.2, 3.5 Hz, 1H), 3.67 (d, J = 11.9 Hz, 2H), 3.43−3.37 (m, 2H), 3.28 (dt, J = 11.0, 5.8 Hz, 1H), 3.25−3.19 (m, 2H), 3.17 (dd, J = 13.5, 5.9 Hz, 1H), 2.72 (t, J = 11.6 Hz, 2H), 1.76 (d, J = 12.3 Hz, 2H), 1.51 (dd, J = 25.7, 14.1 Hz, 4H), 1.44 (s, 11H), 1.35 (d, J = 5.9 Hz, 16H), 1.32 (d, J = 8.5 Hz, 2H). ^{13}C NMR (100 MHz, DMSO-d_6) δ 172.59, 168.86, 168.81, 164.01, 163.59, 160.69 (d, J = 259.8 Hz), 155.71, 152.54, 150.43 (d, J = 259.7 Hz), 135.81 (d, J = 10.0 Hz), 131.33 (d, J = 2.4 Hz), 130.88, 125.74 (d, J = 15.0 Hz), 118.63 (d, J = 22.8 Hz), 105.45, 105.33 (dd, J = 24.5, 6.1 Hz), 105.21, 83.30, 78.56, 78.50, 70.20, 70.04, 67.41, 45.06, 38.76, 31.76, 31.27, 31.25, 28.71, 28.64, 28.45, 28.07. HRMS (ESI): m/z Calcd. for $C_{43}H_{60}F_4N_8O_{12}NaS$ $[M+Na]^+$ 1011.3885; found 1011.3890. HPLC purity: 97.5%.

*4.1.9. Ethyl 6-((1-((2-fluoro-5-((3,4,5-trifluorophenyl)carbamoyl)phenyl)sulfonyl)piperidin-4-yl)amino)-6-oxohexanoate (**8**)*

Monoethyl adipate (1.2 equiv.) and HATU (1.5 equiv.) were mixed in 30 mL of DCM and stirred in an ice bath for 30 min. Subsequently, DIEA (2.0 equiv.) and intermediate **5** (1.0 equiv.) were added to the mixture and then stirred at room temperature for another 5 h (monitored by TLC). The resulting mixture was evaporated under reduced pressure, and the residue was initially washed with 1 mol/L HCl and extracted with ethyl acetate (3 × 20 mL). Then, the combined organic layer was washed with saturated sodium bicarbonate (3 × 20 mL), dried over anhydrous Na_2SO_4, filtered, and concentrated under reduced pressure to afford the corresponding crude product, which was purified by flash column chromatography (ethyl acetate) to afford the intermediate **8**. White solid, yield: 78%. ^{1}H NMR (400 MHz, DMSO-d_6) δ 10.82 (s, 1H), 8.39−8.29 (m, 2H), 7.80 (d, J = 7.5 Hz, 1H), 7.76−7.67 (m, 3H), 4.03 (q, J = 7.1 Hz, 2H), 3.69−3.57 (m, 3H), 2.82 (t, J = 11.3 Hz, 2H), 2.26 (t, J = 6.7 Hz, 2H), 2.03 (s, 2H), 1.86−1.75 (m, 2H), 1.46 (s, 4H), 1.43−1.33 (m, 2H), 1.17 (d, J = 14.2 Hz, 3H). ESI-MS: m/z 588.20 $[M+H]^+$. $C_{26}H_{29}F_4N_3O_6S$ [587.17].

*4.1.10. 6-((1-((2-Fluoro-5-((3,4,5-trifluorophenyl)carbamoyl)phenyl)sulfonyl)piperidin-4-yl)amino)-6-oxohexanoic acid (**9**)*

Intermediate **8** (1.0 equiv.) was dissolved in a mixture of 10 mL THF and 10 mL water. Then, LiOH (3.0 equiv.) was slowly added to the above solution, and the mixture was stirred at room temperature (monitored by TLC). The resulting mixture solution was acidized to pH 2−3 with 1 mol/L HCl. Then, the mixture was filtered under reduced pressure, and the filter cake was washed with water. Finally, intermediate **9** was obtained after drying the filter cake. White solid, yield: 70%. ^{1}H NMR (400 MHz, DMSO-d_6) δ 11.05 (s, 1H), 8.37−8.30 (m, 2H), 7.81 (d, J = 7.5 Hz, 1H), 7.78−7.66 (m, 3H), 3.71−3.62 (m, 1H), 3.58 (d, J = 12.6 Hz, 2H), 2.84 (t, J = 11.0 Hz, 2H), 2.14 (t, J = 6.6 Hz, 2H), 2.01 (t, J = 6.4 Hz, 2H), 1.83−1.73 (m, 2H), 1.45−1.43 (m, 2H), 1.35 (ddd, J = 24.6, 17.0, 4.4 Hz, 4H). ESI-MS: m/z 560.13 $[M+H]^+$, 558.46 $[M-H]^-$. $C_{24}H_{25}F_4N_3O_6S$ [559.14].

*4.1.11. N^1-(Bicyclo[2.2.1]hept-2-en-1-ylmethyl)-N^6-(1-((2-fluoro-5-((3,4,5-trifluorophenyl)carbamoyl)phenyl)sulfonyl)piperidin-4-yl)adipamide (**HyT-S12**)*

Intermediate **9** (1.2 equiv.) and HATU (1.5 equiv.) were mixed in 30 mL of DCM and stirred in an ice bath for 30 min. Subsequently, DIEA (2.0 equiv.) and 1-bicyclo[2.2.1]hept-5-en-2-ylmethanamine (1.0 equiv.) were added to the mixture and then stirred at room temperature for another 5 h (monitored by TLC). The resulting mixture was evaporated under reduced pressure, and the residue was initially washed with 1 mol/L HCl and extracted with ethyl acetate (3 × 20 mL). Then, the combined organic layer was washed with saturated sodium bicarbonate (3 × 20 mL), dried over anhydrous Na_2SO_4, filtered, and concentrated under reduced pressure to afford the corresponding crude product, which was purified by flash column chromatography (CH_3OH: DCM = 1:20) to afford the target compound **HyT-S12**. White solid, yield: 65%. Mp: 192−193 °C. ^{1}H NMR (400 MHz, DMSO-d_6) δ 10.98 (s, 1H, NH), 8.40 (dd, J = 5.5, 3.1 Hz, 1H, NH), 8.36 (d, J = 6.7 Hz, 1H, NH), 7.83 (d, J = 7.5 Hz, 1H, Ph-H), 7.77 (dd, J = 10.4, 6.4 Hz, 3H, Ph-H), 7.74−7.68 (m, 1H, Ph-H), 6.13 (dd, J = 5.5, 2.9 Hz, 1H, CH=CH), 5.94 (dd, J = 5.5, 2.7 Hz, 1H, CH=CH), 3.72−3.64 (m, 1H), 3.61 (d, J = 12.5 Hz, 2H), 2.87−2.70 (m, 5H), 2.61 (ddd, J = 13.1, 8.9, 5.6 Hz, 1H), 2.02 (s, 4H), 1.83−1.69 (m, 3H), 1.47−1.15 (m, 10H). ^{13}C NMR (150 MHz, DMSO-d_6) δ 172.09, 171.83, 164.05, 160.65 (d, J = 259.6 Hz), 150.36 (d, J = 248.6 Hz), 137.27, 135.92 (d, J = 9.2 Hz), 131.26 (d, J = 3.0 Hz), 131.10, 125.88 (d, J = 15.3 Hz), 118.49 (d, J = 22.7 Hz), 105.47, 105.39 (dd, J = 25.5, 4.9 Hz), 105.30, 49.36, 44.81, 44.70, 44.12, 43.00, 42.34, 38.87, 35.68, 35.65, 31.34, 30.22, 25.54, 25.45. HRMS (ESI): m/z Calcd. for $C_{32}H_{36}F_4N_4O_5NaS$ $[M+Na]^+$ 687.2240; found 687.2244. HPLC purity: 96.2%.

4.1.12. General procedure for the synthesis of ***10(a−n)***

Boc-protected amine-terminated linkers (1.2 equiv.) and HATU (1.5 equiv.) were mixed in 30 mL of DCM and stirred in an ice bath for 30 min. Subsequently, DIEA (2.0 equiv.) and intermediate **5** (1.0 equiv.) were added to the mixture and then stirred at room temperature (monitored by TLC). The resulting mixture was evaporated under reduced pressure, and the residue was initially washed with 1 mol/L HCl and extracted with ethyl acetate (3 × 20 mL). Then, the combined organic layer was washed with saturated sodium bicarbonate (3 × 20 mL), dried over anhydrous Na_2SO_4, filtered, and concentrated under reduced pressure to afford the corresponding crude product, which was purified by flash column chromatography (ethyl acetate: petroleum ether = 3:2) to afford the intermediates **10 (a−n)**.

*4.1.12.1. tert-Butyl 4-((1-((2-fluoro-5-((3,4,5-trifluorophenyl) carbamoyl)phenyl)sulfonyl)piperidin-4-yl)carbamoyl)piperidine-1-carboxylate (**10a**).* White solid, yield: 70%. ^{1}H NMR (400 MHz, DMSO-d_6) δ 10.80 (s, 1H), 8.38−8.29 (m, 2H), 7.79 (d, J = 7.6 Hz, 1H), 7.76−7.68 (m, 3H), 3.92 (d, J = 12.2 Hz, 2H), 3.63 (td, J = 12.5, 11.7, 5.6 Hz, 3H), 2.81 (t, J = 11.1 Hz, 2H), 2.75−2.63 (m, 2H), 1.83−1.74 (m, 2H), 1.63−1.56 (m, 2H), 1.46−1.39 (m, 5H), 1.39 (s, 9H). ESI-MS: *m/z* 641.35 $[M-H]^-$, $C_{29}H_{34}F_4N_4O_6S$ [642.21].

*4.1.12.2. tert-Butyl 4-(2-((1-((2-fluoro-5-((3,4,5-trifluorophenyl) carbamoyl)phenyl)sulfonyl)piperidin-4-yl)amino)-2-oxoethyl) piperidine-1-carboxylate (**10b**).* White solid, yield: 67%. ^{1}H NMR (400 MHz, DMSO-d_6) δ 10.82 (s, 1H), 8.38−8.29 (m, 2H), 7.80 (d, J = 7.5 Hz, 1H), 7.77−7.66 (m, 3H), 3.93−3.81 (m, 2H), 3.72−3.55 (m, 3H), 2.82 (t, J = 11.1 Hz, 2H), 2.75−2.57 (m, 2H), 1.95 (d, J = 7.0 Hz, 2H), 1.79 (d, J = 10.0 Hz, 3H), 1.54 (d, J = 12.2 Hz, 2H), 1.38 (s, 11H), 0.96 (qd, J = 12.2, 3.7 Hz, 2H). ESI-MS: *m/z* 679.14 $[M+Na]^+$, 655.40 $[M-H]^-$. $C_{30}H_{36}F_4N_4O_6S$ [656.23].

*4.1.12.3. tert-Butyl 4-(2-((1-((2-fluoro-5-((3,4,5-trifluorophenyl) carbamoyl)phenyl)sulfonyl)piperidin-4-yl)amino)-2-oxoethyl) piperazine-1-carboxylate (**10c**).* White solid, yield: 68%. ^{1}H NMR (400 MHz, DMSO-d_6) δ 10.79 (s, 1H), 8.34 (ddd, J = 13.1, 6.5, 2.3 Hz, 2H), 7.95−7.83 (m, 1H), 7.77−7.67 (m, 3H), 3.67 (ddd, J = 37.0, 7.9, 3.9 Hz, 5H), 3.48−3.41 (m, 3H), 3.14 (dt, J = 10.0, 5.1 Hz, 3H), 2.81 (t, J = 11.5 Hz, 2H), 2.59−2.53 (m, 2H), 1.85−1.75 (m, 2H), 1.55−1.45 (m, 2H), 1.39 (s, 9H). ESI-MS: *m/z* 658.03 $[M+H]^+$, 656.42 $[M-H]^-$. $C_{29}H_{35}F_4N_5O_6S$ [657.22].

*4.1.12.4. tert-Butyl 3-((1-((2-fluoro-5-((3,4,5-trifluorophenyl) carbamoyl)phenyl)sulfonyl)piperidin-4-yl)carbamoyl)piperidine-1-carboxylate (**10d**).* White solid, yield: 74%. ^{1}H NMR (400 MHz, DMSO-d_6) δ 10.82 (s, 1H), 8.39−8.29 (m, 2H), 7.97−7.87 (m, 1H), 7.77−7.67 (m, 3H), 3.87 (dd, J = 21.5, 9.1 Hz, 2H), 3.63 (dd, J = 19.4, 7.5 Hz, 3H), 2.82 (t, J = 11.1 Hz, 2H), 2.72−2.53 (m, 2H), 2.15 (tt, J = 11.0, 3.7 Hz, 1H), 1.78 (dt, J = 20.3, 11.6 Hz, 3H), 1.67−1.57 (m, 1H), 1.55−1.40 (m, 2H), 1.38 (s, 9H), 1.26 (ddd, J = 16.3, 8.3, 3.8 Hz, 2H). ESI-MS: *m/z* 642.84 $[M+H]^+$, 665.16 $[M+Na]^+$, 641.39 $[M-H]^-$. $C_{29}H_{34}F_4N_4O_6S$ [642.21].

*4.1.12.5. tert-Butyl 3-((1-((2-fluoro-5-((3,4,5-trifluorophenyl) carbamoyl)phenyl)sulfonyl)piperidin-4-yl)carbamoyl)pyrrolidine-1-carboxylate (**10e**).* White solid, yield: 72%. ^{1}H NMR (400 MHz, DMSO-d_6) δ 10.80 (s, 1H), 8.34 (ddd, J = 14.6, 5.5, 2.0 Hz, 2H), 7.94 (d, J = 7.7 Hz, 1H), 7.76−7.67 (m, 3H), 3.73−3.57 (m, 4H), 3.17 (dq, J = 25.4, 8.8, 8.3 Hz, 3H), 2.82 (t, J = 11.1 Hz, 3H), 1.98−1.85 (m, 2H), 1.81 (dd, J = 8.7, 4.6 Hz, 2H), 1.40 (d, J = 2.0 Hz, 2H), 1.38 (s, 9H). ESI-MS: *m/z* 651.12 $[M+Na]^+$, 627.39 $[M-H]^-$. $C_{28}H_{32}F_4N_4O_6S$ [628.20].

*4.1.12.6. tert-Butyl 3-(2-((1-((2-fluoro-5-((3,4,5-trifluorophenyl) carbamoyl)phenyl)sulfonyl)piperidin-4-yl)amino)-2-oxoethyl)pyrrolidine-1-carboxylate (**10f**).* White solid, yield: 62%. ^{1}H NMR (400 MHz, DMSO-d_6) δ 10.80 (s, 1H), 8.34 (dtd, J = 10.8, 5.5, 4.5, 2.0 Hz, 2H), 7.86 (d, J = 6.9 Hz, 1H), 7.72 (td, J = 8.2, 6.4, 3.7 Hz, 3H), 3.76−3.54 (m, 4H), 3.33−3.32 (m, 2H), 3.32−3.24 (m, 2H), 3.14 (p, J = 9.8 Hz, 1H), 2.89−2.79 (m, 3H), 2.11 (d, J = 6.6 Hz, 2H), 1.97−1.84 (m, 2H), 1.84−1.75 (m, 2H), 1.38 (s, 9H). ESI-MS: *m/z* 641.37 $[M-H]^-$, $C_{29}H_{34}F_4N_4O_6S$ [642.21].

*4.1.12.7. tert-Butyl 3-((1-((2-fluoro-5-((3,4,5-trifluorophenyl) carbamoyl)phenyl)sulfonyl)piperidin-4-yl)carbamoyl)azetidine-1-carboxylate (**10g**).* White solid, yield: 64%. ^{1}H NMR (400 MHz, DMSO-d_6) δ 10.84 (s, 1H), 8.38−8.29 (m, 2H), 8.00 (d, J = 7.5 Hz, 1H), 7.77−7.66 (m, 3H), 3.94−3.74 (m, 4H), 3.68 (dt, J = 6.9, 3.4 Hz, 1H), 3.60 (d, J = 12.4 Hz, 2H), 3.18 (ddd, J = 14.4, 8.5, 5.9 Hz, 1H), 2.82 (t, J = 11.1 Hz, 2H), 1.87−1.77 (m, 2H), 1.40−1.37 (m, 2H), 1.36 (s, 9H). ESI-MS: *m/z* 637.10 $[M+Na]^+$, 613.40 $[M-H]^-$. $C_{27}H_{30}F_4N_4O_6S$ [614.18].

*4.1.12.8. tert-Butyl (3-((1-((2-fluoro-5-((3,4,5-trifluorophenyl) carbamoyl)phenyl)sulfonyl)piperidin-4-yl)carbamoyl)cyclobutyl) carbamate (**10h**).* White solid, yield: 72%. ^{1}H NMR (400 MHz, DMSO-d_6) δ 10.79 (s, 1H), 8.38−8.28 (m, 2H), 7.76−7.66 (m, 4H), 7.11 (d, J = 7.9 Hz, 1H), 3.84−3.72 (m, 1H), 3.61 (d, J = 12.6 Hz, 3H), 2.79 (t, J = 10.6 Hz, 2H), 2.50−2.43 (m, 1H), 2.26−2.14 (m, 2H), 2.01−1.89 (m, 2H), 1.83−1.74 (m, 2H), 1.40−1.37 (m, 2H), 1.35 (s, 9H). ESI-MS: *m/z* 651.17 $[M+Na]^+$, 627.41 $[M-H]^-$. $C_{28}H_{32}F_4N_4O_6S$ [628.20].

*4.1.12.9. tert-Butyl 1-((1-((2-fluoro-5-((3,4,5-trifluorophenyl) carbamoyl)phenyl)sulfonyl)piperidin-4-yl)carbamoyl)-6-azaspiro [2.5]octane-6-carboxylate (**10i**).* White solid, yield: 61%. ^{1}H NMR (400 MHz, DMSO-d_6) δ 10.81 (s, 1H), 8.39−8.29 (m, 2H), 8.04 (d, J = 7.6 Hz, 1H), 7.71 (dd, J = 10.1, 6.6 Hz, 3H), 3.73−3.57 (m, 3H), 3.50−3.38 (m, 2H), 3.06−2.93 (m, 1H), 2.82 (t, J = 11.0 Hz, 2H), 1.87−1.75 (m, 2H), 1.58−1.43 (m, 4H), 1.38 (s, 9H), 1.38−1.31 (m, 2H), 1.27−1.15 (m, 2H), 0.95−0.90 (m, 1H), 0.71 (dd, J = 7.8, 3.9 Hz, 1H). ESI-MS: *m/z* 691.19 $[M+Na]^+$, 667.43 $[M-H]^-$. $C_{31}H_{36}F_4N_4O_6S$ [668.23].

*4.1.12.10. tert-Butyl 9-((1-((2-fluoro-5-((3,4,5-trifluorophenyl) carbamoyl)phenyl)sulfonyl)piperidin-4-yl)carbamoyl)-3-azaspiro [5.5]undecane-3-carboxylate (**10j**).* White solid, yield: 60%. ^{1}H NMR (400 MHz, DMSO-d_6) δ 10.80 (s, 1H), 8.33 (ddd, J = 13.2, 5.6, 2.1 Hz, 2H), 7.70 (ddd, J = 14.3, 10.7, 6.2 Hz, 4H), 3.69−3.57 (m, 3H), 3.30−3.22 (m, 4H), 2.80 (t, J = 11.0 Hz, 2H), 1.81−1.73 (m, 2H), 1.65 (d, J = 12.9 Hz, 2H), 1.44 (d, J = 8.2 Hz, 5H), 1.38 (s, 13H), 1.22−1.18 (m, 2H), 1.08−0.96 (m, 2H). ESI-MS: *m/z* 709.49 $[M-H]^-$, $C_{34}H_{42}F_4N_4O_6S$ [710.28].

4.1.12.11. tert-Butyl (4-((1-((2-fluoro-5-((3,4,5-trifluorophenyl) carbamoyl)phenyl)sulfonyl)piperidin-4-yl)carbamoyl)bicyclo

*[2.2.2]octan-1-yl)carbamate (**10k**).* White solid, yield: 67%. ^{1}H NMR (400 MHz, DMSO-d_6) δ 10.79 (s, 1H), 8.39−8.28 (m, 2H), 7.76−7.66 (m, 3H), 7.17 (d, J = 7.8 Hz, 1H), 6.37 (s, 1H), 3.72−3.57 (m, 3H), 2.75−2.66 (m, 2H), 1.68 (q, J = 9.9, 8.9 Hz, 14H), 1.45 (qd, J = 12.5, 12.0, 3.4 Hz, 2H), 1.35 (s, 9H). ESI-MS: m/z 681.47 $[M-H]^-$, $C_{32}H_{38}F_4N_4O_6S$ [682.24].

*4.1.12.12. tert-Butyl 6-((1-((2-fluoro-5-((3,4,5-trifluorophenyl) carbamoyl)phenyl)sulfonyl)piperidin-4-yl)carbamoyl)-3-azabicyclo[3.1.0]hexane-3-carboxylate (**10l**).* White solid, yield: 65%. ^{1}H NMR (400 MHz, DMSO-d_6) δ 10.79 (s, 1H), 8.39−8.29 (m, 2H), 8.05 (d, J = 7.6 Hz, 1H), 7.76−7.66 (m, 3H), 3.71−3.62 (m, 1H), 3.62−3.53 (m, 2H), 3.45 (d, J = 11.4 Hz, 2H), 3.27 (d, J = 12.1 Hz, 3H), 2.84 (t, J = 10.9 Hz, 2H), 1.87−1.75 (m, 4H), 1.44−1.39 (m, 1H), 1.37 (s, 9H), 1.31 (t, J = 3.0 Hz, 1H). ESI-MS: m/z 663.13 $[M+Na]^+$, 639.37 $[M-H]^-$. $C_{29}H_{32}F_4N_4O_6S$ [640.20].

*4.1.12.13. tert-Butyl 4-(4-((1-((2-fluoro-5-((3,4,5-trifluorophenyl)carbamoyl)phenyl)sulfonyl)piperidin-4-yl)carbamoyl)phenyl)piperidine-1-carboxylate (**10m**).* White solid, yield: 70%. ^{1}H NMR (400 MHz, DMSO-d_6) δ 10.81 (s, 1H), 8.40−8.30 (m, 2H), 8.23 (d, J = 7.7 Hz, 1H), 7.73 (dd, J = 10.3, 5.7 Hz, 5H), 7.32 (d, J = 8.2 Hz, 2H), 3.73 (d, J = 12.3 Hz, 2H), 3.62 (dt, J = 13.1, 6.5 Hz, 2H), 3.14 (q, J = 7.5 Hz, 2H), 2.81 (t, J = 11.5 Hz, 4H), 1.88 (d, J = 10.3 Hz, 2H), 1.74 (d, J = 11.3 Hz, 2H), 1.67−1.61 (m, 2H), 1.49 (dd, J = 12.6, 3.7 Hz, 2H), 1.41 (s, 9H). ESI-MS: m/z 741.21 $[M+Na]^+$, 717.45 $[M-H]^-$. $C_{35}H_{38}F_4N_4O_6S$ [718.24].

*4.1.12.14. tert-Butyl 4-(4-((1-((2-fluoro-5-((3,4,5-trifluorophenyl)carbamoyl)phenyl)sulfonyl)piperidin-4-yl)carbamoyl)phenyl)piperazine-1-carboxylate (**10n**).* White solid, yield: 72%. ^{1}H NMR (400 MHz, DMSO-d_6) δ 10.81 (s, 1H), 8.42−8.30 (m, 2H), 8.03 (d, J = 7.7 Hz, 1H), 7.75−7.69 (m, 5H), 6.94 (d, J = 8.9 Hz, 2H), 3.86 (dt, J = 7.1, 4.0 Hz, 1H), 3.73 (d, J = 11.8 Hz, 2H), 3.62 (dt, J = 11.3, 5.0 Hz, 2H), 3.50−3.41 (m, 4H), 3.29−3.19 (m, 4H), 1.93−1.82 (m, 2H), 1.55 (td, J = 12.8, 12.2, 2.7 Hz, 2H), 1.42 (s, 9H). ESI-MS: m/z 718.45 $[M-H]^-$, $C_{34}H_{37}F_4N_5O_6S$ [719.24].

*4.1.13. General procedure for the synthesis of **HyT-(S16−S29)*** Intermediates **10 (a−n)** were subjected to deprotection with HCl (4.0 mol/L in 1,4-dioxane, 10.0 equiv.) to afford intermediates **11(a−n)**, which were used without further purification. 1-Adamantaneacetic acid (1.2 equiv.) and HATU (1.5 equiv.) were mixed in 30 mL of DCM and stirred in an ice bath for 30 min. Subsequently, DIEA (2.0 equiv.) and intermediates **11(a−n)** (1.0 equiv.) were added to the mixture and then stirred at room temperature (monitored by TLC). The resulting mixture was evaporated under reduced pressure, and the residue was initially washed with 1 mol/L HCl and extracted with ethyl acetate (3 × 20 mL). Then, the combined organic layer was washed with saturated sodium bicarbonate (3 × 20 mL), dried over anhydrous Na_2SO_4, filtered, and concentrated under reduced pressure to afford the corresponding crude product, which was purified by flash column chromatography (ethyl acetate) to afford the target compounds **HyT-(S16−S29)**.

*4.1.13.1. 1-(2-((1S,3S)-Adamantan-1-yl)acetyl)-N-(1-((2-fluoro-5-((3,4,5-trifluorophenyl)carbamoyl)phenyl)sulfonyl)piperidin-4-yl)piperidine-4-carboxamide (**HyT-S16**).* White solid, yield: 52%. Mp: 198−199 °C. ^{1}H NMR (400 MHz, DMSO-d_6) δ 10.82 (s, 1H, NH), 8.35 (d, J = 6.4 Hz, 1H, NH), 8.34−8.30 (m, 1H, Ph-H), 7.83 (d, J = 7.6 Hz, 1H, Ph-H), 7.77−7.68 (m, 3H, Ph-H), 4.42 (d, J = 12.9 Hz, 1H), 3.97 (d, J = 12.9 Hz, 1H), 3.70−3.57 (m, 4H), 3.13 (dd, J = 10.1, 4.5 Hz, 1H), 2.96 (t, J = 11.7 Hz, 1H), 2.81 (t, J = 11.1 Hz, 2H), 2.47 (d, J = 12.2 Hz, 1H), 2.08 (q, J = 13.5 Hz, 2H), 1.90 (s, 3H), 1.82−1.74 (m, 2H), 1.60 (d, J = 19.2 Hz, 15H), 1.43−1.37 (m, 2H). ^{13}C NMR (150 MHz, DMSO-d_6) δ 173.74, 168.77, 164.01, 160.68 (d, J = 259.9 Hz), 150.43 (d, J = 249.3 Hz), 135.80 (d, J = 9.7 Hz), 131.33 (d, J = 2.9 Hz), 130.90, 125.87 (d, J = 15.9 Hz), 118.62 (d, J = 22.7 Hz), 105.44, 105.35 (dd, J = 25.4, 5.0 Hz), 105.27, 46.21, 45.49, 44.82, 44.71, 42.56, 42.17, 40.81, 36.87, 33.43, 31.30, 29.48, 28.89, 28.55. HRMS (ESI): m/z Calcd. for $C_{36}H_{42}F_4N_4O_5NaS$ $[M+Na]^+$ 741.2710; found 741.2712. HPLC purity: 95.6%.

*4.1.13.2. 3-((4-(2-(1-(2-((3R,5R,7R)-Adamantan-1-yl)acetyl) piperidin-4-yl)acetamido)piperidin-1-yl)sulfonyl)-4-fluoro-N-(3,4,5-trifluorophenyl)benzamide (**HyT-S17**).* White solid, yield: 57%. Mp: 171−172 °C. ^{1}H NMR (400 MHz, DMSO-d_6) δ 10.81 (s, 1H, NH), 8.35 (d, J = 6.4 Hz, 1H, NH), 8.34−8.30 (m, 1H, Ph-H), 7.81 (d, J = 7.5 Hz, 1H, Ph-H), 7.76−7.66 (m, 3H, Ph-H), 4.38 (d, J = 13.9 Hz, 1H), 3.92 (d, J = 14.0 Hz, 1H), 3.73−3.54 (m, 4H), 3.14 (dd, J = 4.3, 2.6 Hz, 1H), 2.94 (t, J = 12.2 Hz, 1H), 2.83 (t, J = 11.0 Hz, 2H), 2.48−2.41 (m, 1H), 2.14−1.99 (m, 2H), 1.96 (d, J = 7.0 Hz, 2H), 1.90 (s, 3H), 1.84−1.76 (m, 2H), 1.61 (d, J = 20.4 Hz, 13H), 1.39 (q, J = 9.2, 7.8 Hz, 2H), 0.95 (dqd, J = 36.8, 12.6, 4.2 Hz, 2H). ^{13}C NMR (150 MHz, DMSO-d_6) δ 170.66, 168.68, 164.01, 160.67 (d, J = 259.4 Hz), 150.43 (d, J = 250.3 Hz), 135.80 (d, J = 9.4 Hz), 131.32 (d, J = 2.7 Hz), 130.91, 125.88 (d, J = 15.9 Hz), 118.60 (d, J = 22.4 Hz), 105.44, 105.35 (dd, J = 25.6, 4.9 Hz), 105.27, 54.00, 46.72, 45.50, 44.86, 44.66, 42.58, 42.25, 41.31, 36.88, 33.51, 33.43, 32.71, 31.96, 31.36, 31.34, 28.55, 18.53, 17.20, 12.90. HRMS (ESI): m/z Calcd. for $C_{37}H_{44}F_4N_4O_5NaS$ $[M+Na]^+$ 755.2866; found 755.2857. HPLC purity: 98.3%.

*4.1.13.3. 3-((4-(2-(4-(2-((3R,5R,7R)-Adamantan-1-yl)acetyl) piperazin-1-yl)acetamido)piperidin-1-yl)sulfonyl)-4-fluoro-N-(3,4,5-trifluorophenyl)benzamide (**HyT-S18**).* White solid, yield: 63%. Mp: 99−100 °C. ^{1}H NMR (400 MHz, DMSO-d_6) δ 10.81 (s, 1H, NH), 8.35 (d, J = 6.6 Hz, 1H, NH), 8.32 (dd, J = 5.3, 3.1 Hz, 1H, Ph-H), 7.76−7.66 (m, 4H, Ph-H), 3.72 (ddd, J = 10.4, 7.3, 4.3 Hz, 1H), 3.62 (d, J = 11.4 Hz, 4H), 3.12 (dd, J = 9.6, 4.9 Hz, 1H), 2.91 (s, 2H), 2.79 (t, J = 11.4 Hz, 2H), 2.43−2.30 (m, 4H), 2.08 (s, 2H), 1.90 (s, 3H), 1.82−1.75 (m, 2H), 1.61 (d, J = 20.0 Hz, 13H), 1.55−1.46 (m, 2H). ^{13}C NMR (150 MHz, DMSO-d_6) δ 168.99, 164.03, 160.68 (d, J = 259.5 Hz), 150.44 (d, J = 252.6 Hz), 135.73 (d, J = 9.9 Hz), 131.38 (d, J = 2.9 Hz), 130.90, 125.94 (d, J = 15.8 Hz), 118.55 (d, J = 22.9 Hz), 105.47, 105.39 (dd, J = 24.9, 5.4 Hz), 105.31, 54.08, 53.47, 53.08, 46.53, 45.37, 44.94, 44.84, 42.62, 36.90, 33.48, 31.24, 28.58. HRMS (ESI): m/z Calcd. for $C_{36}H_{43}F_4N_5O_5NaS$ $[M+Na]^+$ 756.2819; found 756.2813. HPLC purity: 98.3%.

*4.1.13.4. 1-(2-((3R,5R,7R)-Adamantan-1-yl)acetyl)-N-(1-((2-fluoro-5-((3,4,5-trifluorophenyl)carbamoyl)phenyl)sulfonyl)piperidin-4-yl)piperidine-3-carboxamide (**HyT-S19**).* White solid, yield: 71%. Mp: 186−187 °C. ^{1}H NMR (400 MHz, DMSO-d_6) δ 10.81 (s, 1H, NH), 8.35 (d, J = 6.9 Hz, 1H, NH), 8.34−8.28 (m, 1H, Ph-H), 7.89 (dd, J = 11.8, 7.6 Hz, 1H, Ph-H), 7.72 (td,

J = 8.2, 6.4, 3.5 Hz, 3H, Ph-H), 4.29 (dd, J = 54.6, 12.4 Hz, 1H), 3.85 (dd, J = 35.0, 13.7 Hz, 1H), 3.67−3.57 (m, 4H), 3.18−3.10 (m, 1H), 2.99−2.88 (m, 1H), 2.82 (t, J = 11.2 Hz, 2H), 2.60−2.53 (m, 1H), 2.10 (dd, J = 16.1, 4.9 Hz, 2H), 1.90 (s, 3H), 1.82−1.76 (m, 2H), 1.61 (d, J = 19.0 Hz, 15H), 1.44−1.36 (m, 2H). ^{13}C NMR (150 MHz, DMSO-d_6) δ 172.56, 169.01, 164.02, 160.67 (d, J = 259.7 Hz), 150.46 (d, J = 248.4 Hz), 135.75 (d, J = 8.9 Hz), 131.37 (d, J = 3.0 Hz), 130.86, 126.10 (d, J = 15.3 Hz), 118.57 (d, J = 23.0 Hz), 105.48, 105.40 (dd, J = 24.7, 4.5 Hz), 105.31, 54.14, 45.51, 44.65, 42.60, 42.34, 36.91, 33.40, 31.32, 28.59, 18.59, 17.23. HRMS (ESI): *m/z* Calcd. for $C_{36}H_{42}F_4N_4O_5NaS$ $[M+Na]^+$ 741.2710; found 741.2704. HPLC purity: 98.5%.

*4.1.13.5. 1-(2-((1S,3S)-Adamantan-1-yl)acetyl)-N-(1-((2-fluoro-5-((3,4,5-trifluorophenyl)carbamoyl)phenyl)sulfonyl)piperidin-4-yl)pyrrolidine-3-carboxamide (**HyT-S20**).* White solid, yield: 62%. Mp: 140−141 °C. ^{1}H NMR (400 MHz, DMSO-d_6) δ 10.81 (s, 1H, NH), 8.36 (d, J = 6.7 Hz, 1H, NH), 8.32 (dd, J = 5.9, 2.6 Hz, 1H, Ph-H), 7.97 (dd, J = 13.7, 7.6 Hz, 1H, Ph-H), 7.76−7.68 (m, 3H, Ph-H), 3.64 (td, J = 13.2, 12.2, 5.8 Hz, 4H), 3.49 (dd, J = 11.6, 7.9 Hz, 1H), 3.43 (d, J = 8.8 Hz, 1H), 3.24 (dt, J = 11.7, 5.7 Hz, 1H), 3.16 (ddt, J = 11.7, 7.3, 3.8 Hz, 1H), 2.89 (dd, J = 17.4, 9.6 Hz, 1H), 2.84−2.77 (m, 2H), 1.97 (t, J = 3.3 Hz, 2H), 1.90 (s, 3H), 1.85−1.78 (m, 2H), 1.62 (d, J = 13.3 Hz, 13H), 1.47−1.34 (m, 2H). ^{13}C NMR (150 MHz, DMSO-d_6) δ 171.47, 168.95, 164.02, 160.67 (d, J = 259.8 Hz), 150.46 (d, J = 249.1 Hz), 135.75 (d, J = 9.6 Hz), 131.37 (d, J = 3.0 Hz), 130.88, 126.06 (d, J = 15.0 Hz), 118.57 (d, J = 22.8 Hz), 105.39 (d, J = 25.6, 5.4 Hz), 125.91 (d, J = 15.5 Hz), 118.61 (d, J = 23.3 Hz), 105.48, 105.34 (dd, J = 25.4, 4.9 Hz), 105.31, 50.04, 48.59, 47.64, 47.48, 47.15, 45.33, 45.18, 45.11, 44.67, 44.66, 44.32, 42.49, 42.36, 36.94, 33.42, 31.31, 31.27, 29.95, 28.56, 28.41. HRMS (ESI): *m/z* Calcd. for $C_{35}H_{40}F_4N_4O_5NaS$ $[M+Na]^+$ 727.2553; found 727.2555. HPLC purity: 99.6%.

*4.1.13.6. 3-((4-(2-(1-(2-((1S,3S)-Adamantan-1-yl)acetyl)pyrrolidin-3-yl)acetamido)piperidin-1-yl)sulfonyl)-4-fluoro-N-(3,4,5-trifluorophenyl)benzamide (**HyT-S21**).* White solid, yield: 61%. Mp: 102−103 °C. ^{1}H NMR (400 MHz, DMSO-d_6) δ 10.81 (s, 1H, NH), 8.35 (d, J = 6.9 Hz, 1H, NH), 8.34−8.29 (m, 1H, Ph-H), 7.88 (dd, J = 10.8, 7.7 Hz, 1H, Ph-H), 7.77−7.68 (m, 3H, Ph-H), 3.73−3.53 (m, 4H), 3.51−3.43 (m, 1H), 3.18 (dt, J = 11.9, 7.8 Hz, 1H), 3.03 (dd, J = 10.0, 7.6 Hz, 1H), 2.87−2.80 (m, 2H), 2.38 (ddt, J = 40.9, 15.0, 7.3 Hz, 1H), 2.16−2.09 (m, 2H), 1.95 (d, J = 5.9 Hz, 2H), 1.90 (s, 3H), 1.85−1.76 (m, 2H), 1.61 (d, J = 13.8 Hz, 13H), 1.46−1.32 (m, 3H). ^{13}C NMR (150 MHz, DMSO-d_6) δ 170.57, 169.02, 164.00, 163.99, 160.67 (d, J = 259.9 Hz), 150.43 (d, J = 248.5 Hz), 135.80 (d, J = 10.0 Hz), 131.32 (dd, J = 2.8 Hz), 130.88, 125.91 (d, J = 15.5 Hz), 118.61 (d, J = 23.0 Hz), 105.42, 105.34 (dd, J = 25.4, 4.9 Hz), 105.25, 52.58, 50.79, 47.69, 47.35, 46.82, 44.90, 44.87, 44.67, 44.64, 42.49, 42.45, 39.12, 38.76, 36.91, 36.90, 36.42, 34.62, 33.39, 33.36, 31.80, 31.33, 29.90, 28.52. HRMS (ESI): *m/z* Calcd. for $C_{36}H_{42}F_4N_4O_5NaS$ $[M+Na]^+$ 741.2710; found 741.2713. HPLC purity: 98.6%.

*4.1.13.7. 1-(2-((1S,3S)-Adamantan-1-yl)acetyl)-N-(1-((2-fluoro-5-((3,4,5-trifluorophenyl)carbamoyl)phenyl)sulfonyl)piperidin-4-yl)azetidine-3-carboxamide (**HyT-S22**).* White solid, yield: 70%. Mp: 157−158 °C. ^{1}H NMR (400 MHz, DMSO-d_6) δ 10.79 (s, 1H, NH), 8.35 (d, J = 6.7 Hz, 1H, NH), 8.34−8.29 (m, 1H, Ph-H), 7.99 (d, J = 7.5 Hz, 1H, Ph-H), 7.71 (td, J = 8.3, 6.5, 4.0 Hz, 3H, Ph-H), 4.15 (t, J = 8.4 Hz, 1H), 4.09−4.03 (m, 1H), 3.88 (t, J = 9.2 Hz, 1H), 3.75 (dd, J = 9.3, 5.9 Hz, 1H), 3.72−3.65 (m, 1H), 3.61 (d, J = 12.3 Hz, 2H), 3.19 (dq, J = 11.2, 4.3, 2.5 Hz, 1H), 2.83 (t, J = 11.1 Hz, 2H), 1.90 (s, 3H), 1.81 (dd, J = 14.8, 7.3 Hz, 2H), 1.75 (s, 2H), 1.69−1.52 (m, 12H), 1.46−1.32 (m, 2H). ^{13}C NMR (150 MHz, DMSO-d_6) δ 171.17, 170.64, 164.02, 160.67 (d, J = 259.5 Hz), 150.46 (d, J = 248.1 Hz), 135.75 (d, J = 9.5 Hz), 131.38 (d, J = 3.0 Hz), 130.87, 126.05 (d, J = 15.7 Hz), 118.58 (d, J = 22.8 Hz), 105.48, 105.39 (dd, J = 25.4, 5.7 Hz), 105.31, 53.09, 50.28, 45.27, 44.65, 42.44, 36.86, 33.17, 31.78, 31.26, 31.24, 28.51. HRMS (ESI): *m/z* Calcd. for $C_{34}H_{38}F_4N_4O_5NaS$ $[M+Na]^+$ 713.2397; found 713.2397. HPLC purity: 99.5%.

*4.1.13.8. 3-((4-(3-(2-((3R,5R,7R)-Adamantan-1-yl)acet amido) cyclobutane-1-carboxamido)piperidin-1-yl)sulfonyl)-4-fluoro-N-(3,4,5-trifluorophenyl)benzamide (**HyT-S23**).* White solid, yield: 59%. Mp: >200 °C. ^{1}H NMR (400 MHz, DMSO-d_6) δ 10.80 (s, 1H, NH), 8.35 (d, J = 6.4 Hz, 1H, NH), 8.31 (d, J = 3.5 Hz, 1H, Ph-H), 7.96 (d, J = 8.1 Hz, 1H, NH), 7.80−7.65 (m, 4H, Ph-H), 4.05 (h, J = 8.3, 7.8 Hz, 1H), 3.60 (d, J = 12.2 Hz, 3H), 2.80 (t, J = 11.1 Hz, 2H), 2.56 (dd, J = 17.4, 9.5 Hz, 1H), 2.23 (p, J = 9.0, 7.5 Hz, 2H), 2.01−1.92 (m, 2H), 1.89 (s, 3H), 1.77 (d, J = 14.9 Hz, 4H), 1.68−1.47 (m, 12H), 1.44−1.30 (m, 2H). ^{13}C NMR (150 MHz, DMSO-d_6) δ 172.82, 169.52, 164.00, 160.68 (d, J = 259.6 Hz), 150.43 (d, J = 249.0 Hz), 135.80 (d, J = 9.7 Hz), 131.32 (d, J = 2.6 Hz), 130.89, 125.81 (d, J = 15.6 Hz), 118.62 (d, J = 23.1 Hz), 105.43, 105.35 (dd, J = 25.4, 4.9 Hz), 105.26, 50.19, 45.01, 44.76, 42.55, 36.93, 33.84, 32.65, 32.44, 31.31, 28.49. HRMS (ESI): *m/z* Calcd. for $C_{35}H_{40}F_4N_4O_5NaS$ $[M+Na]^+$ 727.2553; found 727.2548. HPLC purity: 97.6%.

*4.1.13.9. 6-(2-((3R,5R,7R)-Adamantan-1-yl)acetyl)-N-(1-((2-fluoro-5-((3,4,5-trifluorophenyl)carbamoyl)phenyl)sulfonyl)piperidin-4-yl)-6-azaspiro[2.5]octane-1-carboxamide (**HyT-S24**).* White solid, yield: 52%. Mp: 128−129 °C. ^{1}H NMR (400 MHz, DMSO-d_6) δ 10.85 (s, 1H, NH), 8.34 (dd, J = 9.1, 3.9 Hz, 2H, NH, Ph-H), 8.12−8.05 (m, 1H, Ph-H), 7.78−7.67 (m, 3H, Ph-H), 3.69 (dd, J = 18.6, 4.2 Hz, 5H), 3.13 (q, J = 7.1, 6.6 Hz, 4H), 2.82 (dd, J = 6.2, 3.2 Hz, 1H), 2.10 (q, J = 7.2, 6.3 Hz, 2H), 1.90 (s, 3H), 1.85−1.75 (m, 2H), 1.61 (dd, J = 23.6, 8.1 Hz, 13H), 1.52−1.32 (m, 7H). HRMS (ESI): *m/z* Calcd. for $C_{38}H_{44}F_4N_4O_5NaS$ $[M+Na]^+$ 767.2866; found 767.2861. HPLC purity: 98.3%.

*4.1.13.10. 3-(2-((1S,3S)-Adamantan-1-yl)acetyl)-N-(1-((2-fluoro-5-((3,4,5-trifluorophenyl)carbamoyl)phenyl)sulfonyl)piperidin-4-yl)-3-azaspiro[5.5]undecane-9-carboxamide (**HyT-S25**).* White solid, yield: 46%. Mp: >200 °C. ^{1}H NMR (400 MHz, DMSO-d_6) δ 10.89 (s, 1H, NH), 8.40−8.32 (m, 2H, NH, Ph-H), 7.72 (ddd, J = 14.0, 8.5, 5.9 Hz, 4H, Ph-H), 3.69−3.55 (m, 4H), 2.80 (t, J = 11.5 Hz, 2H), 2.07 (s, 2H), 2.04−1.94 (m, 2H), 1.90 (s, 3H), 1.82−1.73 (m, 2H), 1.72−1.54 (m, 14H), 1.52−1.32 (m, 9H), 1.30−1.21 (m, 2H), 1.21−1.15 (m, 1H), 1.10−0.98 (m, 2H). HRMS (ESI): *m/z* Calcd. for $C_{41}H_{50}F_4N_4O_5NaS$ $[M+Na]^+$ 809.3336; found 809.3337. HPLC purity: 98.5%.

*4.1.13.11. 4-(2-((3R,5R,7R)-adamantan-1-yl)acetamido)-N-(1-((2-fluoro-5-((3,4,5-trifluorophenyl)carbamoyl)phenyl)sulfonyl)piperidin-4-yl)bicyclo[2.2.2]octane-1-carboxamide (**HyT-S26**).* White

solid, yield: 48%. Mp: >200 °C. ^{1}H NMR (400 MHz, DMSO-d_6) δ 10.79 (s, 1H, NH), 8.34 (d, J = 6.6 Hz, 1H, NH), 8.31 (dd, J = 4.0, 2.1 Hz, 1H, Ph-H), 7.71 (t, J = 8.3 Hz, 3H, Ph-H), 7.16 (d, J = 7.6 Hz, 1H, Ph-H), 7.12 (s, 1H, NH), 3.73−3.50 (m, 4H), 2.75−2.65 (m, 2H), 1.89 (s, 3H), 1.75 (d, J = 12.2 Hz, 9H), 1.71−1.60 (m, 10H), 1.55 (d, J = 14.2 Hz, 9H), 1.43 (dd, J = 18.0, 6.8 Hz, 2H). ^{13}C NMR (150 MHz, DMSO-d_6) δ 176.35, 170.27, 164.01, 160.68 (d, J = 259.8 Hz), 150.43 (d, J = 248.8 Hz), 135.76 (d, J = 9.3 Hz), 131.30 (d, J = 3.0 Hz), 130.87, 125.85 (d, J = 15.6 Hz), 118.60 (d, J = 22.7 Hz), 105.42, 105.34 (dd, J = 25.3, 5.1 Hz), 105.26, 50.87, 50.30, 45.38, 45.16, 42.55, 37.98, 36.99, 32.66, 31.26, 29.98, 28.80, 28.53. HRMS (ESI): *m/z* Calcd. for $C_{39}H_{46}F_4N_4O_5NaS$ $[M+Na]^+$ 781.3023; found 781.3019. HPLC purity: 97.7%.

*4.1.13.12. 3-(2-((1S,3S)-Adamantan-1-yl)acetyl)-N-(1-((2-fluoro-5-((3,4,5-trifluorophenyl)carbamoyl)phenyl)sulfonyl)piperidin-4-yl)-3-azabicyclo[3.1.0]hexane-6-carboxamide (**HyT-S27**).* White solid, yield: 36%. Mp: 163−164 °C. ^{1}H NMR (400 MHz, DMSO-d_6) δ 10.80 (s, 1H, NH), 8.44−8.15 (m, 2H, NH, Ph-H), 8.07 (d, J = 7.5 Hz, 1H, Ph-H), 7.79−7.63 (m, 2H, Ph-H), 7.51 (dd, J = 8.4, 4.4 Hz, 1H, Ph-H), 3.71−3.49 (m, 4H), 3.28−3.22 (m, 1H), 3.18−3.09 (m, 1H), 2.82 (t, J = 11.2 Hz, 1H), 1.97−1.92 (m, 4H), 1.90 (s, 3H), 1.85−1.77 (m, 2H), 1.61 (d, J = 26.4 Hz, 15H), 1.46−1.33 (m, 2H). ^{13}C NMR (100 MHz, DMSO-d_6) δ 170.09, 169.89, 164.00, 160.67 (d, J = 259.5 Hz), 150.42 (d, J = 248.8 Hz), 135.84 (d, J = 9.8 Hz), 131.32 (d, J = 3.3 Hz), 130.94, 125.74 (d, J = 15.6 Hz), 118.63 (d, J = 22.8 Hz), 105.47, 105.35 (dd, J = 25.1, 5.5 Hz), 105.22, 53.99, 49.40, 47.66, 44.98, 44.65, 42.41, 42.25, 36.87, 33.42, 31.38, 31.31, 28.49, 25.66, 24.94, 23.61, 18.52, 17.18, 12.91. HRMS (ESI): *m/z* Calcd. for $C_{36}H_{40}F_4N_4O_5NaS$ $[M+Na]^+$ 739.2553; found 739.2545. HPLC purity: 97.8%.

*4.1.13.13. 3-((4-(4-(1-(2-((1S,3S)-Adamantan-1-yl)acetyl)piperidin-4-yl)benzamido)piperidin-1-yl)sulfonyl)-4-fluoro-N-(3,4,5-trifluorophenyl)benzamide (**HyT-S28**).* White solid, yield: 60%. Mp: 179−180 °C. ^{1}H NMR (400 MHz, DMSO-d_6) δ 10.80 (s, 1H, NH), 8.37 (d, J = 6.5 Hz, 1H, NH), 8.35−8.30 (m, 1H, Ph-H), 8.23 (d, J = 7.7 Hz, 1H, Ph-H), 7.78−7.67 (m, 5H, Ph-H), 7.31 (d, J = 8.1 Hz, 2H, Ph-H), 4.62 (d, J = 12.6 Hz, 1H), 4.10 (d, J = 13.4 Hz, 1H), 3.88 (dq, J = 11.0, 7.3, 5.5 Hz, 1H), 3.73 (d, J = 12.0 Hz, 2H), 3.09 (t, J = 12.4 Hz, 1H), 2.81 (t, J = 11.7 Hz, 3H), 2.56 (t, J = 12.2 Hz, 1H), 2.23 (d, J = 13.5 Hz, 1H), 2.03 (d, J = 13.6 Hz, 1H), 1.89 (d, J = 18.8 Hz, 5H), 1.84−1.73 (m, 2H), 1.63 (q, J = 13.1, 12.6 Hz, 14H), 1.54−1.39 (m, 2H). ^{13}C NMR (150 MHz, DMSO-d_6) δ 168.84, 166.07, 164.03, 160.70 (d, J = 259.6 Hz), 150.43 (d, J = 248.8 Hz), 149.36, 135.80 (d, J = 10.0 Hz), 133.02, 131.33 (d, J = 3.1 Hz), 130.89, 127.95, 127.00, 125.90 (d, J = 15.4 Hz), 118.63 (d, J = 22.9 Hz), 105.44, 105.35 (dd, J = 25.3, 4.8 Hz), 105.27, 47.19, 45.96, 45.59, 45.11, 42.60, 42.09, 41.74, 36.90, 33.86, 33.50, 33.04, 31.34, 28.57. HRMS (ESI): *m/z* Calcd. for $C_{42}H_{46}F_4N_4O_5NaS$ $[M+Na]^+$ 817.3023; found 817.3021. HPLC purity: 97.9%.

*4.1.13.14. 3-((4-(4-(4-(2-((1S,3S)-Adamantan-1-yl)acetyl)piperazin-1-yl)benzamido)piperidin-1-yl)sulfonyl)-4-fluoro-N-(3,4,5-trifluorophenyl)benzamide (**HyT-S29**).* White solid, yield: 59%. Mp: 244−245 °C. ^{1}H NMR (400 MHz, DMSO-d_6) δ 10.81 (s, 1H, NH), 8.37 (d, J = 6.6 Hz, 1H, NH), 8.35−8.29 (m, 1H, Ph-H), 8.03 (d, J = 7.5 Hz, 1H, Ph-H), 7.72 (dt, J = 8.9, 5.0 Hz, 5H, Ph-H), 6.94 (d, J = 8.7 Hz, 2H, Ph-H), 3.92−3.80 (m, 1H), 3.73 (d, J = 12.3 Hz, 2H), 3.68−3.57 (m, 4H), 3.27−3.19 (m, 4H), 2.79 (t, J = 11.7 Hz, 2H), 2.14 (s, 2H), 1.89 (d, J = 21.8 Hz, 5H), 1.62 (q, J = 14.1, 13.5 Hz, 14H). ^{13}C NMR (150 MHz, DMSO-d_6) δ 169.16, 165.83, 164.06, 160.71 (d, J = 260.4 Hz), 152.93, 150.46 (d, J = 248.2 Hz), 135.74 (d, J = 9.9 Hz), 131.37 (d, J = 2.9 Hz), 130.87, 129.07, 125.98 (d, J = 11.8 Hz), 124.60, 118.59 (d, J = 22.2 Hz), 114.20, 105.42 (dd, J = 24.5, 4.6 Hz), 48.13, 47.75, 46.30, 46.17, 45.92, 45.44, 45.18, 42.62, 40.99, 36.90, 33.50, 31.49, 28.58. HRMS (ESI): *m/z* Calcd. for $C_{41}H_{45}F_4N_5O_5NaS$ $[M+Na]^+$ 818.2975; found 818.2981. HPLC purity: 97.6%.

4.2. Cell culture and reagents

Human hepatoblastoma cell line HepG2 was maintained in MEM medium (Invitrogen, Carlsbad, CA, USA) supplemented with 10% fetal bovine serum (Gibco, Grand Island, PA, USA), 100 U/mL penicillin (Invitrogen, Waltham, MA, USA) and 100 μg/mL streptomycin (Invitrogen). HepAD38 cell line, which can support replication of the HBV genome in a tetracycline-inducible manner, was maintained in DMEM medium (Invitrogen) supplemented with 10% fetal bovine serum (Gibco), 100 U/mL penicillin, 100 μg/mL streptomycin, 1 μg/mL tetracycline (Sigma−Aldrich, St. Louis, MO, USA) and 400 μg/mL G-418 (Gibco). Bay 41-4109 (HY-100029), lamivudine (3TC, HY-B0250), 3-MA (HY-19312), and MG132 (HY-13259) were purchased from MedChemExpress (Monmouth Junction, NJ, USA). Bortezomib (S1013), Hydroxychloroquine sulfate (S4430), and 17-AAG (S1141) were purchased from SelleckChem (Houston, TX, USA). NVR 3-778 was synthesized in-house.

4.3. In vitro anti-HBV assay in HepAD38 cells

The synthesized compounds were initially evaluated for their inhibitory effect on the replication of HBV in HepAD38 cell lines. Briefly, cells were plated into 48-well culture plates overnight followed by incubating with a serial dilution of compounds in the absence of tetracycline. After 4−6 days of treatment, the cells were lysed with a buffer containing 10 mmol/L Tris−HCl (pH 8.0), 1 mmol/L EDTA, and 1% NP-40. Cytoplasmic HBV core DNA was extracted and quantified by a real-time PCR assay using TransStart Tip Green qPCR SuperMix (TransGen Biotech, Beijing, China), as described previously[42]. The antiviral efficacy of a compound was expressed as the half maximal effective concentration (EC_{50}) in comparison with the levels of the mock-treated controls.

The cytotoxicity of the compounds on HepAD38 cells was analyzed using the cytopathic effect (CPE) method. The cytotoxicity of a compound was expressed as the concentration that reduced the viability of the cells by 50% (CC_{50}). Both EC_{50} and CC_{50} were determined using the Reed & Muench method.

4.4. Plasmids and cell transfection

The pHBV1.3, pHBV1.3-derived plasmids expressing mutant core proteins with V124F or V124W mutation, pCMV-HBC, and pCMV-HBC-derived plasmids expressing P25A, P25G, D29A/D29L, D29W, T33N, I105F, I105W, I105Y, or T109A were gifts of Dr. Ju-Tao Guo at the Baruch S. Blumberg Institute and have been described previously[42−44].

HepG2 cells were seeded in 24-well plates and grown to approximately 80% confluence. Cells were then transfected with 0.25 μg desired plasmid(s) using 1.5 μL Lipofectamine 3000 (Invitrogen) per well. 6 h post-transfection, the culture media were replaced with fresh media or media containing the desired concentration of compounds and cultured for an additional 18 h. Intracellular HBV core protein was examined with the Western blot assay.

4.5. Western blot assay

Western blot was carried out as described previously[45]. Cells were lysed in an M-PER Mammalian Protein Extraction Reagent (Thermo, Waltham, MA, USA) containing halt protease inhibitor single-use cocktail (Thermo). The extracted total protein was denatured by adding 5× sodium dodecyl sulfate-polyacrylamide gel electrophoresis (SDS-PAGE) sample buffer (Thermo), followed by boiling at 100 °C for 10 min. Next, approximately 10 μg denatured proteins were separated by SDS-PAGE, transferred onto a polyvinylidene fluoride (PVDF) membrane, and blocked with 5% (*w*/*v*) milk at room temperature. After 1 h, the PVDF membranes were incubated with antibodies against GAPDH/*β*-Actin (Cell Signaling Technology, Danvers, MA, USA) or HBV core protein (Synthesized by GenScript, Nanjing, China) at 4 °C overnight. Following a standard wash, the membranes were incubated with a goat anti-mouse or anti-rabbit radish peroxidase (HRP)-conjugated antibody (Cell Signaling Technology). The signal was detected using the Omni-ECL Femto Light Chemiluminescence Kit (EpiZyme, Shanghai, China).

4.6. Determination of the mechanism of action of ***HyT-S7***

4.6.1. Determination of HBC half-life

HepAD38 cells were cultured in a tetracycline-free complete medium for 24 h and then incubated with 6 μmol/L **HyT-S7** or DMSO in the presence of 50 μg/mL CHX (Sigma) for the indicated time. After washing with pre-chilled PBS, the cells were lysed, and HBV core protein levels were determined using a Western blot assay.

4.6.2. Proteomics analysis

HepAD38 cells cultured in a completed medium without tetracycline were treated with DMSO or 6 μmol/L **HyT-S7** for 24 h. Cells were harvested by centrifugation and washed with PBS before snap freezing in liquid nitrogen. Cells were lysed by the addition of lysis buffer with urea at a final concentration of 8 mol/L, along with appropriate protease and phosphatase inhibitors. Then, the mixture was treated by a high-flux tissue grinding machine 3 times, 40 s each. The bicinchoninic acid (BCA) method was used to determine the final protein concentration from the supernatant collected.

100 μg of protein for each sample re-suspended with 100 mmol/L triethylammonium bicarbonate buffer (TEAB) was reduced with 10 mmol/L Tris(2-carboxyethyl)phosphine (TCEP) and alkylated with 40 mmol/L iodoacetamide (IAM). After centrifugation, the pellet was collected and re-suspended in 100 μL of 100 mmol/L TEAB. Proteins were digested with trypsin (1:50; enzyme: protein) overnight at 37 °C.

After digestion, the peptides were drained by a vacuum pump. Then, the enzymatically drained peptides were re-solubilized with 0.1% trifluoroacetic acid (TFA), and the peptides were desalted with HLB and drained by vacuum concentrator. Finally, the peptides were quantified using a ThermoFisher Scientific Peptide Quantification Kit.

Based on peptide quantification results, the peptides were analyzed by a VanquishNeo coupled with an Orbitrap Astral mass spectrometer (Thermo, USA) at Majorbio Bio-Pharm Technology Co., Ltd. (Shanghai, China). Data-independent acquisition (DIA) data were acquired using an Orbitrap Astral mass spectrometer operated in DIA mode. MS data were collected over an *m*/*z* range of 100−1700. Spectronaut software (Version 19) was used to search the DIA raw data. Three peptides per protein and 3 daughter ions per peptide were selected for quantitative analysis. The parameters are as follows: Protein FDR$\leq$0.01, Peptide FDR$\leq$0.01, Peptide Confidence $\geq$99%, XIC width $\leq$75 ppm. The shared peptides and modified peptides were excluded, and the peak areas were calculated and summed to give the quantitative results. Only the proteins that have at least one unique peptide were used for protein identifications.

Bioinformatic analysis of proteomic data was performed with the Majorbio Cloud platform (https://cloud.majorbio.com)[46]. *P*-values and Fold change (FC) for the proteins between the two groups were calculated using the R package "*t*-test." The thresholds of fold change ($>$1.2 or $<$0.83) and *P*-value $<$0.05 were used to identify differentially expressed proteins (DEPs). Functional annotation of all identified proteins was performed using the KEGG pathway (http://www.genome.jp/kegg/).

4.6.3. Surface plasmon resonance (SPR)

The interactions between HBC protein and compound **HyT-S7** were analyzed by an SPR assay performed on a CM5 chip integrated into the Reichert4 SPR system (Reichert, Buffalo, NY, USA). HBC protein was purchased from Sino Biological. All solutions were prepared using ultrapure water obtained from the Master Touch-S15UVF Pure Water Purification system. The running buffer used throughout the analysis was 1% DMSO PBST (pH 7.6 PBS buffer, 0.05% Tween-20, 1% DMSO), which was filtered through a 0.22 μm membrane filter before use. The proteins were prepared in a pH 4.5 sodium acetate solution at 200 μL, 0.25 μg/μL. Compounds were configured with 1% DMSO PBST to the desired gradient concentrations. The analysis temperature was controlled at 25 ± 1 °C. Target/control proteins were immobilized on the surface of the gold film of the chip containing carboxymethyl glucan by covalent amine coupling. The target/control proteins were immobilized on the sensing channels, and the reference channel was employed as a negative control. Furthermore, ethanolamine was used as a blocker to fill in the blanks. The final signal from the sensing channel was normalized by subtracting the signal from the reference channel. Target/control proteins were injected into the respective sensing channels at a rate of 10 μL/min for 300 s, and the CM5 chip was ready with the immobilization of protein. Then, compounds of the concentration gradient were successively injected into the SPR channels at a speed of 25 μL/min to collect the real-time SPR signals. The binding kinetics and affinity were analyzed using TraceDrawer software.

4.6.4. Cellular thermal shift assay (CETSA)

Cellular thermal shift assay (CETSA) is a valuable method to confirm target engagement within a complex cellular environment by detecting changes in a protein's thermal stability upon ligand binding[47]. HepAD38 cells were cultured in a tetracycline-free complete medium for 96 h. After digestion with trypsin, the

cell pellet was resuspended with PBS containing protease inhibitors (Thermo). Then, three freeze−thaw cycles in liquid nitrogen were performed to release cellular proteins. After high-speed centrifugation, cell lysate was incubated with DMSO or different compounds for 30 min at room temperature and heated on a gradient from 37 to 72 °C for 3 min. The supernatant was collected and loaded onto a 10% SDS-PAGE gel. The levels of HBC were detected by Western blot assay. For the thermal gradient analysis, each replicate series ($n = 3$) was fit to a spline curve, and the melting temperature (Tm) was determined by calculating the value of the curve at $y = 50$ using GraphPad Prism software.

*4.7. Molecular docking and molecular dynamics simulation of **HyT-S7***

4.7.1. Molecular docking

Molecular docking was performed using Schrödinger Software Release 2021-4. The X-ray crystal structure of HBC was derived from the Protein Data Bank (PDB: 5T2P). The Protein Preparation Wizard tool of Maestro was used to prepare the protein structure required for subsequent docking calculations, in which missing hydrogen atoms were added and minimized, and bond orders and disulfide bonds were calculated. The structure of the protein was minimized using the OPLS4 force field to optimize the hydrogen bonding network and converge heavy atoms to an RMSD of 0.3 Å. The "receptor grid generation" tool in Maestro was employed to define an active site around the native ligand to cover all the residues within 20 Å. **HyT-S7** was virtually created through the Maestro 2D Sketcher tool. Then, with Ligprep (a utility present in the Schrödinger suite), the ligand was prepared for the docking experiments. Appropriate tautomeric and ionization states were generated, which served as inputs for the docking process. The ligand docking was performed using the Glide v8.4 program with the Standard Precision method. The van der Waals radii of nonpolar atoms for each of the ligands were scaled by 0.8. Ligand poses with the most negative docking scores were chosen for further analysis.

4.7.2. Molecular dynamics simulation

Molecular dynamics simulations were performed further to investigate the dynamic interactions between the HBC and **HyT-S7**. All simulations were conducted by using Schrödinger version 2021-4 and employed the Desmond module. The previously generated docking complex was employed as the starting coordinate, which was then filled into a proper box and solvated with water (TIP3P). The whole system was then added corresponding Na^+ or Cl^- to neutralize all charges of the entire system. 0.15 mol/L NaCl was added to the system to simulate salt concentrations under physiological conditions. The whole system was relaxed with the default setting, and the productive simulation was then performed for 250 ns with a temperature of 300 K and a pressure of 1 bar. The resulting trajectory was then analyzed, and the RMSD of the complex was calculated.

Acknowledgments

We gratefully acknowledge financial support from the Key Research and Development Program, Ministry of Science and Technology of the People's Republic of China (2023YFC2606500), Science Foundation for Outstanding Young Scholars of Shandong Province (ZR2020JQ31, China), Drug Innovation Major Project (2018ZX09101003-003-003, China), CAMS Innovation Fund for Medical Sciences (CAMS-2021-I2M-1-030, China), National Natural Science Foundation of China (81803592) and Shandong Laboratory Program (SYS202205, China).

Author contributions

Shujing Xu: Writing − original draft, Resources, Methodology, Investigation, Conceptualization. Ya Wang: Writing − review & editing, Methodology, Investigation, Data curation. Dazhou Shi: Resources, Investigation. Shuo Wang: Software. Lijun Qiao: Data curation. Ge Yang: Data curation. Yang Zhou: Resources. Xinyong Liu: Writing − review & editing. Shuo Wu: Writing − review & editing, Investigation, Formal analysis, Data curation. Yuhuan Li: Writing − review & editing, Supervision, Project administration, Funding acquisition, Conceptualization. Peng Zhan: Writing − review & editing, Validation, Supervision, Project administration, Funding acquisition, Conceptualization.

Conflicts of interest

The authors have no conflicts of interest to declare.

Appendix A. Supporting information

Supporting information to this article can be found online at https://doi.org/10.1016/j.apsb.2025.02.033.

References

1. WHO. HBV fact sheet. Available from: https://www.who.int/zh/news-room/fact-sheets/detail/hepatitis-b; 2024.02.16.
2. Seto WK, Lo YR, Pawlotsky JM, Yuen MF. Chronic hepatitis B virus infection. *Lancet* 2018;**392**:2313−24.
3. Fung J, Lai CL, Seto WK, Yuen MF. Nucleoside/nucleotide analogues in the treatment of chronic hepatitis B. *J Antimicrob Chemother* 2011;**66**:2715−25.
4. Zoulim F, Durantel D. Antiviral therapies and prospects for a cure of chronic hepatitis B. *Cold Spring Harb Perspect Med* 2015;**5**:a021501.
5. Martinez MG, Boyd A, Combe E, Testoni B, Zoulim F. Covalently closed circular DNA: the ultimate therapeutic target for curing HBV infections. *J Hepatol* 2021;**75**:706−17.
6. Viswanathan U, Mani N, Hu ZY, Ban HQ, Du YM, Hu J, et al. Targeting the multifunctional HBV core protein as a potential cure for chronic hepatitis B. *Antivir Res* 2020;**182**:104917.
7. Niklasch M, Zimmermann P, Nassal M. The hepatitis B virus nucleocapsid-dynamic compartment for infectious virus production and new antiviral target. *Biomedicines* 2021;**9**:1577.
8. Liu KC, Luckenbaugh L, Ning XJ, Xi J, Hu JM. Multiple roles of core protein linker in hepatitis B virus replication. *PLoS Pathog* 2018;**14**:e1007085.
9. Tan ZN, Pionek K, Unchwaniwala N, Maguire ML, Loeb DD, Zlotnick A. The interface between hepatitis B virus capsid proteins affects self-assembly, pregenomic RNA packaging, and reverse transcription. *J Virol* 2015;**89**:3275−84.
10. Lahlali T, Berke JM, Vergauwen K, Foca A, Vandyck K, Pauwels F, et al. Novel potent capsid assembly modulators regulate multiple steps of the hepatitis B virus life cycle. *Antimicrob Agents Chemother* 2018;**62**:e00835-18.
11. Böttcher B, Wynne SA, Crowther RA. Determination of the fold of the core protein of hepatitis B virus by electron cryomicroscopy. *Nature* 1997;**386**:88−91.

12. Ceres P, Zlotnick A. Weak protein−protein interactions are sufficient to drive assembly of hepatitis B virus capsids. *Biochemistry* 2002;**41**: 11525−31.
13. Deres K, Schröder CH, Paessens A, Goldmann S, Hacker HJ, Weber O, et al. Inhibition of hepatitis B virus replication by drug-induced depletion of nucleocapsids. *Science* 2003;**299**:893−6.
14. Stray SJ, Bourne CR, Punna S, Lewis WG, Finn MG, Zlotnick A. A heteroaryldihydropyrimidine activates and can misdirect hepatitis B virus capsid assembly. *Proc Natl Acad Sci U S A* 2005;**102**:8138−43.
15. Wu GY, Liu B, Zhang YJ, Li J, Arzumanyan A, Clayton MM, et al. Preclinical characterization of GLS4, an inhibitor of hepatitis B virus core particle assembly. *Antimicrob Agents Chemother* 2013;**57**: 5344−54.
16. Zhou Z, Hu TS, Zhou X, Wildum S, Garcia-Alcalde F, Xu ZH, et al. Heteroaryldihydropyrimidine (HAP) and sulfamoylbenzamide (SBA) inhibit hepatitis B virus replication by different molecular mechanisms. *Sci Rep* 2017;**7**:42374.
17. Campagna MR, Liu F, Mao RC, Mills C, Cai DW, Guo F, et al. Sulfamoylbenzamide derivatives inhibit the assembly of hepatitis B virus nucleocapsids. *J Virol* 2013;**87**:6931−42.
18. Berke JM, Tan Y, Verbinnen T, Dehertogh P, Vergauwen K, Vos A, et al. Antiviral profiling of the capsid assembly modulator BAY41-4109 on full-length HBV genotype A−H clinical isolates and core site-directed mutants *in vitro*. *Antivir Res* 2017;**144**:205−15.
19. Zhou Y, Xu SJ, López-Carrobles N, Ding D, Liu XY, Menéndez-Arias L, et al. Recent advances in the molecular design and applications of proteolysis targeting chimera-based multispecific antiviral modality. *Acta Materia Med* 2023;**2**:285−98.
20. Xie SW, Zhu JJ, Li JD, Zhan FY, Yao H, Xu JY, et al. Small-molecule hydrophobic tagging: a promising strategy of druglike technology for targeted protein degradation. *J Med Chem* 2023;**66**:10917−33.
21. Wang S, Ren YJ, Li QL, Wang Y, Jiang XY, Xu SJ, et al. Design, synthesis, and biological evaluation of novel sulfamoylbenzamide derivatives as HBV capsid assembly modulators. *Bioorg Chem* 2022; **129**:106192.
22. Wang M, Zhang J, Dou YT, Liang MH, Xie Y, Xue P, et al. Design, synthesis, and biological evaluation of novel thioureidobenzamide (TBA) derivatives as HBV capsid assembly modulators. *J Med Chem* 2023;**66**:13968−90.
23. Lam AM, Espiritu C, Vogel R, Ren S, Lau V, Kelly M, et al. Preclinical characterization of NVR 3-778, a first-in-class capsid assembly modulator against hepatitis B virus. *Antimicrob Agents Chemother* 2018;**63**:e01734-18.
24. Shao XY, Xu SJ, Wan XF, Zhou Y, Wang S, Wu S, et al. Medicinal chemistry strategies in the discovery and optimization of HBV core protein allosteric modulators (2018−2022 update). *Chin Chem Lett* 2023;**34**:108349.
25. Sun Y, Xue YL, Sun PK, Mu SY, Liu HB, Sun Y, et al. Discovery of the first potent, selective, and *in vivo* efficacious polo-like kinase 4 proteolysis targeting chimera degrader for the treatment of TRIM37-amplified breast cancer. *J Med Chem* 2023;**66**:8200−21.
26. Ladner SK, Otto MJ, Barker CS, Zaifert K, Wang GH, Guo JT, et al. Inducible expression of human hepatitis B virus (HBV) in stably transfected hepatoblastoma cells: a novel system for screening potential inhibitors of HBV replication. *Antimicrob Agents Chemother* 1997;**41**:1715−20.
27. Pennington LD, Moustakas DT. The necessary nitrogen atom: a versatile high-impact design element for multiparameter optimization. *J Med Chem* 2017;**60**:3552−79.
28. Pennington LD, Aquila BM, Choi Y, Valiulin RA, Muegge I. Positional analogue scanning: an effective strategy for multiparameter optimization in drug design. *J Med Chem* 2020;**63**:8956−76.
29. Pennington LD, Croghan MD, Sham KK, Pickrell AJ, Harrington PE, Frohn MJ, et al. Quinolinone-based agonists of $S1P_1$: use of a N-scan SAR strategy to optimize *in vitro* and *in vivo* activity. *Bioorg Med Chem Lett* 2012;**22**:527−31.
30. Mallo-Abreu A, Prieto-Díaz R, Jespers W, Azuaje J, Majellaro M, Velando C, et al. Nitrogen-walk approach to explore bioisosteric replacements in a series of potent A2B adenosine receptor antagonists. *J Med Chem* 2020;**63**:7721−39.
31. Garai S, Kulkarni PM, Schaffer PC, Leo LM, Brandt AL, Zagzoog A, et al. Application of fluorine- and nitrogen-walk approaches: defining the structural and functional diversity of 2-phenylindole class of cannabinoid 1 receptor positive allosteric modulators. *J Med Chem* 2020;**63**:542−68.
32. Ciechanover A, Kwon YT. Degradation of misfolded proteins in neurodegenerative diseases: therapeutic targets and strategies. *Exp Mol Med* 2015;**47**:e147.
33. Berkers CR, Verdoes M, Lichtman E, Fiebiger E, Kessler BM, Anderson KC, et al. Activity probe for *in vivo* profiling of the specificity of proteasome inhibitor bortezomib. *Nat Methods* 2005;**2**: 357−62.
34. Shanmugasundaram K, Shao P, Chen H, Campos B, McHardy SF, Luo TP, et al. A modular PROTAC design for target destruction using a degradation signal based on a single amino acid. *J Biol Chem* 2019; **294**:15172−5.
35. Choi SR, Wang HM, Shin MH, Lim HS. Hydrophobic tagging-mediated degradation of transcription coactivator SRC-1. *Int J Mol Sci* 2021;**22**:6407.
36. Solit DB, Ivy SP, Kopil C, Sikorski R, Morris MJ, Slovin SF, et al. Phase I trial of 17-allylamino-17-demethoxygeldanamycin in patients with advanced cancer. *Clin Cancer Res* 2007;**13**:1775−82.
37. Sheng Y, Sun B, Guo WT, Zhang YH, Liu X, Xing Y, et al. 3-Methyladenine induces cell death and its interaction with chemotherapeutic drugs is independent of autophagy. *Biochem Biophys Res Commun* 2013;**432**:5−9.
38. Li M, Khambu B, Zhang H, Kang JH, Chen XY, Chen DH, et al. Suppression of lysosome function induces autophagy *via* a feedback down-regulation of MTOR complex 1 (MTORC1) activity. *J Biol Chem* 2013;**288**:35769−80.
39. Lagunas-Martínez A, García-Villa E, Arellano-Gaytán M, Contreras-Ochoa CO, Dimas-González J, López-Arellano ME, et al. MG132 plus apoptosis antigen-1 (APO-1) antibody cooperate to restore p53 activity inducing autophagy and p53-dependent apoptosis in HPV16 E6-expressing keratinocytes. *Apoptosis* 2017;**22**:27−40.
40. Harhouri K, Navarro C, Depetris D, Mattei MG, Nissan X, Cau P, et al. MG132-induced progerin clearance is mediated by autophagy activation and splicing regulation. *EMBO Mol Med* 2017;**9**:1294−313.
41. Fan T, Huang ZX, Wang W, Zhang BY, Xu Y, Mao ZF, et al. Proteasome inhibition promotes autophagy and protects from endoplasmic reticulum stress in rat alveolar macrophages exposed to hypoxia-reoxygenation injury. *J Cell Physiol* 2018;**233**:6748−58.
42. Wu S, Luo Y, Viswanathan U, Kulp J, Cheng JJ, Hu ZY, et al. CpAMs induce assembly of HBV capsids with altered electrophoresis mobility: implications for mechanism of inhibiting pgRNA packaging. *Antivir Res* 2018;**159**:1−12.
43. Luo Y, Cheng JJ, Hu ZY, Ban HQ, Wu S, Hwang N, et al. Identification of hepatitis B virus core protein residues critical for capsid assembly, pgRNA encapsidation and resistance to capsid assembly modulators. *Antivir Res* 2021;**191**:105080.
44. Wu S, Zhao Q, Zhang PH, Kulp J, Hu L, Hwang N, et al. Discovery and mechanistic study of benzamide derivatives that modulate hepatitis B virus capsid assembly. *J Virol* 2017;**91**:e00519-17.
45. Wang HQ, Li K, Cui BM, Yan HY, Wu S, Wang K, et al. Tribbles pseudokinase 3 promotes enterovirus A71 infection *via* dual mechanisms. *Emerg Microbes Infect* 2024;**13**:2307514.
46. Ren Y, Yu G, Shi CP, Liu LM, Guo Q, Han C, et al. Majorbio Cloud: a one-stop, comprehensive bioinformatic platform for multiomics analyses. *Imeta* 2022;**1**:e12.
47. Jafari R, Almqvist H, Axelsson H, Ignatushchenko M, Lundbäck T, Nordlund P, et al. The cellular thermal shift assay for evaluating drug target interactions in cells. *Nat Protoc* 2014;**9**:2100−22.